Università degli Studi di Ferrara

DOTTORATO DI RICERCA IN

Farmacologia e Oncologia Molecolare

CICLO XXVIII

COORDINATORE Prof. Cuneo Antonio

The pan-HDAC inhibitor AR42 downregulates CD44 expression, a new circulating prognostic factor for multiple myeloma

Settore Scientifico Disciplinare BIO/17

Dottorando

Dott. Canella Alessandro

Tutore

Prof. Volinia Stefano

Anni 2013/2015

ABSTRACT

Multiple myeloma (MM) is a hematological malignancy of plasma cells (PCs) in the bone marrow. The interplay between MM-PCs and bone marrow microenvironment, including cell-cell contacts and release of pro-survival factors and extracellular vescicles (EV), promotes cancer cell survival and drug resistance. At first my research was focused on the characterization of the proteomic content of EVs secreted by MM cell lines. Among them, the glycoprotein CD44 is one of the most abundant proteins and has been already associated, both in vivo and in vitro, with lenalidomide and dexamethasone resistance in multiple myeloma. The analysis of serum samples from a cohort of 200 MM patients shows that circulating CD44 carried by MM-EVs correlates with ISS stage and β2-microglobulin and constitutes a potential prognostic factor, thus providing the rationale to further explore novel molecular players associated with MM disease.

Despite multiple treatment options, MM is inevitably associated with drug resistance and poor outcomes. Histone deacetylase inhibitors (HDACi's) are promising novel chemotherapeutics under evaluation in clinical trials for the treatment of MM patients. Although in preclinical studies HDACi's have proven anti-myeloma activity, in the clinics single-agent HDACi treatments have been limited due to low tolerability. We believe that HDACi could constitute a valid support if used in combination with the MM state of care. In this thesis I show that a novel pan-HDACi AR42 downregulates CD44. Moreover, the CD44 downregulation is in part mediated by *miR-9-5p*, targeting insulin-like growth factor 2 mRNA binding protein 3 (IGF2BP3), which directly binds to CD44 mRNA and increases its stability. Importantly, we demonstrate that AR42 enhances anti-myeloma activity of lenalidomide in primary MM cells isolated from lenalidomide resistant patients and in MM mouse model. In conclusion, our observations suggest a potential novel combinatorial therapeutic approach modulating CD44 expression, which may help overcome lenalidomide resistance in myeloma patients.

CONTENTS

ABBREVIATIONS

ACY-1215	Ricolinostat - HDAC6i
AML	Acute myeloid leukemia
ANXA2	Annexin A2
AR42	HDACi
ARF	Tumor suppressor ARF
β2M	β_2-microglobulin
Bcl-2	Apoptosis regulator Bcl-2
BM	Bone marrow
BMSC	Bone marrow stromal cells
CAM-DR	Cell adhesion-mediated drug resistance
CCL2	C-C motif chemokine 2
CDKN1A	Cyclin-Dependent Kinase Inhibitor 1A
C.I.	Combinatorial index
CLL	Chronic lymphocytic leukemia
Cryo-TEM	Cryogenic transmission electron microscopy
CSCs	Cancer stem cells
CTCL	Cutaneous T-cell lymphoma
CXCR4	Chemokine (C-X-C Motif) Receptor 4
DLBCL	Diffuse large B-cell lymphoma
DLS	Dynamic Light Scattering
DMSO	Dimethyl sulfoxide
ECM	Extracellular matrix
EGFR	Epidermal Growth Factor Receptor
EMT	Epithelial mesenchymal transition
EVs	Extracellular vesicles
FDA	Food and drug administration
FK228	Romidepsin - HDACi
FIH-1	Factor inhibiting HIF-1
GAPDH	Glyceraldehyde-3-Phosphate Dehydrogenase
gDNA	Genomic DNA
GFP	Green fluorescent protein
GSK3β	Glycogen synthase kinase 3 beta
H	Histone
H&E	Hematoxylin and eosin
HA	Hyaluronic Acid
HAT	Histone acetyltransferase
HCT	Hematopoietic cell transplant.
HDAC	Histone deacetylase
HGF	Hepatocyte Growth Factor
HIF-1	Hypoxia-inducible factor 1
Hsp	Heat shock protein
Ig	Immunoglobulin
IGF2BP	Insulin grow factor 2 binding protein
IKB	Nuclear factor of kappa light polypeptide gene enhancer in B-cells inhibitor
IL	Interleukin
ISS	International Staging System
LBH589	Panobinostat - HDACi
LC-MS/MS	Liquid chromatography-mass spectrometry/mass spectrometry
Len	Lenalidomide
Luc	Luciferase
MDR	Multidrug resistance
MET	Proto-Oncogene, Receptor Tyrosine Kinase
MGUS	Monoclonal Gammopathy of Unknown Significance
MM	Multiple Myeloma
MM-EVs	Multiple myeloma-derived extracellular vesicles
MMP9	Matrix Metallopeptidase 9
NF-κB	Nuclear factor κB
NK	Natural killer
NKG2D	Natural-killer group 2, member D
OCs	Osteoclasts
OS	Overall Survival

p16	Cyclin-dependent kinase inhibitor 2A
p53	Tumor suppressor protein 53
PBMCs	Pheripheral blood mononuclear cells
PDX101	Belinostat - HDACi
PKM	Pyruvate Kinase, Muscle
PI	Propidium iodide
PTEN	Phosphatase tensin homolog
RF	Tumor suppressor ARF
RHAMM	Hyaluronan-mediated motility receptor
ROS	Reactive oxygen species
SAHA	Vorinostat - HDACi
SIRT1	Sirtuin 1
Scr	Scramble
SMM	Smoldering MM
SOC	Standard of care
TFs	Transcription factors
TGFβ	Transforming growth factor β
TLR7	Toll-like receptor 7
TME	Tumor microenvironment
TRAP5	Tartrate Resistant Acid Phosphatase 5
TrpC5	Transient receptor potential cation channel subfamily C member 5
TNF	Tumor necrosis factor
VCAM-1	Vascular cell adhesion protein 1
VEGF	Vascular endothelial growth factor
VLA-4	Very late antigen 4
3' UTR	Three prime untranslated region
ZNF224	Zinc finger protein 224
WT	Wild type

CHAPTER 1. INTRODUCTION

1.1 MULTIPLE MYELOMA

1.1.1 Epidemiology

Multiple myeloma (MM) is a hematological malignancy of plasma cells in the bone marrow (Fig. 1) accounting for approximately 114,000 diagnoses, 0.8% of all cancer diagnoses and 80,000 deaths, 1.0% of all cancer related deaths, annually worldwide [1]. MM represent approximately 1.4% of all cancer diagnoses, more than 15% of all leukemia and lymphomas, and 1.8% of all cancer related deaths in the United States [2]. Men have a slightly higher risk for diagnosis and death from MM than women worldwide (1.2:1). Patients with MM have a 5 year overall survival (OS) rate of about 45% and a median survival of 3-4 years [1]. Even though various risk factors have been characterized, no specific cause for the initial development of MM has been identified. Nevertheless, the most established risk factors for MM development are age (median age of diagnosis is 69), male gender, African American race and a familiarity of the illness [3].

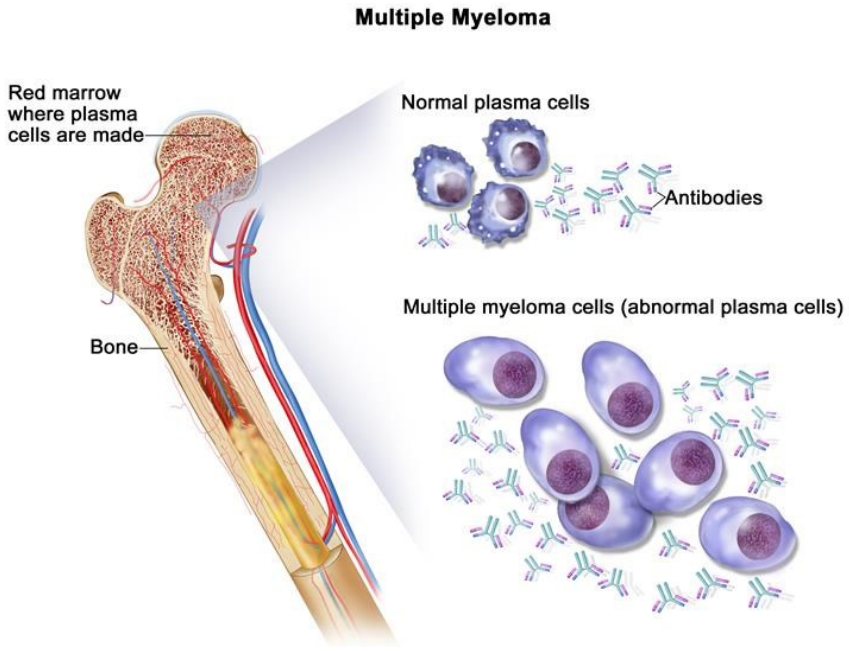

Fig. 1 *Multiple Myeloma*

1.1.2 Diagnosis, staging and treatment

Multiple Myeloma is a heterogeneous disease, which frequently develops by progression of premalignant disorders called Monoclonal Gammopathy of Unknown Significance (MGUS) and Smoldering MM (SMM, asymptomatic MM) [4]. A MGUS diagnosis is determined by detection of less than 3 g/dL monoclonal protein in the serum, low level or absence of proteinuria, less than 10% of monoclonal plasma cells in the bone marrow and no evidence of end organ damage [5]. Estimates suggest around 3% of the population over the age of 50 have a symptomatic MGUS [6]. Three types of MGUS are recognized clinically, non-IgM, IgM, and light chain MGUS, each associated with unique end-stage diseases [7]. However, only a small subset (approximately 1% per year) of patients diagnosed with MGUS will develop active multiple myeloma [7].

SMM differs from MGUS for the presence of higher monoclonal protein content (>3 g/dL) in serum and/or higher concentration of monoclonal plasma cells in the bone marrow (10-60%) [8]. Patients diagnosed with SMM are more likely to develop active MM (approximately 10% per year compared to 1% in MGUS) due to the bone marrow contribution [4]. Symptoms of active multiple myeloma include anemia, bone pain, elevated creatinine, fatigue/weakness, hypercalcemia and weight loss [8]. Once diagnosed with active disease, MM patients are staged based on cytogenetic abnormalities to determine prognostic significance and treatment options. Patients diagnosed with active MM who do not receive effective therapy have a median survival of six months [9].

MM classification, the International Staging System (ISS, Table 1), is based on serological levels of two proteins, β_2 microglobulin (β2M) and albumin. The median OS correlated with each ISS stage is (I) 62, (II) 44, and (III) 29 months [10]. Furthermore, beside the ISS, many factors and cytogenetic alterations have been evaluated to determine their prognostic value in MM [11]. Among them, the cytogenetic abnormality t(4;14)(p16;q32) is associated with more aggressive disease leading to shorter survival when treated with common chemotherapeutics [12-14]. Overall, the distinction between MGUS, SMM, active MM and ISS must be cautiously considered to determine prognosis and best therapy for each patient.

ISS STAGE	Prognostic factors	Median survival
I	β2M < 3.5mg/L - Albumin ≥ 3.5 g/dL	5Y,2M
II	5.5<β2M5>3.5mg/L - Albumin any level or β2M<3.5mg/L - Albumin<3.5g/L	3Y,8M
III	β2M5>5.5mg/L - Albumin any level	2Y,5M

Table 1. *Multiple myeloma staging, main prognostic factors and median OS (Y=Years; M=Months)*

In eligible MM patients, high dose chemotherapy followed by autologous hematopoietic cell transplantation (HCT) is the treatment option presenting the best event-free and OS, when compared to chemotherapy alone [15].

In intermediate and standard risk MM patients (meeting the criteria for HCT), the induction therapy before the transplant consists in low doses of lenalidomide plus dexamethasone. Lenalidomide is an immunomodulatory drug, while dexamethasone reduce the tumor burden and organ damage typically associated with MM [16]. After the induction therapy, hematopoietic stem cells are harvested from the peripheral blood of the patients, isolated and stored until reinfusion which follows preparative chemotherapeutics to eradicate the residual malignant cells [16]. Although this standard of care (SOC) prolongs event-free survival, autologous HCT is not curative and disease relapse is inevitable.

While Intermediate and Standard risk groups are the most common in MM, approximately 15% of MM patients have high risk disease [11]. High risk MM has been shown to have a more rapid progression following chemotherapy and HCT. Following HCT patients with high risk MM are placed on maintenance doses of therapeutics, commonly the proteasome inhibitor bortezomib, to suppress disease relapse. However in most cases, relapse occurs quickly [11].

The final subgroup of MM patients are those ineligible for autologous HCT due to age, hepatic, renal, pulmonary and cardiac function [17]. The treatment options for this group of patients rely heavily on combinatorial chemotherapeutics such as lenalidomide and dexamethasone, bortezomib, cyclophosphamide and dexamethasone [11,17], depending on the ability of the patient to tolerate the heavy side effects of the combinatorial therapy. Unfortunately, none of the reported therapeutic options are considerate curative.

1.1.3 Pathogenesis and principal mediators of tumor progression

The evolution from the pre-malignant condition to active MM status, requires the onset of additional cytogenetic rearrangements, microenvironmental protection and other mechanisms [18]. The MGUS status is assumed to be the result of unusual cytogenetic rearrangement due to an abnormal response to antigen with a subsequent cytogenetic defects occurring during the tumor progression. For example, in the germinal center, approximately 50% of pre-MGUS acquire aberrant immunoglobulin (Ig) heavy chain translocations at common oncogenic loci, such as the cyclin D1 gene on chromosome 11q13 [18,19]. This abnormality is observed in approximately 15-20% of tumors, conferring immortalization to these cells. Other commonly recurring oncogenic Ig translocations are found on chromosomes 6q21 (cyclin D3), 4p16 (fibroblast growth factor receptor 3 and MMSET domain), 16q23 (c-maf) and 20q11 (mafB) [19,20]. The remaining 50% of MGUS cases have no Ig heavy chain rearrangement but present multiple chromosomal trisomies [12]. Furthermore, nearly 40% of MM tumors were shown to have activating RAS mutations which is known to reduce the dependence of the MM cells for Interleukin-6 (IL6) mediating survival [21]. Many other mutations, translocations deletions and epigenetic mechanisms are essential to MM progression and development, regulating the expression of several key proteins such as tumor suppressors p53, p16, ARF and PTEN [18].

Beside the genetic changes well known to be involved in MM progression, also the bone marrow microenvironment plays a key role in MM development. The current hypothesis of MM pathogenesis suggests that initiating cytogenetic abnormalities, either Ig heavy chain translocation or hyperploidy, of oncogenes, such as cyclin D1, makes early pre-MGUS cells prone to microenvironmental stimuli ultimately leading to progression of disease [18,20,22].

The bone marrow microenvironment consists of many different cell types and elements, such as bone marrow stromal cells (BMSC), endothelial cells, osteoclasts, osteoblasts and extracellular matrix (ECM) proteins, actively contributing to the MM development. For example, MM cells have been shown to adhere to both BM-ECM proteins, such as Fibronectin (FN), and interact with BMSC via vascular cell adhesion protein 1 (VCAM-1) and very late antigen 4 (VLA-4), promoting the modulation of cytokine production [23,24]. Moreover, VLA-4 associations have been reported to increase BMSC secretion

of interleukin-6 (IL6), a key mediator of MM cell growth and survival, through nuclear factor κB (NF-κB) signaling [24,25]. In addition to cellular adhesion and other functions, bone marrow MM cells have been shown to secrete cytokines, such as transforming growth factor β (TGFβ) and vascular endothelial growth factor (VEGF), to promote IL6 release from BMSC [26,27].

From the other side, the effect of bone marrow cells on MM growth and survival is primarily mediated through IL6 signaling [28]. IL6 has been shown to function both as an autocrine, secreted by MM cells, and a paracrine signal, secreted by BMSC and osteoblast cells [29]. Following receptor binding, IL6 initiates multiple signaling pathways, including MEK/MAPK, JAK/STAT and PI3K/Akt, which confer survival, resistance to apoptosis, promote migration and proliferation [30-32]. In addition to apoptotic evasion and survival, paracrine soluble factors and direct cell adhesion, have been shown to confer drug resistence to MM cells of the bone marrow [22,25,33-37]. For instance, the activation of signaling mediated by IL6 in MM cells has demonstrated to reduce dexamethasone induced apoptosis [38]. Additional mechanisms have been reported to be important in MM chemo-resistence, in particular the aquisition of genetic mutations of key apoptotic mediators, such as p53 [39].

The preliminary data on the biological interactions of multiple myeloma with the bone marrow microenvironment has only begun paved the way to the development of novel targeted therapeutics. Further invesitgations into the microenvironmental interactions and communication between MM and BM cells are warranted to identify innovative therapeutic strategies and targets.

1.2 EXTRACELLULAR VESICLES (EVs)

The biological importance of the EVs was unknown until a study published in 1981 [40] described the shedding of lipid microvesicles by normal and neoplastic cells. Since the exfoliated membrane vesicles contained proteins with enzymatic activities it was speculated that those kinds of vesicles may have some biological functions. For the following 15 years, research on extracellular vesicles (or exosomes) has been minimal. It was not until the discovery that B-lymphocytes also secreted exosomes carrying membrane-bound molecules essential for the adaptive immune response [41] that these molecules became major research focus. It is now well known that EVs are

produced by several kinds of cells, and are found in all physiological fluids, including blood, urine and saliva [42]. EVs can be classified in different subpopulations based on the cellular origins. The term “extracellular vesicles or exosomes” refer to vesicles created intracellularly in multivesicular compartments (endosomes) of the cells and secreted by fusion with the cellular membrane. In contrast, the microvesicles (and ectosomes) are shed from plasma membrane. Microvesicles, ectosomes and exosomes also differ in shape and size [43,44] and can have different lipids, proteins, DNA and, RNA cargo [45]. EVs can be defined by common characteristics, such as size (50–100 nm in diameter), morphology, enrichment of proteins and miRNAs. Exosomes (Fig. 2) also contain bioactive molecules that reflect the pathological state of the originated cells, thus providing an enriched source of biomarkers.

Originally supposed to be involved in removal of the cellular metabolites, EVs are nowadays recognized for their role in cell-cell communication by transporting proteins, lipids, mRNAs and microRNAs, and therefore contributing to the maintenance of normal physiology [46]. More in detail, EVs can participate in control of tissue repair, blood coagulation, inflammation, stem cells maintenance, or angiogenesis [46]. Moreover, they may also play a role in pathogenesis, such as the establishment of a pre-metastatic tumor niche and stimulation of tumor development and growth [47-49].

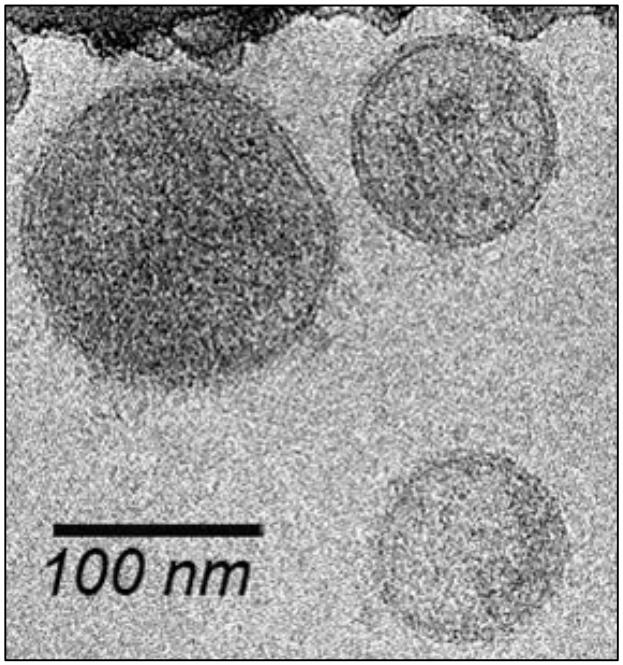

Fig. 2 *Extracellular vescicles by electron microscopy*

1.2.1 Extracellular vesicles and cancer

The interconnection between cancer and EVs has been recently investigated in several kinds of solid and soft tumors and many indicators suggesting that EVs may be involved in microenvironment remodeling, tumor progression and drug resistance mechanisms. The following examples indicate how EVs derived from cancer cells could mediate different effects depending on the mRNAs and proteins content. However the functional relevance of exosomal miRNAs and proteins are still areas of expanding research.

1.2.2 EVs and tumor microenvironment (TME)

The constant interaction and signal exchange between malignant cells and microenvironment are essential for the tumor progression, survival, metastasis and chemoresistance, but the function of many elements still remains to be investigated. More recently, EVs have come up as an alternative way for cell-cell interaction in cancer. Their generation from cancer cells can discipline the surrounding environment to become a supportive niche for tumor growth and survival, reprogram the BM progenitors or intensify the metastatic diffusion [50,51]. EVs derived from cancer cells can alter the tumor microenvironment through multiple mechanisms.

In a remarkable study on breast cancer, Fong M et al. [52] demonstrated that *miR-122* enriched exosomes derived from breast cancer are transferred to normal niche cells, promoting the downregulation of the PKM gene (encoding the pyruvate kinase, involved in glycolysis) subsequently blocking the glucose metabolism and reprogramming the glucose metabolism in premetastatic niche to promote metastasis.

One of the most important element of the extracellular matrix is the Fibronectin (FN), which plays a significant role in cell adhesion, growth, migration and differentiation. Heat shock protein 90 (Hsp90) can directly bind the extracellular FN and promote its stabilization. It has been demonstrate that breast cancer derived EVs, enriched in Hsp90, can directly interact with the extracellular Fibronectin, thus supporting the cancer invasion [53].

In prostate cancer, large EVs (oncosomes, > 100 nm) secreted by amoeboid cells are enriched in *miR-200* family and *miR-125a*. *miR-200* is involved in epithelial mesenchymal transition (EMT) and amoeboid-mesenchymal transition, while *miR-125a* can suppress the macrophages growth in this type of cancer [54].

Furthermore, Bronisz et al [55] discovered that Glioblastoma (GBM) secretes EVs enriched in ANXA2, a pro-oncogenic factor and it's implicated in proliferation, invasion and angiogenesis [56]. Treatment of GBM with EVs enriched in *miR-1* (onco-suppressor) determine downregulation of intracellular and EVs-ANXA2, repression of the tumor growth, reduction of endothelial cell recruitment and neurovascularization. These results confirms the importance of GBM derived EVs, enriched in ANXA2, in the TME remodeling and tumor growth.

The EVs secretes by the cells of the microenvironment can also influence and modify the cancer phenotype. Different kinds of stromal cells are able to release EVs; for example, exosomes secreted from fibroblasts promote breast cancer cell migration via Wnt-PCP signaling [57] and NK cell-derived exosomes from human blood contain proteins that promote cytotoxicity of tumor cells [58]. Notably, NK cell-derived exosomes are not cytotoxic to resting-immune cells, suggesting that their specific cytolytic effects are exclusively directed to cancer cells. Finally, exosomes released from Dendritic Cells (DCs), defined dexosomes, have been investigated as potential cancer vaccine [59,60]. This is supported by preclinical melanoma models, whereby dexosome immunization induced CD8+ cytotoxic T cells and slower tumor growth [61].

1.2.3 EVs derived from cancer stimulate tumor growth and metastasis

In aggressive melanoma, EVs derived from cancer cells promote tumor growth and metastasis in primary tumors and reprogrammed bone marrow-derived DCs to assume a pro-angiogenic phenotype [48], mechanism mediated by the inhibition of the receptor MET due to its direct interaction with the cancer derived EVs.

EVs generated by chronic myeloid leukemia cells contain BCR/ABL and the transfer of the oncoprotein to the normal neutrophils provoke a phenotypical change *in vivo* that improve the invasive and metastatic process [62].

As I mentioned before, *miR-200* has been also found enriched in EVs circulating in metastatic breast cancer and promotes metastasis [63]. Of note, circulating EVs containing *miR-200* not only increase the metastatic activity, but are also capable of transferring the metastatic phenotype from high metastatic to poorly metastatic human breast cancer cells.

As an alternative biological function of miRNAs carried by EVs, Fabbri et al. showed that exosomal miRNAs have the ability to activate Toll-like receptors, thus mediating a prometastatic inflammatory response [64]. A similar mechanism was found by We et al. [65], who have been able to demonstrate that miRNAs, such as *miR-21*, carried by circulating EVs derived from pancreatic and lung cancers, can directly interact with the Tool like receptor 7 (TLR7) of myoblasts. The interaction between *miR-21* and TLR7 triggers the downstream activation of JNK, which promotes apoptosis and cell death, finally inducing Cachexia on murine model.

1.2.4 EVs confer chemoresistance and immuno-modulation

Specific proteins contained in EVs have been shown to be very important in several mechanisms such as immune suppression and regulation.

Recently, studies conducted in lung cancer [66] and melanoma [67] showed a reduced sensitivity to cisplatinum upon cellular treatment with cancer derived exosomes. Moreover, Ma et al. [68] unequivocally demonstrated that the extracellular vesicles containing TrpC5, secreted from chemoresistant breast cancer cells, are able to transmit chemoresistance behavior to the chemosensitive cells. Lundholm M et al. [69] discovered a sophisticated immune-escape mechanism in prostate cancer: EVs prostate cancer-derived and highly expressing NKG2D ligand, interact directly with NK and CD8+ T cells, therefore blocking the NKG2D receptor and bypassing the cytotoxic activity. Furthermore, mesothelioma and myeloid leukemia derived EVs has been shown to facilitate inhibition of lymphocyte response to the survival cytokine interluken-2 (IL-2), through a mechanism mediated by transforming growth factor β1 (TGF-β1) expressed on EVs [70]. Additionally, vesicles from EBV-infected nasopharyngeal carcinoma cells induced apoptosis of $CD4^+$ T-cells via a galectin-9 pathway [71]. Another study reported that FasL can be expressed on melanoma tumor derived vesicles and induced apoptosis of activated T-cells [72].

These examples illustrate a variety of mechanisms in immunology and cancer biology, that can be influenced by proteins of enriched in EVs. As a result, further research into the identification, characterization and function of cellular derived EVs is encouraged to identify novel mechanisms and new therapeutic targets in neoplastic syndromes.

1.2.5 Biomarkers in cancer-derived EVs

The use of exosomal miRNAs as biomarkers is very promising and there is a wealth of literature supporting their relevance [73].

So far, many groups have used proteomics to characterize the protein content of extracellular vesicles derived both *in vitro* and *in vivo* [74-84]. Recently the complete proteomic-miRNAs profile has been determined in EVs derived from different kinds of tumors, for example breast cancer [85] and esophageal cancer [86]. Interestingly, while the origin of the vesicles used in these studies varied greatly from saliva to cell lines, their content was extremely similar [78,87]. The three most commonly identified proteins were heat shock protein 70 (Hsp70), β-actin, and glyderaldehyde-3-phosphate dehydrogenase (GAPDH) [78]. Overall, identified proteins in common are distributed into several categories including antigen presenting molecules, adhesion molecules, membrane transport and fusion molecules, cytoskeletal proteins, and others [78].

While RNA has been already demonstrated to have high potential for prognostic and predictive value in a host of diseases, protein content of extracellular vesicles may also yield significant functional consequences and prognostic capabilities. In addition to their function, the sole abundances of individual exosomal miRNA has been shown to correlate with disease status. For example, the miRNA profiles of ovarian cancer patients differ from those with a benign disease and specific miRNAs levels in the EVs were representative of the tumor cells themselves [88]. Tanaka et al. have shown that expression level of exosomal *miR-21* was higher in esophageal squamous cell carcinoma patients when compared to healthy controls suggesting the potential use of *miR-21* as a biomarker for the status of the disease [89]. Analogous results were obtained in lung cancer [90], where studies on the secreted EVs put in relation their content with the progression of the disease. Of note, Boeri et al [91] and Hu et al. [92] discovered in lung cancer respectively 9 and 4 miRNAs (Boeri et al.: *miR-221, miR-660, miR-484-5p, miR-28-3p, miR-197, miR-106a, miR-451, miR-140-5p, miR-16;* Hu et al.: *miR-486, miR-30d, miR-1, miR-499*) highly related to the cancer malignancy and poor prognosis. Lazaro-Ibenez et al. [93] demonstrated that EVs derived from serum of patients affected by prostate cancer contain higher concentration of double strand DNA fragments (gDNA) compared to healthy patients. Finally, another interesting study conducted in chronic liver disease [94] highlighted the enrichment of *miR-122* in

circulating EVs, despite its already known decreased level in the liver tissue of the patients.

1.2.6 Extracellular Vesicles in multiple myeloma

The constant and dynamic interaction between multiple myeloma (MM) and BM microenvironment is the key for tumor survival, growth, drug resistance, and pathogenesis [95,96]. In the past years, these kinds of interactions was attributed entirely to growth factors and cytokines such as IL6, VEGF and many others [25,97]. However, these well-known cellular messengers were not sufficient to completely explain the whole process.

Several researches has in part demonstrated the role of the extracellular vesicles (EVs) as mediators of the cell-cell communications in solid tumors but only recently MM-derived EVs have been characterized and suggested as promoters of tumor progression and potential mediators between MM and BM microenvironment. Despite recent studies have remarkably contributed to address the MM-EVs mechanism of production, interaction with the target cells and functions, many questions remain still unanswered.

1.2.7 Production of EVs in MM

The characterization of the intracellular molecules implicated in the EVs production process is extremely complicated. Thompson et al. [98] discovered that the edoglycosidase enzyme heparanase has an important role in regulating the production of MM-EVs and is able to dramatically increase their secretion. The heparanase not only plays a key role on the EVs production, but also modifies the quality of protein contents, enriching in syndecan-1, VEGF, HGF (proteins correlated with the aggressive tumor phenotype) and heparanase. They also provided the evidence that heparanase stimulates the exosomes production in other types of cancer such as in breast cancer, demonstrating the crucial role of this enzyme in the exosome biology. Interestingly, the qualitative and quantitative change of production of EVs due to the heparanase overexpression, and the consecutive treatment of tumor and normal cells increased the tumor cells spreading and the endothelial cells proliferation, key processes for tumor progression, metastasis and microenvironment alteration.

1.2.8 Role of MM-derived EVs on target cells

MM-derived EVs have been demonstrated to have biological effects on other cell types, both malignant and normal in the bone marrow (BM) microenvironment (Fig. 3).

The bone disease induced by altered balance between osteoclasts (either pre -pOCs- or mature -OCs), and osteoblasts is one of the most frequent complication in multiple myeloma and is rarely arrested by chemotherapy. Of note, EVs secreted by MM cells specifically cause a phenotypical change in Osteoclasts [99]. The absorption of MM derived EVs by pre and mature OCs increases the expression of CXCR4 (supporting the cellular migration), induces the extra cellular secretion of MMP9 (proteases involved in the bone resorption activity), overexpresses the TRAP-positive multinucleate OCs (degrades the bone matrix phospho-proteins, influencing the bone resorption) and finally promotes the differentiation of pCOs cells by inhibiting the apoptotic mechanism (downregulation of activate caspase 3).

Recently, the overexpression of *miR-135b* has been related to the osteogenic differentiation of mesenchymal stem cells derived from MM patients [100]. In an interesting study conducted by Umezu et al. [101] and supported by Fan G. [102], EVs isolated from MM patients were shown to be highly enriched in *miR-135b*. This miRNA is already known as tumor progression mediator in several kinds of solid tumors (colorectal cancer [103], osteosarcoma [104], lung cancer [105]). Beside the role in osteogenesis, treatment of endothelial cells under hypoxic conditions with MM-EVs overexpressing *miR-135b* induced the downregulation of FIH-1 (an inhibitor of the HIF-1 transactivation), eventually promoting the angiogenesis *in vivo*. The effect of EVs secreted by MM on angiogenesis was also reported by another research [106], where in vitro treatment of endothelial cells with MM derived exosomes promoted production and secretion of IL6 and VEGF, invasion, tube formation and *in vivo* vascularization.

To support the previously reported results on EVs and induction of angiogenesis in the BM microenvironment, a recent study by Arendt et al. demonstrated for the first time that MM-derived EVs were capable of stimulating the cellular proliferation through a mechanism mediated by CD147 [107]. Indeed, the internalization of MM exosomes enriched in CD147 enhances the upregulation of the mTOR-MAPK pathway in target cells, hence increasing the cell proliferation.

Finally, another study conducted on serum deprived EVs [108] proved the enhancement of the tube formation in endothelial cells treated with MM-EVs and highlighted the role the protein ZNF224 (Zinc finger protein 224), highly expressed in MM-EVs, on the activation of NF-kB signaling pathway in target myeloma cells, thus promoting the cell proliferation.

1.2.9 Influence of the BM microenvironment-derived EVs on MM

The BM microenvironment is an essential ally for the MM as it supports the tumor growth, survival, drug resistance and pathogenesis (Fig. 3). A recent and important study, developed by Roccaro et al. [109], clearly demonstrate for the first time that both BM microenvironment and MM cells produce transferable extracellular vesicles, suggesting a novel oncogenic mechanism mediated by EVs secreted by BM in MM. In this study, the interexchange of EVs between BM and MM cells was clearly demonstrated, leading to transfer of protein or regulation in miRNA expression. In particular, they found that EVs derived from normal and MM-BM cells have a different effect on MM cells, respectively reducing or increasing the MM proliferation rate. In fact the MM derived EVs showed higher level of CCL2 (C-C motif chemokine 2), IL6 and Fibronectin which play a crucial role in MM pathogenesis and tumor progression. Of note, the qualitative miRNA contents was also different. Indeed, *miR-15a* was one of the most downregulated miRNA in MM-EVs, as well as in the MM BM microenvironment cells and in EVs derived from BM of relapsed/refractory patients compared to the normal BM cells and derived EVs. Treatment of MM cells with EVs extracted from healthy bone marrow increased the *miR-15a* intracellular level and reduced the MM proliferation, supporting the tumor suppressor role of the *miR-15a* on MM and clearly indicating that MM growth, proliferation and dissemination are sustained by downregulation of the *miR-15a*. To support the protective role of miR-15a against MM, another study proved the evidence that in plasma of MM patients with a better outcome there were higher levels of circulating *miR-15a* and *miR-16* compared to severe MM patients [110].

Further, Wang et al. obtained significant results investigating the effect on MM of EVs derived from the tumor microenvironment [111]. They confirmed the role of extracellular vesicles derived from bone marrow stromal cells (EVs-BMSC) in transferring proteins

on target cells, supporting survival, proliferation and migration in MM. BM derived EVs internalized by MM cells mediated the upregulation of antiapoptotic Bcl-2 and downregulation of caspase 9 and 3, lastly promoting the cellular survival. Furthermore, they demonstrated the acquired drug resistance of MM cells upon BMSC-EVs uptake. In conclusion, the extracellular vesicles produced by the MM tumor microenvironment are able to transfer proteins, cytokines and modulate the miRNA expressions, inducing MM survival, proliferation, migration and eventually increasing the drug resistance.

1.2.10 Biomarkers in multiple myeloma-derived EVs

Nowadays, one of the most complete *in vitro* study focused on the characterization of the protein contents in MM-derived EVs has been conducted by the group I've been part of at The Ohio State University [83]. We identified 583 total proteins isolated from EVs derived from 2 different kinds of MM cells; the secreted EVs, are mostly expressing a common pattern of proteins with minimum differences between different kinds of MM cell lines: antigen presenting molecules (MHC class I and class II), adhesion molecules (CD44, tetraspanins, integrins), membrane transport and fusion molecules (annexins, flotillin, Rab proteins), cytoskeletal proteins (actin, tubulin), and many others (pyruvate kinase, GAPDH, 14-3-3 proteins, Hsp70, Hsp90, elongation factor 1α, histones H2B, H2A, and H4). These data support the hypothesis that MM extracellular vesicles have common protein profiles (with small sets of unique proteins depending on the parent cells of origin) and can potentially represent important diagnostic biomarkers upon validation on EVs isolated from MM patients. Among them, Hsp70 seems to be one of the most promising potential candidate.

Recently, Di Noto et al. [112] revealed that EVs isolated from serum of MM patients were strongly enriched in Hsp70 (accordingly with Harshman et al.) and in C-src, compared to EVs collected from MGUS and healthy patients.

Moreover, a remarkable study [113] discovered the presence of two different kinds of MM-EVs, one with Hsp70 expressed on the membrane and the other one with Hsp70 expressed only into the cytoplasm. The difference in Hsp70 localization reflected a different immune response mediated by NK and CD8+ CTL. In particular, the MM-derived EVs expressing superficial Hsp70 were more capable of activating the immune response compared to the ones expressing only the cytosolic one, suggesting that EVs

carrying Hsp70 on the membrane can be potentially used for the development of an anti-MM vaccine.

Furthermore, as expected in MM circulating EVs (isolated from peripheral blood samples of MM patients), the tumor related antigen CD38 is overexpressed and correlated with the International Staging System (ISS stage) [114].

As previously discussed, several studies revealed peculiar protein enrichments in MM-derived EVs and prove the relation between protein enrichments and biological effects to eventually support the tumor growth and drug resistance. For example, MM-EVs are also enriched in syndecan-1, VEGF and HGF [98], CD147 [107], ZNF224 [108], CCL2, IL6 and Fibronectin [109].

miRNAs have been involved in several diseases and miRNAs carried by EVs have been demonstrate to be able to drive the tumor progression. The pathogenic nature of the miRNAs and their capacity to be secreted into biological fluids through EVs, where they remain relatively stable, suggest miRNAs as promising biomarkers for diagnostic and therapeutic monitoring.

Only recently, few studies have demonstrated that miRNAs carried by EVs secreted by MM could have an effect on the tumor progression. As already discussed, EVs isolated from MM patients contains high levels of *miR-135b* [101] and low levels of the oncosopressor *miR-15a* [109]. The detection of higher level of circulating *miR-15a* and *miR-16* in MM patients have been instead associated to a better overall survival [110].

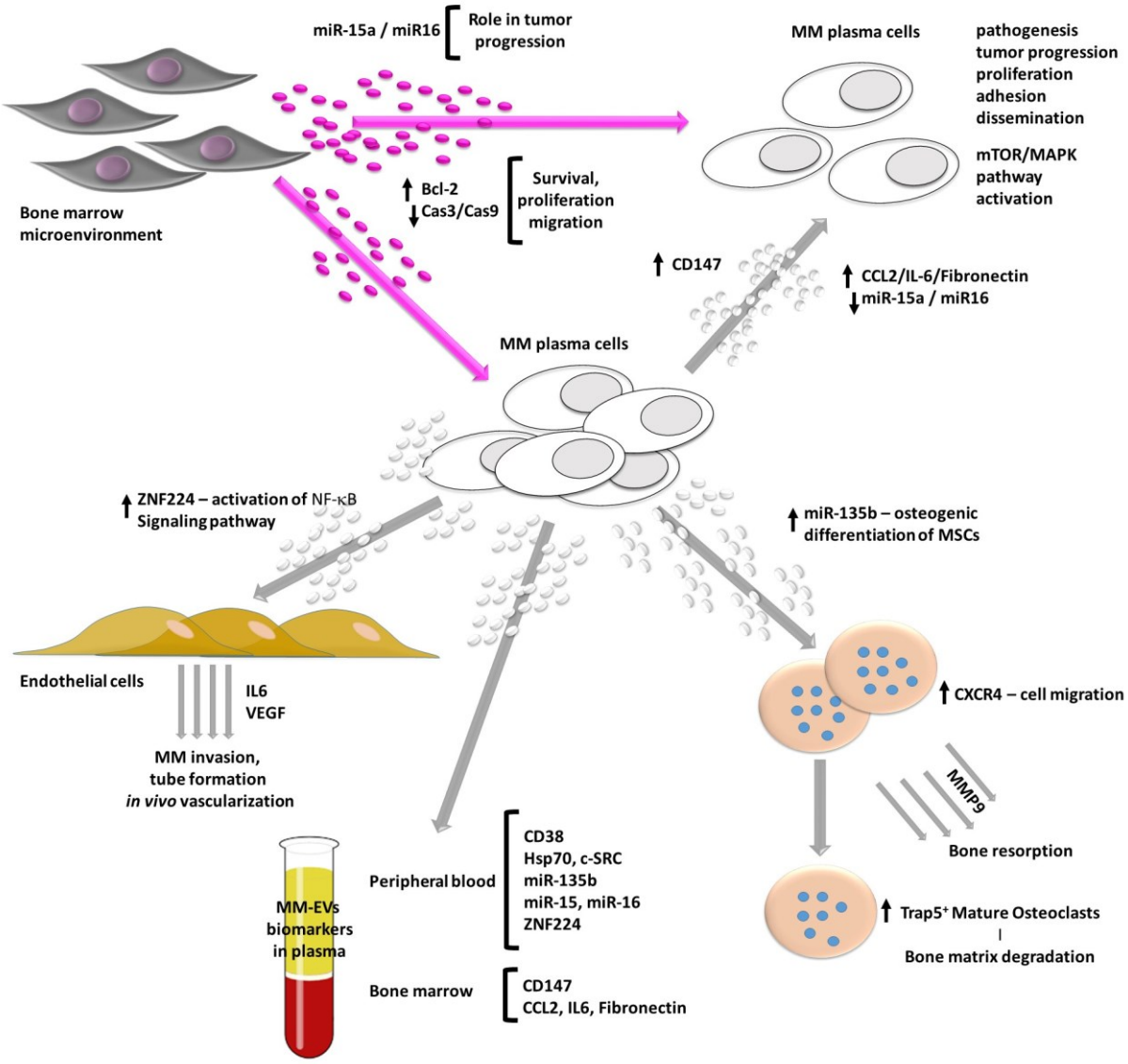

Fig. 3 *Multiple Myeloma-microenvironment crosstalk mediated by EVs*

1.3 CD44

CD44 is a transmembrane glycoprotein of 742 aminoacids and the main role is the interaction with the hyaluronic acid (HA), one of the components of the extracellular matrix [115]. The CD44 gene is located on Chromosome 11p13 and contains 20 exons. The first five and the last five exons are constant; Exons 1-5 and Exons 15-19 encode the N-terminal (extracellular, interact with the Hyaluronic acid), and C-terminal (extracellular, transmembrane, and cytoplasmic) domains respectively, and share homologous domains among all the CD44 family members. On the contrary, the ten exons (Exons 5a-14, typically defined as v1-v10) located between these regions are subjected to alternative splicing, resulting in the generation of CD44 standard (CD44s) and several CD44 variants (CD44v). More than 20 isoforms have been described, with a size ranging from 85 to 230KDa [116] (Fig. 4).

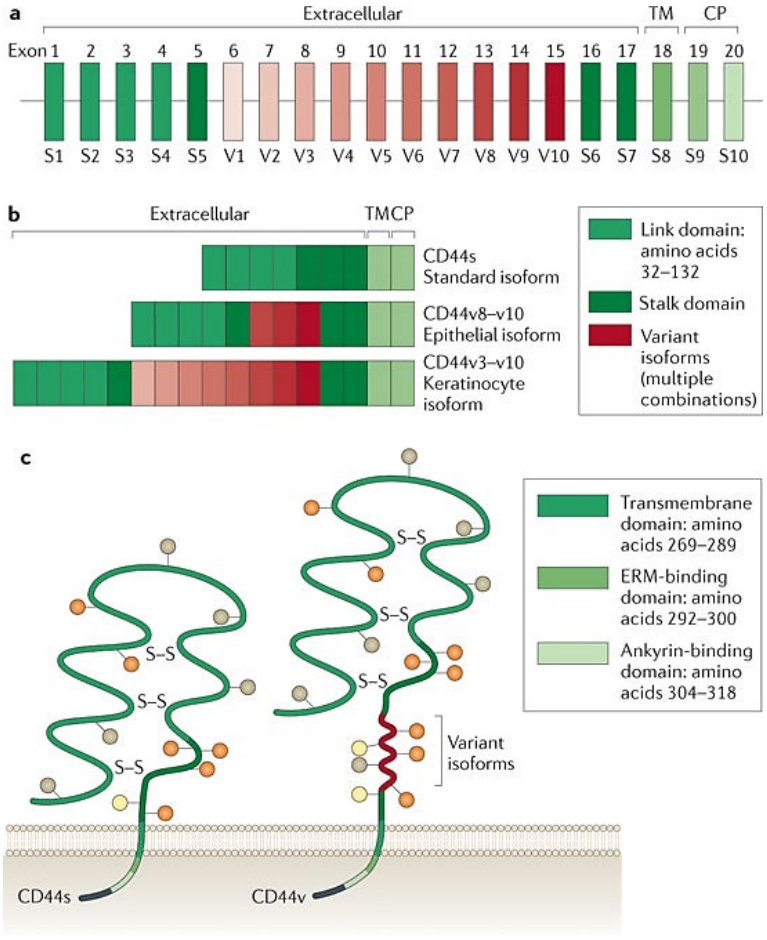

Fig. 4 *CD44 structure and principal isoforms*

CD44s is generally expressed on lymphohaematopoietic cells (CD44H). CD44 isoforms can be upregulated by T-lymphocytes and other leukocytes after immunological activation and the expression patterns are tissue specific: CD44 lacking v2-v10 is the most common form on hematopoietic cells while larger CD44 splice variants dominate on certain normal and neoplastic epithelia, activated lymphocytes and malignant lymphomas. A CD44 isoform consisting of the last three exon of the variable region (CD44V8-10) is preferentially expressed on epithelial cells, hence it is also called epithelial CD44 or CD44E. In contrast, CD44V3-10, the longest CD44 isoform that expresses eight exons of the variable region, has been observed in keratinocytes.

CD44 is a multifunctional receptor which plays a role in cell adhesion (cell-cell and cell-ECM interactions), cell traffic, lymph node homing, presentation of chemokines and growth factors, apoptosis, transmission of growth signals and signals mediating hematopoiesis.

CD44 is involved in the uptake and intracellular degradation of HA. Other CD44 ligands include ECM components such as collagen, Fibronectin, laminin, and chondroitin sulphate. ECM-unrelated ligands include mucosal addressin, serglycin, osteopontin, and the class II invariant chain.

1.3.1 Role of the CD44 in cancer

CD44 belong to a huge family of cell adhesion molecules (CAMs) involved in the control of cell behavior by mediating direct interaction between cells or between cells and the extracellular matrix and are essential for preserving tissue integrity. Because of these functions they are frequently involved in tumor progression and survival. High levels of expression of CD44 have been observed in numerous cancer cell types and interactions between HA and CD44 have been shown to play essential roles in tumor cell growth, survival, migration, and metastasis. Indeed, introduction of an antisense construct against two of the three human enzymes responsible for HA synthesis, namely HAS2 and HAS3, inhibited invasion of these otherwise metastatic cells into matrigel. In addition, CD44 antibodies inhibiting the HA-CD44 interaction blocked invasion of these metastatic cells.

Furthermore, the use of HA oligosaccharides as competitors for HA–CD44 binding induce suppression of tumor cell growth *in vivo* by suppression of the

phosphatidylinositol 3-kinase (PI3K)/Akt pathway [117]. The CD44 silencing is associated to the loss of adhesiveness of human colon cancer cells to HA and reduce colony-forming ability and tumorigenicity in xenograft model [118]. CD44 also correlated with tumor recurrence after surgery removal [119], and has been proved to promote multidrug resistance (MDR) in cancer cells, which is a marker of therapeutic resistance. In a study conducted on breast cancer, antibodies targeting CD44 repressed tumor growth and prevented tumor relapse after chemotherapy-induced remission in an orthotopic xenograft *in vivo* model [120]. All of these results highlight the important roles of CD44 in cancer progression and relapse. Multidrug resistance (MDR) in Cancer stem cells (CSCs) is a key obstacle for an effective cancer therapy and can be partially attributed to the induction of survival/anti-apoptotic signals. An additional limitation to the efficacy of chemotherapy is rapid drug evacuation from cancer cells which is mediated by drug transporters and MDR genes. Recently, it has been demonstrated [121] that HA-CD44 interactions-induced association of Nanog and Stat-3 to stimulate Stat-3-dependent *MDR1* gene expression. Moreover, HA-CD44 interactions up-regulate multidrug resistance protein 2 in non-small cell lung cancer [122].

Additionally, several studies have highlighted the importance of the CD44 in CSC maintenance and self-renewal. In a remarkable study, a group of scientist has proved that the activation of GSK3β mediated by CD44 is necessary for the preservation of CSCs properties, and CSCs going through EMT are dependent on GSK3β activity for the development of the mesenchymal phenotype [123]. As already mentioned above, HA/CD44-mediated Nanog activation induced the expression of the CSCs regulators, for example Rex1 and Sox2, while CD44 silencing reduced the expression of stem cell markers, including Oct4, Nanog, and Sox2 [123]. Taken together, these data underline the role of HA and CD44 in CSC self-renewal, clonal formation, and chemotherapy resistance [121].

Furthermore, CD44 can mitigate the activation of c-Jun N-terminal kinase, and p53 signaling pathways, resulting in resistance to oxidative and cytotoxic agent-induced stress in glioblastoma cells [124], thus suggesting that CD44 can also maintain low levels of reactive oxygen species (ROS) and coordinate defensive mechanisms against ROS-mediated damage.

CD44 also plays a pivotal role in preserving the survival of many tumor cells by transmitting anti-apoptotic signals. CD44 and receptor tyrosine kinases (RTKs) have been shown to cooperate on promoting cell survival, and HA–CD44 interaction triggers the activation of Src and PI3K [125]. Cancer cells expressing CD44 and derived from colon carcinoma are associated with the alteration of pro (caspase 9 and 3) and anti (Bcl-2, Bcl-xL) apoptotic agents [126]. To further support this discovery, CD44 knockdown was followed by a reduction of expression of anti-apoptotic Bcl-2 and Bcl-xL and by an increase of expression of cleaved caspase 3, 8, 9 and Bax [127] in the same kind of tumor. Another example of association between high expression of CD44 and the inducement of anti-apoptotic agents, promoting survival, was found in chronic lymphocytic leukemia (CLL) cells, in fact CLL cells have been proved to overexpress CD44, and the CD44-HA binding activated the PI3K/Akt and MAPK pathways to induce the expression of anti-apoptotic proteins, thus promoting survival [128]. Also, several studies have demonstrated the activation of apoptosis resistance mechanisms via CD44 variant isoforms. For example, binding of CD44v6 to HGF-initiated c-Met is essential for the signaling that regulate MEK and Erk pathways [129].

CD44-expressing cancer cells can acquire the ability to escape the immune response. For instance, the CD44-HA interaction led to immune escape of lung cancer cells from killing mediated by cytotoxic T-lymphocytes [130]. Of note, Yasuda et al. proposed a mechanism by which the interactions between CD44 and HA reduced the vulnerability of cancer cells by suppressing Fas expression and inactivating the Fas/Fas mediated cytotoxicity. In squamous cell carcinoma of the head and neck the CD44 positive cells repressed T-cell proliferation and efficiently induced regulatory T cells (Tregs) and myeloid-derived suppressor cells, thus confirming the immune-protective properties of CD44.

1.3.2 Role of CD44 in TME-mediated drug-resistance and in multiple myeloma

In multiple myeloma, the activity and expression of these adhesion molecules are controlled by intra and extracellular factors including enzymes, growth factors and microenvironmental conditions [131]. Several signaling pathways are influenced by adhesive interactions of multiple myeloma cells, and their consequences affect the survival, proliferation, migration, homing to the bone marrow microenvironment and in many cases induce drug-resistance phenotype. Therefore, the adhesive interactions of multiple myeloma cells are extremely important and may thus be potential therapeutic targets. So far, numerous studies are being developed to inhibit the activities of adhesion molecules in multiple myeloma cells, including small antagonist molecules and signal transduction inhibitors.

The BM stroma is a sophisticated microenvironment, containing cellular and non-cellular components. The BM solid part is constituted by extracellular matrix (ECM) components (e.g. fibronectin, hyaluronan, collagens) [132,133], different cell types (for example mesenchyme stromal cells, osteoclasts, adipocytes) and endothelium [134]. Of note, in MM patients the BM ECM could result altered compared to the normal BM, with a reduced quantity of fibronectin, collagen type-I, and increased levels of collagen type-IV [135].

BM stromal cells synthetize and integrate several types of macromolecules into the ECM, mostly glycosaminoglycans [136]. Among them, hyaluronan is a high molecular weight glycosaminoglycan composed of glucuronic acid and N-acetylglucosamine disaccharides [133,137]. Both stromal cells and hematopoietic progenitor cells are the producers of the main component of the hyaluronian [136,138]. The interactions of MM cells with hyaluronan is principally mediated by CD44 [139] and the receptor for hyaluronan mediated motility RHAMM (CD168), which was identified also in other types of B-cell malignancies [140,141]. The standard CD44 form is down-regulated in MM cells, while some splice variants are highly expressed by these cells [139]. Indeed, CD44 variants 3v, 4v, 6v or 10v were identified in MM cells, but not in normal individuals or in MGUS patients [142,143]. The variant CD44v6 is frequently expressed in high-risk MM, and its expression is associates with chromosome 13q (−), which is a risk factor in MM [144].

Tissue inhibitor of metalloproteinase 1 (TIMP-1) induces the post-germinal center differentiation of lymphoid cells, which is associated with the up-regulation of several plasma cell-associated genes including CD44, indicating that extracellular factors may modulate the CD44 expression in MM cells [145]. IL6, the major MM related cytokine, strongly increases CD44 gene expression, modulates CD44 RNA alternative splicing, and promotes the over-expression of all CD44 variant exons in MM cells [146]. The interaction between cells and hyaluronan through CD44 and its splice variants triggers signaling pathways that impact on cell adhesion, migration, and protects MM cells from apoptosis [147,148]. Likewise, some of the activities of CD44 splice variants in MM cells can be addressed to their binding to stromal or endothelial cells, instead of interaction with hyaluronan and the ECM [149,150].

Notably, highly important is the drug-resistance mechanism caused by the MM adhesion to ECM defined “cell adhesion mediated drug resistance” (CAM-DR) which has been discovered recently in MM cells, and is now extended to other types of cancer, as part of environment-mediated drug resistance [151-154]. CAM-DR to a wide range of drugs (e.g. bortezomib, doxorubicin and dexamethasone) in MM cells can be induced by FN or BM stromal cells, and is regulated by integrins [151,152,155] . For example, it has been reported that adhesion of MM cells to FN up-regulates the levels of p27Kip1 which is important to maintain the drug-resistant phenotype, possibly due to its involvement in cell cycle regulation [152]. Activation of the NF-kB pathway was found to be stimulated by adhesion to FN, and may be possibly associated with CAM-DR in MM [156]. CAM-DR is not connected with loss in drug-induced DNA damage, but more in protection from mitochondrial distress and caspase activation [157]. However, FN cannot defend MM cell lines from apoptosis triggered by Fas, hence demonstrating that the FN induce partial protection, not including all types of programmed cell death [158]. In MM cell lines, not only integrin-mediated adhesion but also hyaluronan binding with CD44 can confer resistance to dexamethasone [148]. Dexamethasone inhibit NF-kB through induction of IkB-α inhibitory protein, which traps activated NF-kB in an inactive complex [159,160]. Different stimuli including TNF-α and IL6 trigger IkB-α protein phosphorylation, resulting in their proteasome-mediated degradation, consequently allowing the release of active NF-kB and its nuclear translocation [161]. In an important study conduct by Ohwada et al. [148], the engagement of CD44 induced serine

phosphorylation and degradation of IkB-α on CD44-high MM cells and myeloma cells overexpressing CD44 co-cultured with Dexamethasone and anti-CD44 mAb (IM7) did not exhibit IkB-α up-regulation, indicating that CD44 engagement with IM7 inhibits the drug activity by inducing phosphorylation and subsequently degradation of IkB-α.

It has been demonstrated that CD44 can be targeted by therapeutic antibodies. The CD44v6 variant, expressed by MM cells, can be inhibited by bivatuzumab, a humanized monoclonal antibody specific to this variant, in association with the potent anti-microtubule agent mertansine [144]. Unfortunately, phase-I clinical trials conducted in head and neck cancer and in metastatic breast cancer showed variable responses, with serious adverse side effects, indicating poor clinical importance of this drug [162,163]. Nevertheless, bivatuzumab was able to stabilize some of the severely pretreated metastatic breast cancer patients [109].

In summary, CD44 is an attractive therapeutic targets in MM due to several reasons:

- molecular structure and function in MM is well established;
- adhesive interactions CD44-HA protect MM cells (including minimal residual malignant cells) in their BM microenvironment;
- CD44 interactions have impact on important MM key functions such as tumor progression, proliferation, and cell adhesion mediated drug resistance.

Among the potential therapeutic strategies to incorporate anti-CD44 into MM treatment, one possibility consists in the integration of anti-adhesion substances into current Standard of care (SOC). Finally, a fruitful incorporation of anti-CD44 into the MM treatment may extend its use in other hematological malignancies.

1.4 HDAC inhibitors

1.4.1 Chromatin remodeling and regulation of transcription mediated by Histone Acetyltransferase (HAT) and Histone Deacetylase (HDAC)

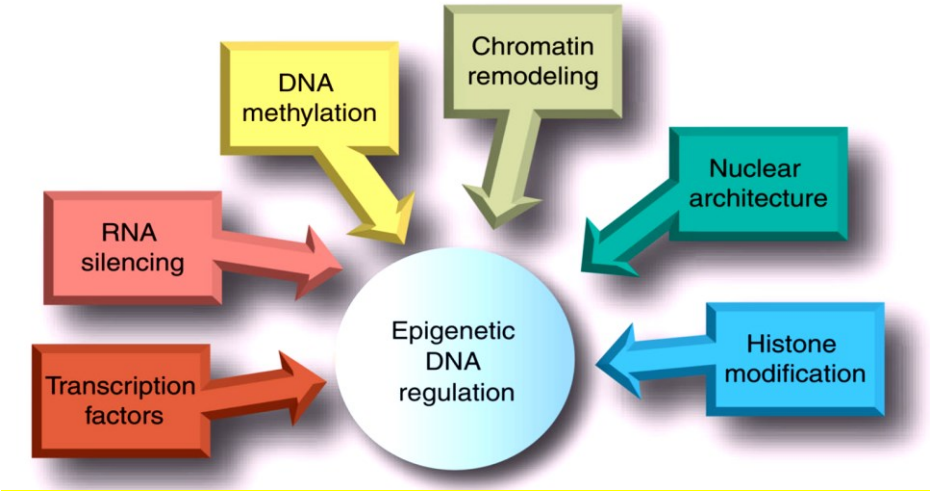

Figure 5. *Factors influencing the epigenetic regulation of gene expression.*

Chromatin consists of DNA and proteins confined into the nucleus of mammalian cells. To form chromatin, DNA is firmly condensed by being wrapped around nuclear proteins defined histones and nucleosome is a repetition of DNA-histone complexes (146 base pairs of double-stranded DNA wrapped around an octamer of two molecules each of the core histone proteins H2A, H2B, H4 and H4). The epigenetic DNA regulation is mediated by chromatin remodeling, consisting in the rearrangement of chromatin from a condensed state to a transcriptionally accessible open conformation, lately allowing transcription factors or other DNA binding proteins to access DNA and control the gene expression. In general, the condensed shape of the chromatin (heterochromatin) doesn't allow the DNA access to transcription factors and other DNA binding proteins for the gene expression. Instead, the relaxed conformation of the chromatin (euchromatin) allowed the molecular interaction between DNA and gene regulators, promoting the gene expression.

Among all the possible epigenetic modifications, acetylation/deacetylation (Fig. 6) and methylation/demethylation promote the structural rearrangement of the chromatin, thus resulting in transcriptional activation or repression [164,165].

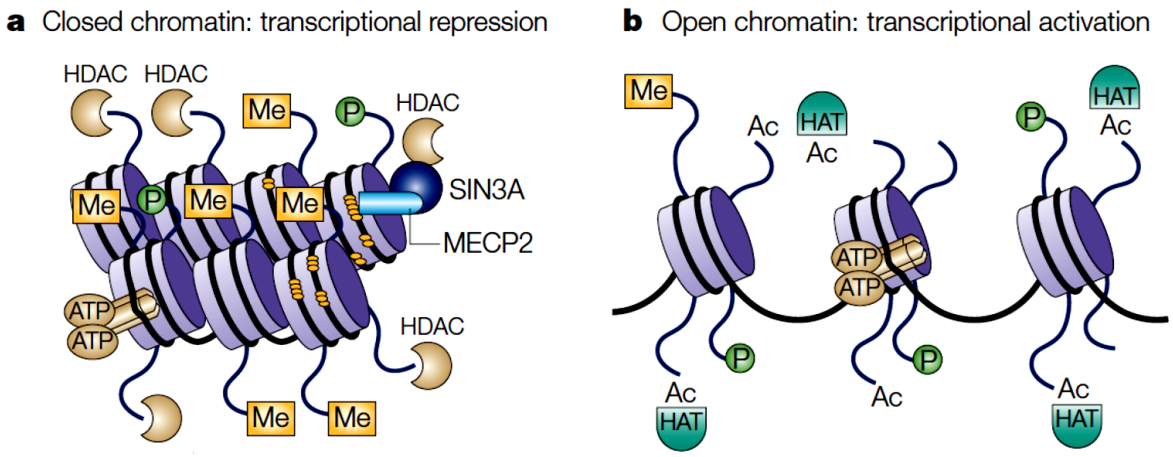

Figure 6. *Histone acetylation and deacetylation emerges as a central switch that allows inter conversion between permissive and repressive chromatin domains in terms of transcriptional competence.*

Respectively, HATs and HDACs perform the reversible acetylation and deacetylation of the ε-amino group of specific lysine residues. The acetylation precludes the formation of positive charges on the lysine amino group, and affects protein activity. HDACs, oppositely, repress the gene transcription through the deacetylation of nucleosomal histones, leading to chromosomal condensation and the exclusion of transcriptional activating complexes. Moreover, large HDAC-containing repressor complexes can exclude the binding to specific gene loci of activating molecules, including HATs, from interacting with TFs. Specific TFs are also targets of HDACs activity, decreasing their DNA-binding, inducing their degradation [166].

Thus, HATs and HDACs can regulate transcription: 1) modifying histone acetylation patterns, modulating chromatin structure and its accessibility to transcriptional regulatory proteins [167,168], and 2) acetylating consequently affecting the activity of molecules that directly regulate transcription, including different Transcription Factors (TFs) [169].

1.4.2 Classes of HDACs

Human HDACs 18 isoforms are commonly divided into four classes based on homology to yeast: class I (HDAC1, 2, 3 and 8), class IIa (HDAC4, 5, 7,and 9), class IIb (6 and 10), class III (sirtuins; SIRT1, 2, 3, 4, 5, 6, and 7), and class IV (HDAC11) [170,171] . HDAC classes vary in structure, substrate specificity, enzymatic activity, subcellular localization and tissue-specific expression.

The “typical” HDACs are the ones belonging to classes I, IIa, IIb, and IV, they have a conserved catalytic domain (~390 aminoacids) and a Zn-dependent deacetylase activity. Instead, members of the third class, sirtuins (~275 aminoacids), require NAD+ for their enzymatic activity [172] and are unrelated to the catalytic domain of the typical HDACs [173,174]. Among the HDACs belonged to the class III, sirtuin 1 (SIRT1) cooperate in association with p53, and NF-κB, intermediaries in cellular stress mechanisms. At the mitochondrial level, well known is the role of sirtuins 3, 4 and 5 (SIRT3, 4, 5) in the regulation of mitochondrial function and respiration [175]. Notably, some sirtuins (SIRT4 and 6) don’t deacetylase targets, but are capable of ADP-ribosyl-transferase activity and they are involved in DNA repair and metabolism.

Due to the differences in catalytic mechanisms, complete inhibition of HDAC activity is extremely difficult, and consequently, several HDAC inhibitors (HDACi) tested in cancer target the most common HDACs.

Other differences between HDAC classes are:

- Class I HDACs are ubiquitously expressed, with a prevalent nuclear localization.
- Class II HDACs are usually larger than class I, demonstrating tissue-specific expression patterns, can be primarily cytoplasmic and/or migrate between the cytoplasm and nucleus.
- Class III differ in their subcellular localization and interact with a wide variety of TFs and other primarily non-histone substrates [176]. The class III HDACs’ activity is not inhibited by compounds such as vorinostat or trichostatin A (TSA), that inhibit class I and II HDACs.
- HDAC 11 is the only member of the class IV, has conserved residues in the catalytic core region shared by both class I and II enzymes [177], but it does not take part in any of the known HDAC complexes.

Both classes I and II have been found being part of big transcriptional repressing complexes, which are recruited and transported to the DNA by specific DNA-binding proteins. These large protein complexes play the important roles in HDAC localization and target specificity, can act as support to recruit DNA-binding proteins, and provide the cofactors required for HDAC function. Indeed, lack of these cofactors limits the activity of some recombinant HDACs [178].

Many transcription factors such as GATA3 and the p65 (a component of NF-kB involved in the regulation of DNA transcription), are also targets of post transcriptional modifications such as acetylation and deacetylation, which regulate their activity. In fact, the acetylation of specific lysine residues on p65 increases its DNA affinity and leads to transcriptional activation, without modifying the DNA binding [179-181]. Moreover, HDAC1 and HDAC2 deacetylase the acetylated forms of NF-kB and promote its binding to the inhibitor inside the nucleus, favoring the translocation of the inactive NF-kB/IkB-α newborn complex into the cytoplasm [180]. Inhibition of these HDACs by TSA determined the activation of NF-kB and also raised the expression of inflammatory-related genes, such as IL-8. Of note, differences in the phosphorylation status of p65 can modulate its interaction with either HDAC or HAT [181].

1.4.3 HDAC inhibitors and implications in cancer

HDAC inhibitors, categorized based partly on chemical structures and in part on target specificity, are also distributed into five groups: 1. hydroxyamic acids; 2. cyclic tetrapeptides; 3. benzamides; 4. ketones and 5. aliphatic acids. HDACi can have broad-based pan-HDACi inhibitory activity, class specificity, or even isozyme specificity.

The first evidence that changes in histone acetylation may support initial growth and development of cancer was presented in a study that demonstrated the complete loss of monoacetylation and trimethylation on histone H4 in malignant tumor cells [182]. Subsequently, several researches have confirmed the aberrant expression in human tumors of HDACs such as HDAC1, -5, and -7, thus suggesting their possible role as cancer-related biomarker [183]. It is reasonable to expect that HDACs could emerge as potential targets for therapy. In several kinds of tumors such as prostate [184], colorectal [185], breast [186], lung [187,188], liver [189], and gastric cancer [190], overexpression of peculiar HDACs correlated with important reductions in OS and

predicted poor patient outcome, independently from other common factors, for example kind of tumor or progression of the disease. The overexpression of HDACs has been associated to crucial events of tumorigenesis such as the epigenetic repression of the tumor suppressor gene CDKN1A [191] and other important genes encoding DNA damage repair enzymes such as BRCA1 and ATR [192]. In a wide range of tumors (colon, lung, and breast just to name a few), the downregulation of the HDACs expression promotes cell cycle arrest and apoptosis, unequivocally demonstrating the fundamental role of HDACs in tumor survival. For example, HDACs deacetylase p53 (tumor suppressor) thus reducing its transcription, while the activation of TFs SP1 and C/EBP, also due to HDAC activity, promotes the transcription of oncogenes belonging to the BCL2 family [193,194].

To summarize, treatment with HDACi increases the acetylation of histones on chromatin, thus increasing the gene expression, and the acetylation of non-histone proteins (TFs, NF-kB). In TFs, the increased level of acetylation can either increase or decrease their activity. So far, HDACi have been used in clinical trial as a treatment of several kinds of tumors. Among the multiple possible effects induced by treatment in different cancers, HDAC inhibition:

- Selectively modulates gene expression. One of the most common induced gene is the cyclin-dependent kinase inhibitor p21 (WAF1/CIP1) [195-197]; as opposite HDACi silence the expression of the androgen receptor (AR) [198] .
- Promotes cell cycle arrest. Sub-lethal doses provoke G1 arrest, while high doses induces either G1 or G2+M arrests [196] due to p21 overexpression.
- Triggers the extrinsic apoptotic pathway, and the upregulation both death receptors (Apo-1, CD95) and TNF-associated pro-apoptotic ligands (for example TRAIL, Apo2-L) [199,200].
- Induces the intrinsic apoptotic pathway by stimulating the release of cytochrome-C and the activation of Caspase-9 [201].
- Promotes the autophagy-mediated cell death. The cell death, associated with the presence of autophagic vacuoles in the cytoplasm, was noted on HeLa cells upon treatment [202].

- Induces the accumulation of ROS. Several studies reported cell death upon HDACi treatment associated with a massive intracellular accumulation of ROS in cancer cells [203,204].
- Inactivates the chaperon Hsp90 [205]. Hsp90 is the responsible of the correct folding of hundreds of intracellular proteins, including some key player in cancer, such as EGFR in Glioma. The Hsp90 inhibition mediated by HDACi leads of the degradation of Hsp90 client proteins.
- Inhibits fundamental elements involved in angiogenesis, such as hypoxia inducible factors (HIF), and the pro-angiogenesis molecule VEGF [201,206].

Because of the uncountable effects of acetylation/deacetylation on gene expression and protein activity, it is well known that the influence of HDACi on tumor growth and survival is not mediated by single or a small number of targets. Moreover, the consequences of treatment with HDACi may vary between tumor types, within a specified tumor type, and even within a given tumor due to tumor heterogeneity.
From the clinical prospective, the genetic alterations driving the tumor of interest have very important role in determining the therapeutic outcome of HDACi treatment. In general, as already mentioned above, HDACi induces tumor cell apoptosis, growth arrest, senescence, differentiation, immunogenicity, and inhibit angiogenesis. Among them, the inducement of apoptosis is the most common effect [201]. Altered gene expression and the induction of apoptosis are strictly connected: histone hyper acetylation upregulates pro-apoptotic genes such as TNFSF10, TRAIL [207], and BMF. In tumor cells, BCL-2 family expression is one of the most modulated by the HDACi treatment to favor a pro-apoptotic expression pattern [201,208,209] and frequently, the apoptosis induced by HDAC inhibition is associated with the overexpression of pro-apoptotic BIM, PUMA, BAX, [201,210]. Mechanism and mediators that make cancer cells be more sensitive to the apoptosis mediated by HDACi compared to the normal cells, are still controversial. One possible reason could be the massive accumulation of ROS species due to the treatment with HDACi in cancer cells as compared to the healthy cellular controls [211]. Other researches showed that the HR23B gene expression regulation upon HDAC inhibition improved the tumor sensitivity to apoptosis, even though mediated by weak HDAC inhibitors. Moreover, little is known

about the mechanism that bring to the selective regulation of a subset of genes in cancer cells treated with HDACs, compared to matched normal cells. This subset of genes ultimately triggers tumor-specific apoptosis.

Of note, it has been reported the development of chemoresistance in diffuse large B-cell lymphoma (DLBCL) upon HDACi treatment due to the concomitant overexpression of the anti-apoptotic genes Bcl-2 and BCL-X_L, a tumor response to the cellular stress induced by the treatment.; another example of developed chemoresistance in lymphoma associated with HDAC inhibition is due to the overexpression of the antioxidant thioredoxin, and CHK1 (member of the DNA damage repair family) [212].

In soft tumors, a conspicuous number of HDACi have been approved for clinical trials so far. The first HDAC inhibitors “FDA approved” had been the pan-HDACi vorinostat (SAHA, oral medication), and the class I HDACi romidepsin (administered intravenously). Vorinostat is effective in the treatment of cutaneous T- cell Lymphoma (CTCL), with favorable response rates, while belinostat has been used for relapsed and refractory peripheral T-cell lymphomas [213]. In CTCL cell lines, vorinostat induced hyper acetylation of all histones, resulting in the upregulation of gene expression (up to 22% of all genes resulted to be altered by the treatment upon few hours of treatment) and subsequent inhibition of the MAPK pathway, generation of cell cycle dysregulation due to the inhibition of several cyclins [201,209], induction of apoptosis and arrest of proliferation [196,214].

One limitation in the use of HDACi in cancer is the role of HDACs in normal immune cell function; shutting down the HDAC activity leads to the increment of apoptosis in cancer cells, but simultaneously provokes the suppression of the immune responses required for anti-cancer therapy [215].

1.4.4 HDAC inhibitors in multiple myeloma

The epigenetic modulation, that is the modification of gene expression without alteration of DNA sequences, is essential in the pathogenesis and development of MM [216]. In general, epigenetic modifications are categorized into 2 main subgroups: DNA methylation and histone modification, which regulate several oncogenes and tumor-suppressor genes. Consequently, therapies targeting epigenetic modifications are under continuous development in several kinds of soft and solid cancers.

Abnormal DNA methylation of specific genes is well known to be responsible for their altered expression and association with tumor development and progression in multiple myeloma [217,218]. Nonetheless, the mechanism that leads to the increased DNA methylation in MM compared to normal plasmacells, still remains unclear and all the efforts focused on developing successful therapeutic strategies against DNA methylation in MM have been useless so far. On the contrary, histone modifications have been well described in MM, and HDACi have been already tested in the pathology, revealing promising preclinical results. For instance, class I and II pan-HDACi such as vorinostat (SAHA) [219], panobinostat (LBH589) [220,221], and belinostat (PXD101) [222] have already demonstrated antitumor efficacy in MM. It has been also shown *in vitro* that a class I HDACi, romidepsin (FK228) [223], also stimulates apoptosis in MM. Even though nonselective HDACi used in combination with bortezomib have demonstrated some efficacy, the OS advantage of the combination compared to the bortezomib alone was less than 1 month, with concomitant development of toxic side effects including fatigue, diarrhea, and thrombocytopenia [224]. Remarkably, LBH589, (FDA approved drug) used in combination with dexamethasone in MM has shown an increase of 4 months of OS compared to the SOC (bortezomib/dexamethasone) [225]. However, adverse side effects induced by HDACi still constitute a great obstacle for their use and for this reason, novel pan- and selective HDAC inhibitors are constantly under development.

Recently, the scientific interest has been focused on HDAC6, which has a critical role in aggresome formation, a mechanism of degradation of ubiquitinated proteins in lysosomes. First of all, HDAC6 binds unfolded ubiquitinated proteins to dynein motility complexes, then it is responsible for the transport of those proteins to the aggresome. The recent development of the HDAC6-specific inhibitor and its preclinical use in combination with bortezomib demonstrated the total arrest of degradation of ubiquitinated protein in proteasomes and lysosomes. Of note, the HDAC6i tubacin and bortezomib showed synergistic inducement of cytotoxicity in MM in association with a substantial accumulation of polyubiquitinated proteins, a clear hallmark of cellular stress [226]. Due to this important effect, a novel selective HDAC6 inhibitor, ricolinostat (ACY-1215), has been quickly developed for clinical therapy. So far, it has shown

synergistic anti-MM activities with both bortezomib and lenalidomide in preclinical settings [227], and phase I/II clinical trials in MM are ongoing [228,229].

Additionally, the use of the second generation proteasome inhibitor carfilzomib in combination with HDAC6i demonstrated an improved in vitro cytotoxicity in MM as compared to bortezomib alone, thus prompting the development of clinical trials with this combination in MM [230].

Recently, a novel orally bioavailable class I/II, phenylbutyrate-based pan-HDAC inhibitor ($C_{18}H_{20}N_2O_3$, M.W. 312.36), AR42 (Fig. 7) has been developed by The Ohio State University, licensed to Arno Therapeutics and showed a better anti-proliferative effect in cancer compared to the vorinostat (SAHA), either *in vitro* or *in vivo* [231] in several kinds of cancer [232,233], such as CLL, AML, schwannoma, meningioma, and it's a potential effective anti-cancer agent in hematological malignancies. AR42 is also able to inhibit STAT3 activation whether or not of IL6-activation signals are present, consequently promoting apoptosis and MM death. Some histone-independent activity has also been reported for AR42. A phase I clinical trial is actually ongoing for the characterization of side effects and best dose calibration of AR42 in advanced or relapsed MM, CLL or Lymphoma patients at The Ohio State University.

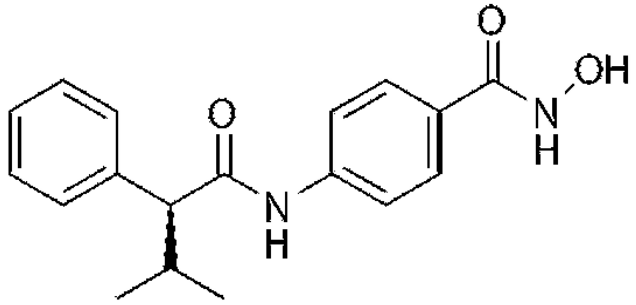

Fig. 7. *AR42 chemical structure.*

CHAPTER 2. AIMS OF THE THESIS

Based on the most recent published data, Multiple Myeloma is not considered an incurable form of cancer anymore. However, according to the statistics reported by the American NCI agency, updated at the 2015, only 46.6% of MM patients survive within 5 year with 26.000 new cases (1.6% of all cancer cases) and 11.240 deaths (1.9% of all cancer deaths) yearly. Indeed, severe MM patients still have an unfavorable prognosis and more than 50% of the newly diagnosed cases die before 5 years. Currently, none of the reported therapeutic options are considerable totally curative in Multiple Myeloma and a better characterization of the tumor biology is mandatory to define novel therapeutic targets, and ultimately improve overall survival and outcome.

The first point I decided to address in this thesis was the *in vitro* characterization of the protein contents of Extracellular Vesiscles secreted by Multiple Myeloma cells. The purpose was to better understand one of the most unexplored mediator of biological messages exchanged among MM cells, and between cancer cells and surrounding environment.

Afterwards, my aim was to identify *in vivo* novel circulating MM biomarkers to improve the diagnosis and eventually design a better therapeutic strategy.

Finally, the last objective of the thesis was the *in vitro* and *in vivo* characterization of a novel pan-HDAC inhibitor and its therapeutic role in combination with Lenalidomide.

My goal was to develop a new strategy to potentially overcome drug resistance mechanisms, which are associated with the interaction between adhesive molecules expressed by Multiple Myeloma and the extracellular matrix of the bone marrow microenvironment.

CHAPTER 3. METHODS

3.1 Cell lines and transfection

The following human cell lines cells have been used and obtained from American Type Culture Collection (ATCC; Manassas, VA), or courtesy of Dr M. Kuehl (National Cancer Institute, MD): MM.1S, MM.1R, NCI-H929, KMS18, RPMI-8226, U266, EJM, LP1, OPM2, TBI, ARH77, L363 (Multiple Myeloma cell lines), HeLa (CCL-2, Adenocarcinoma) and HS-5, HS-27A (human marrow stromal cells).

MM cell lines were cultured in RPMI-1640 (Sigma; St. Luis, MO) supplemented with 10% fetal bovine serum (FBS, Sigma). HeLa (CCL-2) and human marrow stromal cells were maintained in DMEM with 10% FBS. MM.1S-GFP$^+$/Luc$^+$ cells have been maintained in RPMI-1640, 10% FBS and 800ng/ml of Geneticin (G418, Sigma). All the cell lines have been grown at 37°C, 5% CO2.

Bone marrow aspirates were obtained from patients after appropriate informed consent. Primary myeloma cells isolated from the BM were classified as Lenalidomide refractory if the patient had disease progression during or within 60 days of receiving a Len-containing regimen. All primary MM samples, including newly diagnosed and Lenalidomide refractory were obtained through the Multiple Myeloma Registry and Leukemia Tissue bank at the Ohio State University.

Transfections: one million MM.1S, U266 and L363 were transfected by electroporation using the Nucleofector 4D system (Lonza, Basel, Switzerland). A specific optimized electroporation protocol and a determined nucleofector solution was used for each cell type. Cells were grown in T75 flasks, trypsinized, and collected via centrifugation (1200 × rpm, 6m). Cells were then resuspended in the nucleofector solution at 10^6 cells/100µl, mixed with 1–10µg DNA (1µg/µl CAT), and transferred to a cuvette. For all transfected cell lines, SF Nucleofector 4D solution was used, with program DS-137 for MM.1S cells, DN-100 for U266, and DS-100 for L363. Following electroporation, cells were immediately transferred into 6 well plates in pre-warmed medium supplemented with 10% FBS. HeLa cells were transiently transfected using Lipofectamine 2000 (ThermoFisher Scientific, Wilmington, DE), following the manufacturer' protocol.

3.2 Isolation of Extracellular Vesicles (EVs)

Before the EVs isolation, MM cells were kept in serum-deprived culture conditions for 48h (starvation). Starved cells and media were centrifuged at 300 x g for 10 minutes at 4ºC. Supernatant was transferred and centrifuged at 2000 x g for 20 minutes at 4ºC. Supernatant was harvested and vacuum ultracentrifuged at 10,000 x g for 30 minutes at 4ºC (these initial steps were necessary to deplete the samples from cells and debris). Supernatant was collected and ultracentrifuged at 100,000 x g for 70 minutes at 4ºC with vacuum. The resulting supernatant was discarded, and EVs pellets were resuspended in cold sterile PBS for the cellular treatments, frozen and stored at -80ºC for mass spectrometry investigations. Serum samples collected from MM patients and Healthy donor were processed in the same way.

3.3 Enzyme-linked immunosorbent assay (ELISA)

ELISA was conducted as described by the manufacturers: CD44 Elisa kit was provided by Abcam (Cambridge, MA), IL6 kit by R&D Systems (Minneapolis, MN).

For the CD44 determination on human samples, serum was diluted 1:40 in Standard Diluent Buffer and 100µl of each sample were plated in duplicate in a 96-well plate.

For the CD44 evaluation on the animal model, blood from xenografted mice (0.6 ml/kg) was collected by retro-orbital bleeding and serum samples were obtained by centrifugation at 1500 x g for 10 minutes. Subsequently, samples were diluted as described above.

For the IL6 measurement, 100µl of HS-5 or HS-27A supernatant was collected 24h after EVs treatment, depleted by cellular debris and seeded in duplicate in 96-well plates. Standard and 1x control solution were added to the appropriate wells and incubated for 1 hour. The plate was washed, biotinylated anti-CD44 or anti-IL6 was added to each well and plate was incubated for 30 minutes. The plate was washed again and 100µl 1x Streptavidin-HRP solution was added into each well, allowed to stand for 30 minutes and washed one more time. Chromogenic TMB substrate (100µl) was added to each well and incubated in the dark for 15 minutes. Finally, 100µl/well of Stop Reagent was added and absorbance was read on a spectrophotometer at 450 nm. All incubations were conducted at room temperature.

3.4 Proliferation assay

Cell proliferation was assessed using the WST-1 cell proliferation assay (Roche, Indianapolis, IN). 5.000 cells/well were seeded in triplicate for each treatments or controls into a 96 flat bottom well plate (Corning, New York, NY) and incubated at 37°C overnight before the treatment. After treatment, the plate was incubated for 72 hours, in a final volume of 100µl/well. The cellular proliferation, compared to untreated control, was determined by addiction of 10µl/well of WST-1 reagent, following 30 minutes of incubation at 37°C. At the end of the incubation period, the formazan dye formed was quantitated at 450nm with a scanning multi-well spectrophotometer Infinite (Tecan, Morrisville, NC). The measured absorbance directly correlated with the number of viable cells.

3.5 RNA extraction and analysis

RNA extraction: total RNA was prepared using TRIzol (Invitrogen) and purified using RNA Clean-Up and Concentration Kit (Norgene Biotek corp., Thorold, ON Canada), accordingly with the manufacturer's guidelines. The RNA quantity and purity were measured by Nanodrop (ThermoFisher Scientific).

qRT-PCR: mRNA and *miRNA* were quantified with quantitative reverse-transcription PCR (qRT-PCR) using TaqMan probe sets (Life Technologies), accordingly to the manufacturer's instructions. The following probes were used: *hsa-miR-9-5p, hsa-mir-9-1, hsa-miR-9-2, hsa-mir-9-3*, CD44, IGF2BP3. All reactions were performed in triplicate, simultaneous quantification of small endogenous nuclear RNU44 or RNU48 was used as a reference for miRNA assay data normalization, and simultaneous quantification of OAZ1 or GAPDH mRNAs was used as a reference for mRNA and pri-miRNA assay data normalization. The comparative cycle threshold (Ct) method for relative quantification of gene and miRNA expression (User Bulletin #2; Applied Biosystems) was used to determine miRNA, pri-miRNA, or mRNA expression levels.

Microarray: the analyses were performed by the Genomic shared resource at The Ohio State University. The RNA samples were analyzed by GeneChip® Human Genome U133 (Affymetrix, Santa Clara, CA). The probe sets represented in the chip is designed for the screening of approximately 47.000 transcripts. The sequences from which these probe sets were derived were selected from GenBank®, dbEST, and RefSeq. The sequence clusters were created from the UniGene database (Build 133, April 20, 2001) and then refined by analysis and comparison with a number of other publicly available databases, including the Washington University EST trace repository and the University of California, Santa Cruz Golden-Path human genome database (April 2001 release).

Nanostring arrays: the analysis was performed by the Genomic shared resource at The Ohio State University. The RNA samples were analyzed by nCounter GX Human Immunology Kit, or nCounter Human microRNA Kit, as recommended by the manufacturer (NanoString Technologies, Inc.).

A total of 511 immunology related genes and 800 microRNAs were profiled. The nanostring Counter GX Human Immunology Kit is a comprehensive set of 511 human genes (and 15 internal reference genes) known to be differentially expressed in immunology. The gene list was compiled from the Gene Ontology Consortium List of Immunologically Important Genes (GO-LIIG) with additional input from experts in the field of immunology. All genes with a priority score of 8 or higher in the GO-LIIG are included in the panel. A panel of experts designated additional genes (with priority scores lower than 8) for inclusion in the panel based on their relevance in addressing key research questions.

The NanoString miRNA panel detects 664 endogenous miRNAs (with 654 probes), 82 putative viral miRNAs from nine viruses including HIV-1, five housekeeping transcripts [(actin beta (NM_001101.2), beta-2 microglobulin (NM_004048.2), GAPDH (NM_002046.3), RPL19 (NM_000981.3), and RPLP0 (NM_001002.3)], six positive and eight negative controls (proprietary spike-in controls). Unlike traditional hybridization microarrays, NanoString does not associate targets with spatial coordinates; instead, the system generates copy numbers of target-specific molecular barcodes attached to detection probes, theoretically eliminating position-dependent effects.

Raw data, which are proportional to copy number, were log-transformed and normalized by the quartile method after application of a manufacturer-supplied

correction factor for several miRNAs. Data were filtered to exclude relatively invariant features (IQR = 0.5) and features below the detection threshold (defined for each sample by a cutoff corresponding to approximately twice standard deviation of negative control probes plus the mean of them) in at least half of the samples. P values were used to rank miRNAs of interest, and correction for multiple comparisons was done by the Benjamini-Hochberg method [234].

3.6 Western blotting

Cells were harvested by centrifugation, washed with PBS and lysed using buffer composed of 50mM Tris (pH 7.5), 150mM NaCl, 10% glycerol, 1.0% NP-40, 0.1% SDS, supplemented with protease and phosphatase inhibitors. Protein concentrations were estimated by Bradford assay and equivalent quantities of the lysates were resolved on 4-20% Tris-HCl SDS-PAGE TGX gels (Bio-Rad, Hercules, CA). Proteins were transferred to nitrocellulose membranes and stained for acetyl-histone H3 (Millipore, Billerica, MA), acetyl-histone H4 (Millipore), IGF2BP1 (IMP-1, Cell Signaling Technology, Danvers, MA), IGF2BP3 (IMP-3, Santa Cruz Biotechnology, Dallas, TX), CD44 (Santa Cruz Biotechnology), Drosha (Cell Signaling Technology), CD9 (Santa Cruz Biotechnology), Lamin B1 (Abcam), β_2-Microglobulin (Abcam) or glyceraldehyde 3-phosphate dehydrogenase (GAPDH, Cell Signaling Technology), followed by anti-mouse, or anti-rabbit IgG-HRP (GE Healthcare, Pittsburgh, PA). Signals were developed using Pierce ECL Western Blotting Substrate (Thermo Fisher Scientific) and X-ray films (BioExpress, Kaysville, UT).

3.7 Flow cytometry

MM.1S, MM.1R, U266, H929, RPMI-8226, KMS11, LP1, EJM MM cell lines, and three PBMCs samples collected from healthy donors were analyzed for apoptosis by Annexin-V/Propidium Iodide flow cytometry according to the manufacturer's protocol (Clonetech, Mountain View, CA).

MM.1S, MM.1R, U266, H929, L363, OPM2, ARH77, TBI, RPMI8226, KMS11, KMS18, LP1, and EJM MM cell lines were analyzed for the CD44 expression, using an anti-human CD44-FITC antibody (BD Bioscience, San Jose, CA).

Cells were harvested and washed 2 times in PBS before performing the staining (15 minutes for apoptosis kit, 30 minutes for CD44 staining). All the staining were performed in the dark at room temperature. At the end of the staining, cells were resuspended in PBS and acquired at the FC500 flow cytometer (Beckman Coulter, Brea, CA).

For the multiparametric analysis, the bone marrow samples harvested from 8 MM patients were stained with CD38-PE (BD Bioscience), CD138-APC (BD Bioscience), CD44-FITC (BD Bioscience) or AnnexinV-FITC (Clonetech) for 30 minutes, washed with PBS and immediately analyzed with Gallios flow cytometer (Beckman Coulter).

Subsequent analysis was conducted using FlowJo vX.0.7 (Tree Star Inc., Ashland, OR).

The size distribution analysis of the EVs was performed on a Nanosight NS300 (Malvern Instruments Ltd., Malvern, UK): two separate vesicle preparations for each cell line and single MM patient and healthy donor preparations were analyzed five times each. Batch capture was conducted on a sCMOS camera with variable shutter length and frame rate, 1000 shutter setting and 400 camera gain. Computational analysis was evaluated on the Nanoparticle Tracking Analysis Software (Malvern Instruments Ltd.).

3.8 DNA constructs and Luciferase reporter assay

Human CD44 promoter-luciferase reporter gene (CD44P pGL3, Fig. 8A) [235] was obtained from Addgene (Plasmid 19122; Addgene, Cambridge, MA).

The 3'UTR of CD44 was PCR amplified using the following primers: (Forward) 5'-gctagcCACCTACACCATTATCTTG -3' and 5'- gctagcAATTCTTGGTGTTGTTATG-3'

(engineered NheI sites are in lower case). The products were cloned into XbaI site downstream from the luciferase gene in pGL3-control vector (Fig. 8A; Promega).

To generate IGF2BP3 luciferase reporter constructs, the 3‘UTR was amplified by PCR using primers:

(Forward) 5’-TCTTTGGTTATCTAGCTGTATGA-3’

(Reverse) 5’-TCTTTGGTTATCTAGCTGTATGA-3’

The product was cloned into XbaI site of pGL3-control vector (Promega). Mutations in the *miR-9-5p* binding site of the IGF2BP3 3′UTR were introduced by the QuikChange Mutagenesis Kit (Stratagene) using the following primers:

(Forward) 5'-CAGAGGCAGATGCCAAACGGGGTACAGATTGCTTAACC-3'

(Reverse) 5'-GGTTAAGCAATCTGTACCCCGTTTGGCATCTGCCTCTG-3'.

Luciferase assay: Hela cells were transfected with 500ng of 3’UTR-pGL3-control plasmid and 50ng of Renilla luciferase expression construct (pRL-TK; Promega), Fig. 8B, using Lipofectamine 2000 (ThermoFisher Scientific). After 24hrs cells were lysed and tested by Dual Luciferase Assay (Promega), according to the manufacturer’s instructions. MM.1S, U266 and L363 cells were transfected by nucleofection with 1.8µg of pGL3-based luciferase vector and 200ng of pRL-TK, harvested 24 hours later and assayed as above.

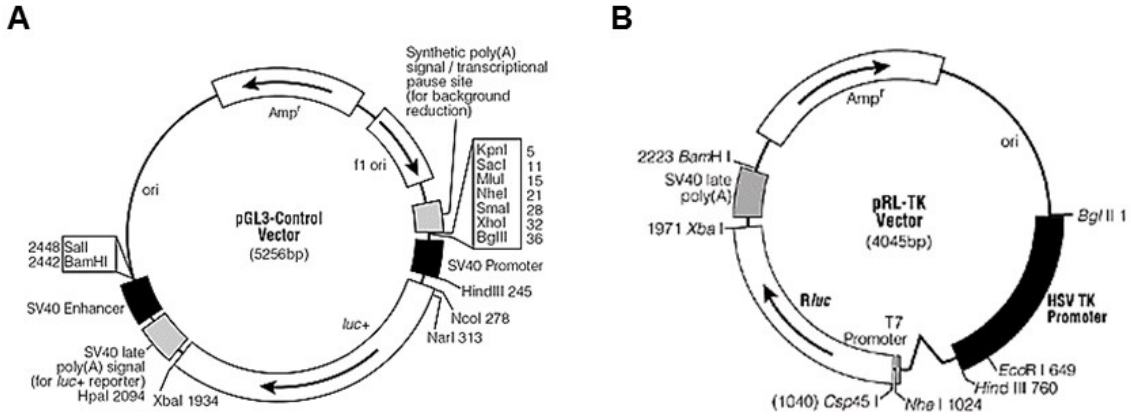

Fig.8. Expression plasmids used in Luciferase reporter gene assays *A) pGL3 plasmid used with Multiple Myeloma and HeLa cells for the expression of CD44 or IGF2BP3 promoter regions. B) pRL-TK plasmid for the Renilla luciferase expression.*

3.9 Cryo-Transmission Electron Microscopy (Cryo-TEM) and Dynamic Light Scattering (DLS)

Vesicles derived from the MM.1S and U266 cell lines were prepared for cryo-TEM within a Controlled Environment Vitrification System at 25°C and 100% relative humidity. A 10µl suspension of vesicles was applied onto glow discharged Lacey Formvar/Carbon 200 Mesh copper grids (Ted Pella, Inc., Redding, CA), blotted and plunged into ethane. Vitrified grids were transferred to a Gatan cryo-sample holder and visualized by a FEI Tecnai G2 Spirit electron microscope (FEI, Hillsboro, OR). The microscope was operated at 120 kV under low dose conditions to minimize radiation damage to the samples. The total electron dose was held between 10 and 100 e-/Å2. Images were captured on a 4k x 4k Gatan Ultrascan CCD camera (Pleasanton, CA) at 4,800x, 18,000x and 30,000x magnification. Size distributions were obtained from images using the NIS Element Imaging Software (Nikon, Melville, NY).

Relative vesicle size distributions of the MM.1S and U266 derived vesicles were measured using a BI-200SM Laser Light Scattering Goniometer (Brookhaven Instruments, Holtsville, NY). 1ml of vesicles were equilibrated at room temperature and eventually diluted to 10-200 kilocounts/sec. DLS measurements were made using a 633 nm laser. Vesicle translational diffusion coefficients were converted to apparent hydrodynamic diameters using the Stokes-Einstein Relation. The relative size distributions were obtained using the CONTIN algorithm.

3.10 Proteomic Analysis

Preparation of Samples for Mass Spectrometry: vesicle isolations (in triplicate, secreted from 100 million of MM cells) or 48 hours serum starved cell pellets (100.000 MM cells) were resuspended in 50mM ammonium bicarbonate (Sigma Aldrich, St. Louis, MO) supplemented with 0.5% Rapigest SF surfactant (Waters, Milford, MA). 800ng of sequencing grade modified trypsin (Promega, Madison, WI) was added to each sample and incubated overnight (>16h) at 37ºC. The reaction was stopped and Rapigest was precipitated by addition of 98% formic acid to 30% v/v. Samples were incubated at 37ºC for 30 minutes, centrifuged 3 times at 21,000g and the supernatant removed after each

centrifugation. Peptides were speedvacuumed to dryness and resuspended in 20µL of 2% acetonitrile with 0.1% formic acid. Final peptide concentrations were measured by 280nm absorbance using a Nanodrop ND-1000 spectrometer.

Liquid Chromatography and Mass Spectrometry (LC-MS/MS): 1-2µg of peptides were loaded for RP-HPLC separation on a Dionex Ultimate 3000 capillary/nano HPLC (Dionex, Sunnyvale, CA) and mass analyzed by a ThermoFisher LTQ Orbitrap XL mass spectrometer (ThermoFisher, Waltham, MA). The LTQ Orbitrap XL was fitted with a micro/nanospray ionization source (Michrom Bioresources Inc, Auburn, CA). HPLC separations were carried out at a flow rate of 2µl/min on a 0.2 mm x 150 mm C18 column (5µm, 300Å, Michrom Bioresources Inc., Auburn, CA). Mobile phases were HPLC water and acetonitrile each supplemented with 0.1% (v/v) formic acid. Top 5 data dependent mode was utilized, on the mass spectrometer, in positive ion mode with dynamic exclusion of: repeat count=3, repeat duration=30.00, exclusion list size=500, exclusion duration=350 s and exclusion mass width of ± 1.50m/z. Protein identifications were obtained using the MassMatrix search engine and the UniprotKB complete H. sapiens proteome (updated at 18Sep12).

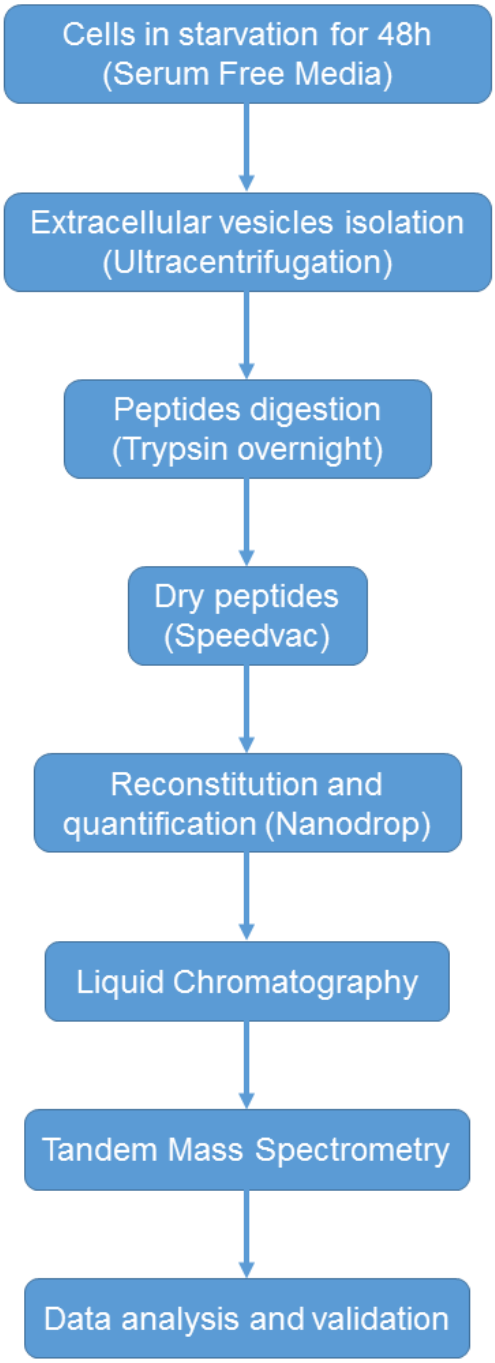

Fig. 9. EV analysis flowchart

Cytoskeletal, epidermal and cuticle keratin identifications were considered as contaminant proteins and removed from the analysis. The false discovery rate (FDR) was estimated using the reversed sequences of the target database. The parsing of protein identifications and spectral counts was conducted from each data file and combined using a Python application. Protein matches were retained based on an FDR threshold of 0.05%, 2 unique peptide matches and a decoy cutoff of 2 for each protein identification returned.

3.11 Animal experiments

Tumor implantation: animal experiments were performed according to The OSU institutional guidelines. To generate MM xenograft model, 10^7 viable MM.1S cells were injected subcutaneously into the right flank of twelve 5-week-old female nude mice (Foxn1nu/Foxn1nu; Charles River, Burlington, MA). The tumor size was measured once a week using a caliper, and the volume was calculated in cubed millimeters (mm^3), using the formula $LxW^2/2$. At 3 weeks after injection, a group of 8 mice with comparable tumor size ($250 \pm 60mm^3$) were randomly divided into two groups, using 4 mice for each treatment. Mice were treated with intra-peritoneal injection of AR42 (25mg/kg) or DMSO (8% in PBS) once a day on Monday and Wednesday. The day after the second treatment, when the tumor sizes between the 2 different groups were comparable, blood from mice was collected by retro-orbital bleeding and the mice were sacrificed for IHC analysis.

For studies involving AR42 in combination with Lenalidomide, MM.1S-GFP^+/Luc^+ stable line was harvested during logarithmic growth phase, washed with PBS and injected intravenously into NOD-SCID nude mice ($5x10^6$ cells in 0.2ml/mouse) under general anesthesia (isoflurane, 2-4% to effect). Beginning at 7 days post-injection, mice were monitored every day for the appearance of tumors by fluorescence using *In Vivo* Imaging System (IVIS). On day 15, when the engraftment reached approximately $\geq 2x10^6$photons/sec/cm^2/sr mice with similar tumor burden were divided into different groups of treatments. Intraperitoneal injections with vehicle control (8% DMSO in PBS), AR42 (25mg/kg; Mon-Tue-Fri) and Lenalidomide (50mg/kg, daily) were administered by intraperitoneal injection under general anesthesia (isoflurane, 2-4% to effect).

Treatments continued for 3 weeks, and ended when the control group showed sign of disease, including paralysis and extreme weight lost, or when tumor mass was equivalent to 10% of body weight.

Detection of tumor progression by bioluminescence imaging: mice were injected with 75mg/kg Luciferin (Xenogen), and tumor growth was detected by bioluminescence 10 minutes after the injection. The home-built bioluminescence system used an electron multiplying charge-coupled device (Andor Technology Limited) with an exposure time of 30 seconds and an electron multiplication gain of 500 voltage gain x 200, 5-by-5 binning, and with background subtraction. Images were analyzed using ImageJ software (National Institutes of Health).

Immunohistochemistry: Xenograft tumor samples were fixed in 10% neutral-buffered formalin embedded in paraffin, and sectioned at 4μm. Slides were then placed in a 60°C oven for 1 hour, cooled, deparaffinized, and rehydrated by passing slides through xylene, a series of graded ethanol solutions, and ending with water. All slides were placed for 5 minutes in a 3% hydrogen peroxide solution to block the endogenous peroxidase. Antigen retrieval was performed by heat induced epitope retrieval (HIER), in a citric acid solution, pH 6.1, for 25 minutes at 96°C followed by cooling down for 15 minutes. Slides were placed on a Dako Autostainer and sections were treated with primary antibodies for human CD138 and CD44 followed by biotinylated secondary antibodies and the DAB chromogen.

3.12 Statistical analysis

All preclinical data were obtained from at least three independent experiments and are expressed as mean ± standard deviation (SD). Comparisons between groups were performed using two-tailed t-tests, and comparisons between multiple groups were performed using 1-way analysis of variance (ANOVA). For evaluate the *in vitro* combinatorial therapy, the Chou-Talalay method was used to calculate combination indices (CI). Mouse data were evaluated by ANOVA, and synergy between AR42 and Lenalidomide was tested by interaction contrast. For AnnexinV and CD44 level in primary patients geometric mean values were analyzed by using mixed effect model, incorporating repeated measures for each patient's sample. For the AnnexinV experiment, p-values were adjusted by Holm's method to control the family wise error rate at 0.05.

Overall survival on patients was defined as the time from study enrollment to the time of death. Patients who did not die during the study follow up were censored at the end of study follow up or the date of last follow up. The assumption of proportional hazards was assessed through tests of the Schoenfeld residuals with no violations observed. All reported p-values are two-sided and analyses were performed using the statistical program Stata (StataCorp, College Station, TX).

Computational Annotations, Clustering and Bioinformatics: Venn diagrams were created using the BioVenn web application. Clustering analysis and visualization was performed using open source software Cluster 3.0 and Java Tree View. Bioinformatics annotations of gene ontology for identified proteins were searched against the PANTHER Classification System.

CHAPTER 4. RESULTS

4.1 EVs isolation from MM cell lines and proteomic characterization

The initial set of experiments of this project was focused on the characterization of size and protein contents of Extracellular Vesicles (EVs) isolated from 2 different kinds of Multiple Myeloma cell lines, MM.1S and U266, which share similar malignant potential but grow in adhesion and suspension respectively. At the electron microscope (Cryo-TEM, Fig. 10A), the morphology of EVs derived from these kinds of cells appeared spherical in shape with a single lipid bilayer, and hydrodynamic diameters with ranging from 50 to 200 nm.

Dynamic Light Scattering (DLS) microscopy was performed to assess the size distributions of the enriched vesicles. The DLS analysis of the U266-derived vesicles showed a monomodal distribution of diameters ranging from 80 to 200 nm (average diameter of 138 nm), while the MM.1S vesicle diameters were larger, ranging from 100 to 200 nm (average diameter of 177 nm) with a small population of even larger vesicles with diameters between 240 and 260 nm (Fig. 10B).

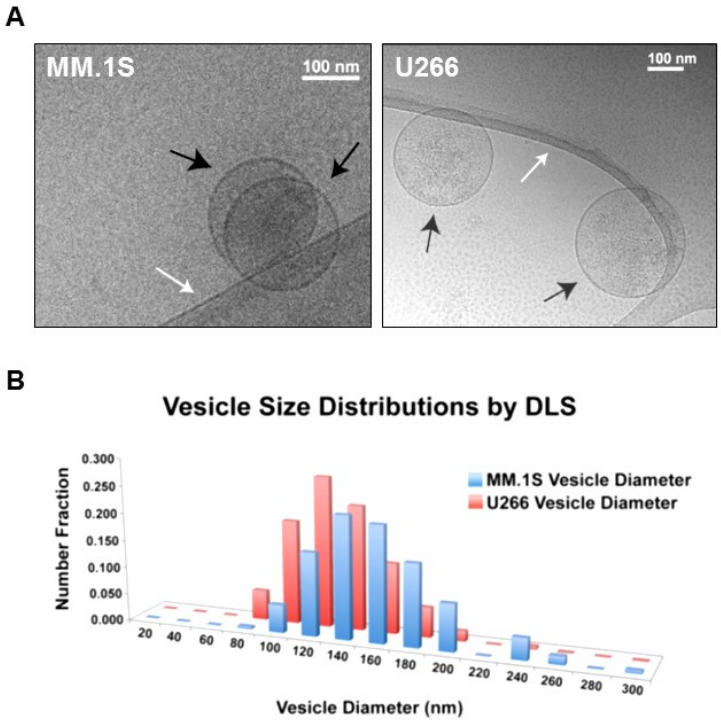

Fig.10. Morphology and size distribution of MM derived EVs. *A) Cryo-TEM of EVs isolated by ultracentrifugation from MM.1S and U266 MM cells. B) Size distribution of EVs determined by DLS.*

These results indicated that EVs secreted by the two different MM cell lines have comparable size distribution and shape. At that time we were not sure about the quality of the EVs collected due to the method of isolation by ultracentrifugation, and I wanted to determine if the vesicles visualized through the electronic microscope were effectively Extracellular Vesicles or in part contaminated with apoptotic bodies (harvested due to the similarity in shape and mass). To address the possibility of apoptotic bodies' contamination, I subsequently analyzed by flow cytometry the apoptosis status of the serum-starved MM cells before and after EVs collection and the result, showed in Fig. 11, clearly indicated no sign of apoptosis in the parental cells (more than 98% of cells were negative for AnnexinV/Propidium Iodide staining), confirming that the majority of the vesicles were derived from non-apoptotic cells.

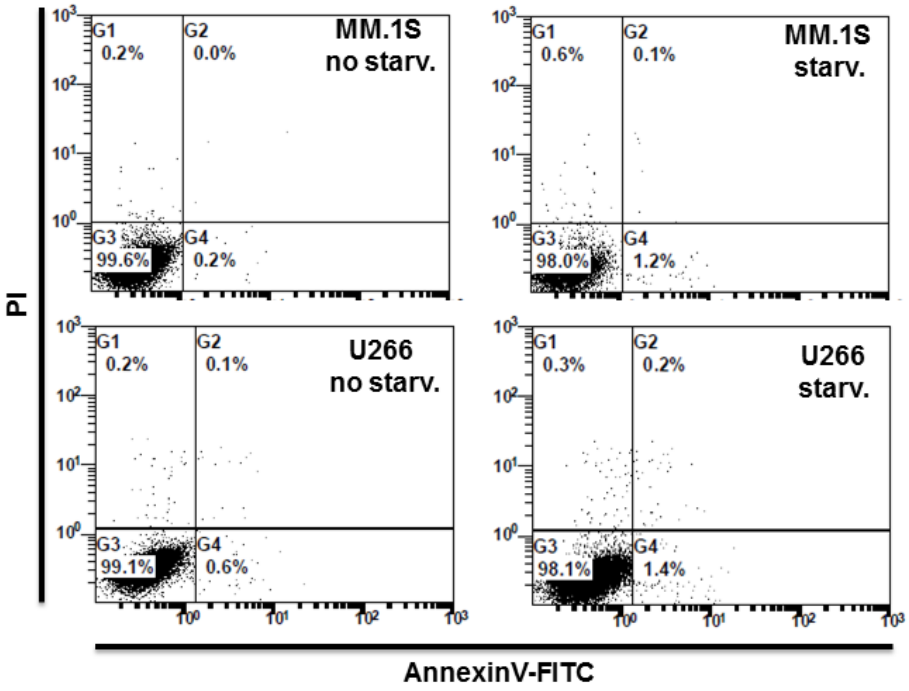

Fig.11. Level of apoptosis in EVs-parental MM cells. *AnnexinV and Propidium Iodide expression by flow cytometry analysis in MM.1S (above) and U266 (below) in normal (no starv.) and in starved (starv, before EVs collection) conditions.*

To analyze the entire proteomic contents of MM cells and their derived EVs, we proceeded to perform a proteomic characterization by liquid chromatography-mass spectrometry-mass spectrometry (LC-MS/MS). All the information related to the LC-

MS/MS results for the vesicles and cell lysates can be found in the APPENDIX, page 105. A database search of the LC-MS/MS for each kinds of vesicles (from three independent replicates) generated the identification of 374 and 368 proteins for MM.1S and U266, respectively. Moreover, the proteomic analysis of the entire MM.1S and U266 proteome (cell lysates and EVs together) produced 429 and 479 protein identifications. The Venn diagrams (Fig. 12A) show the overlap of identical proteins between the cell-derived vesicles and their global lysates. Although the majority were identified as common proteins, few distinctive proteins were observed in cell line derived EVs (24%, 72 for MM.1S, and 15%, 49 for U266) and in cellular lysates (18%, 55 for MM.1S, and 35%, 111 for U266). Indeed, numerous recent papers indicates a similarity between protein contents in EVs and parental cells [78,236]. To assess the differences between the MM-EVs collected from the two cell lines, we compared the quantity of the carried proteins. The diagram in Fig. 12B shows 324 common proteins, 32 (10%) specific to the MM.1S vesicles and 13 (4%) distinctive of U266. Among the 324 common proteins, 125 showed a different enrichment between EVs derived from U266 and MM.1S, as indicated by the clustering analysis on Fig. 12C.

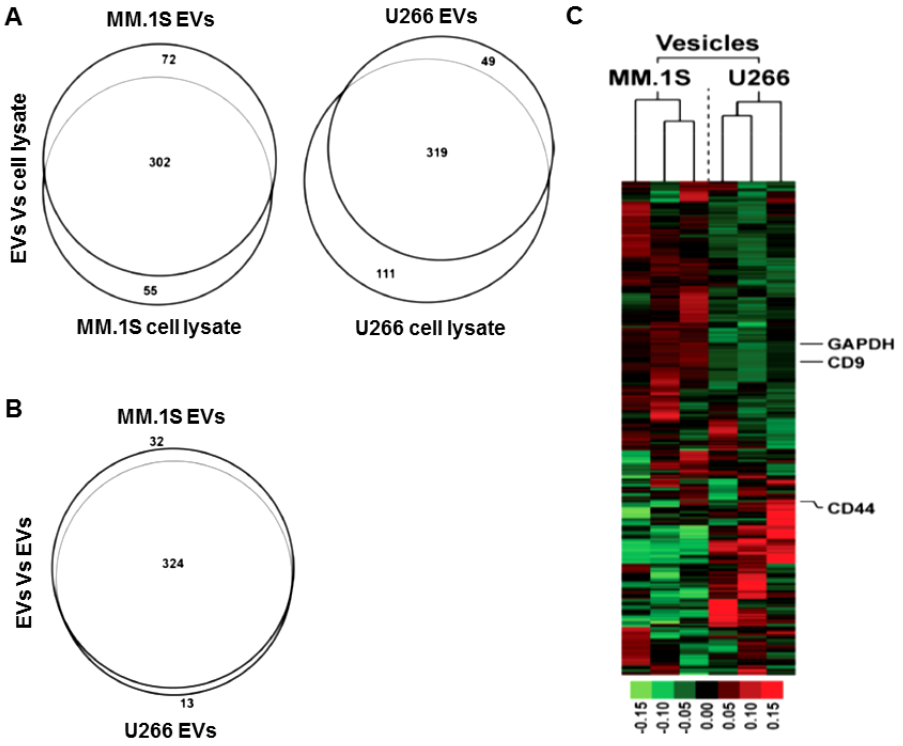

Fig. 12. Differences in protein contents in between MM cells and secreted EVs.
A) B) Venn graphic representation of the protein distribution between A) cells and secreted EVs, or B) U266 Vs MM.1S EVs. C) Hierarchical clustering of proteins differentially expressed between EVs secreted by MM.1S and U266.

One of the possible explanations for these differences can be attributed to the different amount of the same kind of proteins in the different parental cells that secreted the EVs, MM.1S and U266.

Interestingly, some of the proteins carried by the EVs resulted enriched compared the cells of origin, such as CD44 and CD9 (Fig. 12C).

Of note, the obtained data set was in agreement with the previously published protein database from the same MM cell lines and with recent proteomic studies on EVs [45,78,236]. Overall, excluding some exceptions, what we found into the EVs was mostly representative of the protein contents, either qualitative or quantitative, into the different kinds of MM cells of origin.

I focused my attention on proteins that were enriched in the MM-EVs compared to the protein set derived from the cells of origin (Appendix). Using the bioinformatics tool “PANTHER” we analyzed the protein distribution based on the gene ontological classification. To simplify, the results have been divided in molecular functions (Fig. 13A, above) and biological processes (Fig. 13A, below). Our data indicated a wide range of molecular processes and biological functions, but the majority of the discovered proteins were involved in catalytic activity and metabolic processes and they were the most variable in terms of quantity between the different kinds of EVs, suggesting a possible correlation with the characteristics of parental cell lines that produced and secreted them.

Finally, to corroborate the results obtained by mass spectrometry, I validated by western blotting the enrichment of CD9 in EVs secreted by MM.1S compared to the cells of origin, the CD44 and GAPDH enrichment in both kinds of MM-EVs compared to the MM cells contents. Overall, the western blotting confirmed the differences documented in the LC-MS/MS analysis, including differential protein abundances within EVs-EVs and EVs-cells (Fig. 13B).

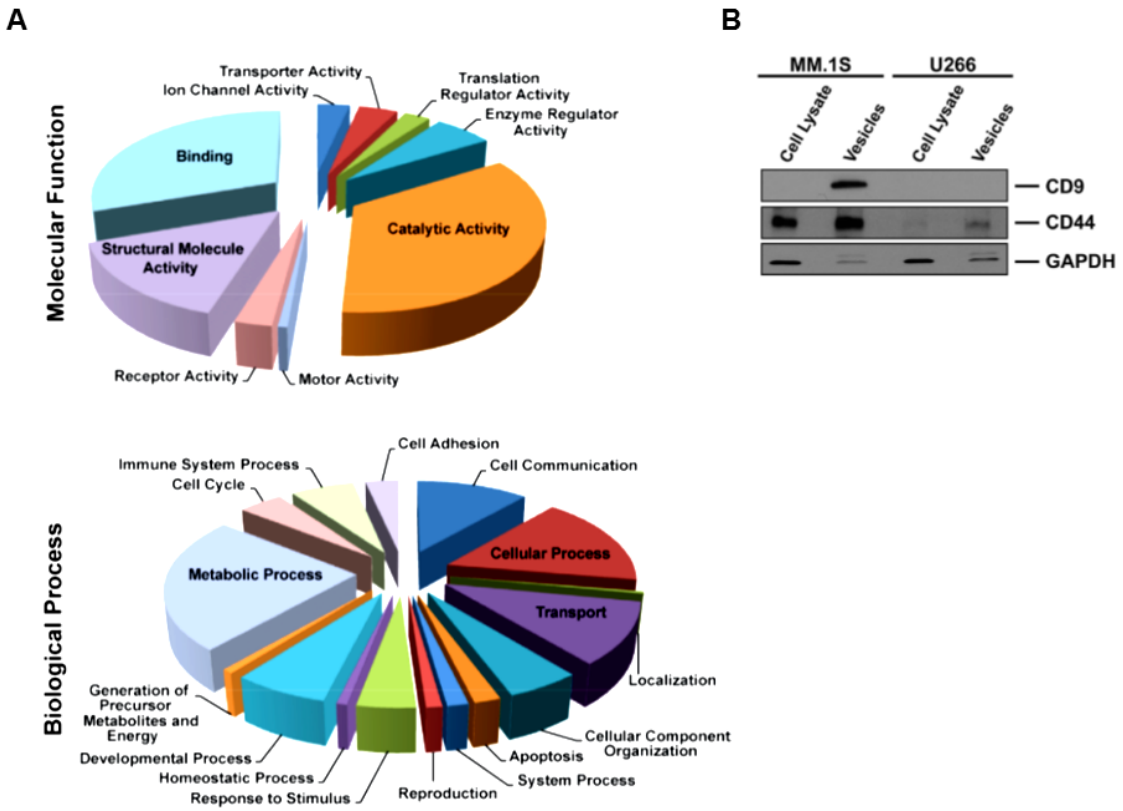

Fig. 13. Protein differentially expressed between EVs and EVs-cells, *A) Pie chart of the PANTHER analysis shows differences in molecular function (above) and involvement in biological processes (below) in MM.1S-EVs Vs U266-EVs. B) Differential expression of CD9, CD44, GAPDH between EVs and parental cells determined by western blotting.*

Furthermore, to characterize the differences in vesicles size and protein contents, the study has been extended to the comparison of the mass spectrometry results obtained from 2 additional MM cell lines, MM.1R and RPMI8226 (Fig. 14). Altogether, the four parental cell types were dissimilar in terms of growth rate, *in vitro* adhesion and resistance to Dexamethasone. Indeed, MM.1R grows in adhesion as well as MM.1S, while U266 and RPMI8226 in suspension. Notably, regarding the resistance to the treatment with Dexamethasone, MM.1R is the most resistant, MM1.S and U266 are moderately sensitive, and RPMI8226 is very sensitive. The results showed: a similarity in EVs size (even if MM.1R are more heterogeneous and bigger in size, and RPMI8226 has the lower size) (Fig. 14D), a cohort of 339 common proteins (Fig. 14C) expressed in all different kinds of MM-EVs with few peculiar exemptions (complete data set

available in the supplementary material of paper # 1 at the paragraph LIST OF PUBLICATIONS DURING THE PhD), and the hierarchical clustering clearly indicated quantitative differences in expression of common proteins such as the CD9 and GAPDH (Fig. 14A and B).

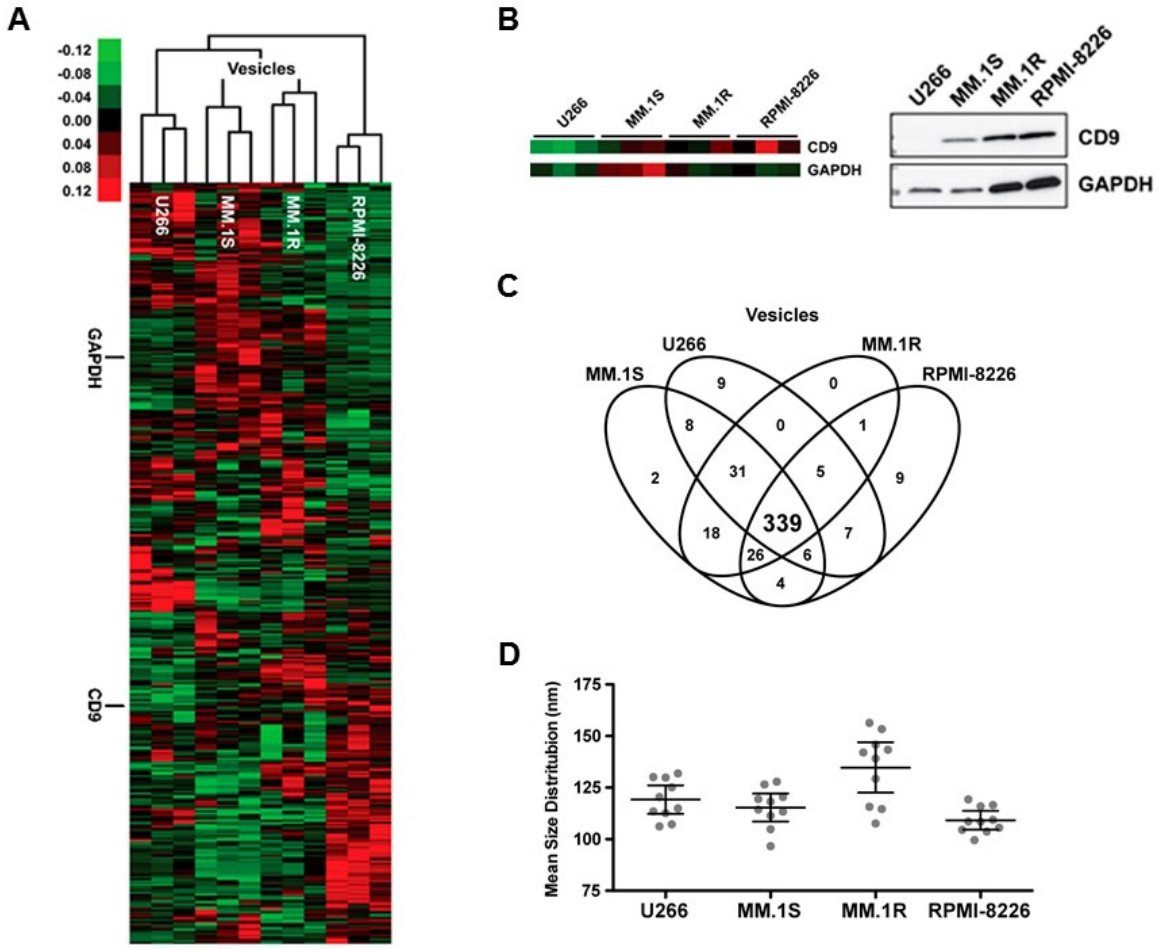

Fig. 14. Differences in protein contents between cell lines and in vitro secreted MM-EVs. *A) Hierarchical clustering of proteins differentially expressed between EVs secreted from U266, MM.1S, MM.1R, and RPMI8226. B) Western blotting analysis of the CD9 and GAPDH expression in MM-EVs. C) Venn graphic representation of the protein distribution among all the secreted MM-EVs. D) Nanosight analysis of the size distribution of U266, MM.1S, MM.1R, and RPMI8226 EVs.*

4.2 The in vitro activity of the MM-EVs on MM and BM cells

Numerous studies have already demonstrated the biological effect of the EVs on the target cells in different kinds of solid and soft tumors [51-72]. It is also well known the supportive effect of the tumor microenvironment on the Multiple myeloma through the IL6 release (necessary for the tumor growth, drug resistance and survival) [25,95-97], and the crosstalk mediated by EVs may have effect on both MM and BM cells. First of all, to assess the *in vitro* biological consequence of secreted Multiple Myeloma-EVs, I evaluated their effect on proliferation in MM.1S cells performing a WST-1 assay. Briefly, cells were seeded in a 96 well plate and treated the following day with fresh isolated EVs derived from MM.1S or RPMI8226 cells with a 1:50 ratio (cells:EVs). The increase of proliferation was visible after 48h, with the maximum effect achieved upon 72h of treatment with both kinds of EVs (Fig. 15A), as compared to the untreated control ($p=0.0002$ for MM.1S EVs, $p=0.0011$ for RPMI8226 EVs).

To assess if the MM-EVs were able to induce BM cell lines to release IL6, I treated HS-5 and HS-27A (derived from human bone marrow/stroma, morphologically classified as fibroblasts) with EVs isolated from MM.1S and RPMI8226 for 24h (1:50 ratio). The major difference between the two BM-derived cell lines is the secretion of cytokines, which is very low in HS-27A, and normal in HS-5. After 24h of incubation, the supernatant was recovered, depleted of cellular debris and used to quantify the release of IL6 by Elisa. The data, normalized on the basal IL6 production by the untreated HS-27A, showed an increase of IL6 secretion upon treatment of HS-5 with MM.1S EVs and no effect was observed with the RPMI8226-derived EVs (Fig. 15B), compared to the untreated control. This important result demonstrates the capacity of MM-EVs of stimulating proliferation on MM cells, and selectively promoting IL6 release in BM cells (depending on the nature of MM parental cells). Of note, MM.1S-EVs showed the ability to promote proliferation and to stimulate the IL6 release, whereas RPMI8226 were able to promote the MM proliferation but had no effect on cytokines production and secretion in BM cells. Our data further confirm that qualitative differences in proteins carried by MM-EVs may be used for screening of circulating MM biomarkers and have different impact on the target cells.

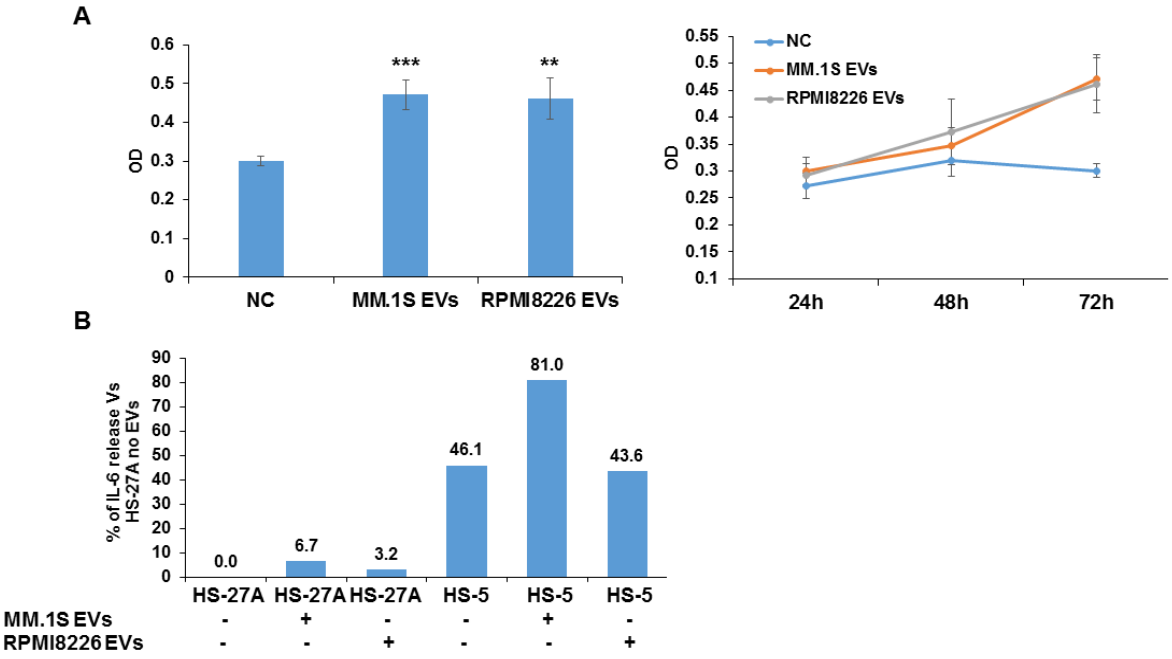

Fig. 15. MM-EVs effect on MM and BM cells. *A) WST-1 assay on MM.1S cells treated for 72h (left) or for 24,48 and 72h (right) with MM.1S and RPMI8226-derived EVs, ratio cells-EVs 1:50. p=0.0002 for MM.1S cells treated with MM.1S EVs for 72h, p= 0.0011 for MM.1S treated with RPMI8226 EVs for 72h. B) Quantitation by Elisa of IL6 secreted by HS-27A and HS-5 cells upon 24h of treatment with MM.1S or RPMI8226 EVs. Ratio cells-EVs 1:50. Data are expressed in % of secreted IL6 normalized to the amount of IL6 released by untreated HS-27A cells (baseline).*

4.3 Potential association between CD44 enrichment in EVs and drug resistance in MM

One of the peculiar characteristics related to the MM cells is the resistance to the treatment with Dexamethasone. For example, MM.1R and MM.1S are resistant and sensitive to the treatment with this chemotherapeutic agent, respectively. Using a proteomic approach to the one already described, we tried to investigate if the difference in drug resistance was in some way influencing also the protein contents of the extracellular vesiscles. Fig. 16A and B display the clustering of proteins differentially expressed between EVs secreted by MM.1S and MM.1R. Among them, two of the most enriched protein carried by MM.1R-EVs compared to MM.1S-EVs were the transmembrane glycoprotein CD44 and the prognostic factor β2-microglobulin. Interestingly, no differences were measured in the CD44 protein levels in the lysates

coming from both MM.1S and MM.1R, also confirmed by immunoblotting analysis as shown in Fig. 16C. To further corroborate these results, differences in GAPDH contents and absence of Lamin B1 was established in EVs compared to the parental cells, as confirmed by the western blotting (Fig. 16C). Notably, CD44 is an adhesion molecule that interacts with the hyaluronic acid in the extracellular matrix and it has been already associated with drug resistance in several kinds of tumors [148,151-155,157,237].

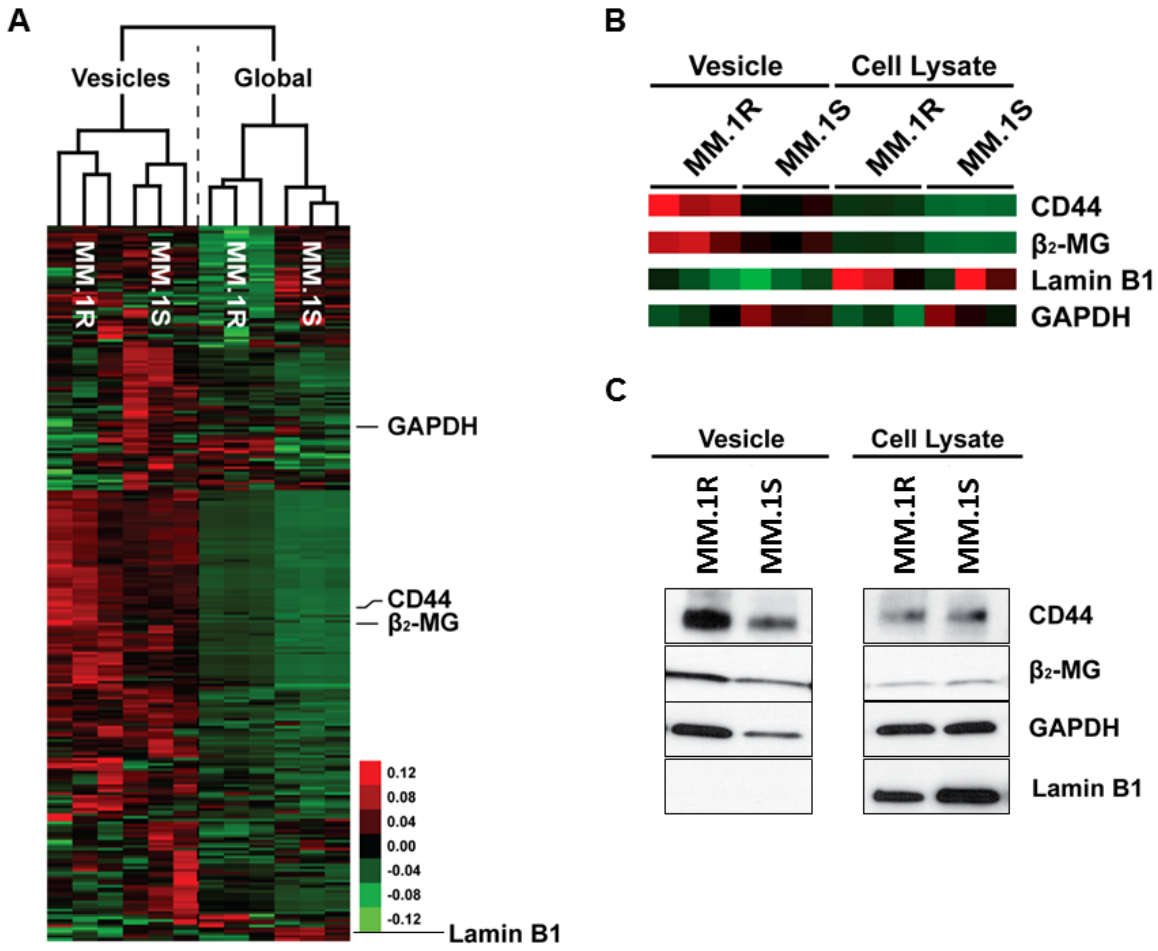

Fig. 16. Comparison between protein cargo in MM.1R and MM.1S EVs. *A) B) Hierarchical clustering of proteins differentially expressed between MM.1S and MM.1R EVs and cells. B) Western blotting analysis of the CD44, β2-microglobulin (β2-MG), GAPDH and Lamin B1 expression in MM-EVs.*

4.4 Circulating CD44 as new prognostic factor in MM

Evidences of the role of CD44 in drug resistance mechanisms convinced us to investigate the EVs circulating in peripheral blood of newly diagnosed MM patients. More than 300 serum samples collected from newly diagnosed MM patients were available under IRB protocols at The Ohio State University, and I first checked the CD44 status in 31 of these samples and in 13 healthy donors by immunoblotting. The blots in Fig. 17A showed variability in protein contents and the expression of different CD44 variants patient-dependent. Overall, the CD44 expression in MM patients was higher than healthy donors. Of note, only the MM patients carried different CD44 isoforms, confirming the presence of variants related to the gene-aberrant splicing as already demonstrated in several tumors [238]. Using the nanosight technology, a novel flow cytometry application principally dedicated to the measurement of size and concentration of micro and nanoparticles in liquids, we tried to determine if there were differences in EVs size between healthy donors (H) and patients (MM), who were divided in MGUS, SMM, and Active MM (Fig. 17B). Interestingly, the EVs size were homogeneous in dimensions across all the different kinds of patients, around 75nm, but smaller compared to the *in vitro* study previously done on MM continuous cell lines (Fig. 14D).

To determine whether CD44 circulating in the peripheral blood was preferentially carried by EVs or not, I depleted the EVs from 2 healthy and 3 MM serum samples already tested and performed a CD44 western blotting. As shown in Fig. 17C, the EVs depletion induced a strong reduction of circulating CD44. Furthermore, to validate what previously discovered, I measured the quantity of CD44 by Elisa in the same kind of samples before and after EVs depletion and, as shown in Fig. 17D, the downregulation of the circulating CD44 upon vesicles-depletion was confirmed. Of note, the CD44 was not completely removed after EVs depletion. In my opinion, the residual CD44 after EVs depletion could be ascribed to the limits of the EVs isolation technique in high concentrated and dense biological fluids such as serum samples.

Based on these results, we decided to evaluate the potential implication of CD44 as a MM circulating biomarker. I measured CD44 levels on serum samples collected from a large cohort of newly diagnosed MM patients who were uniformly treated, and subsequently I matched the circulating CD44 levels with clinical data.

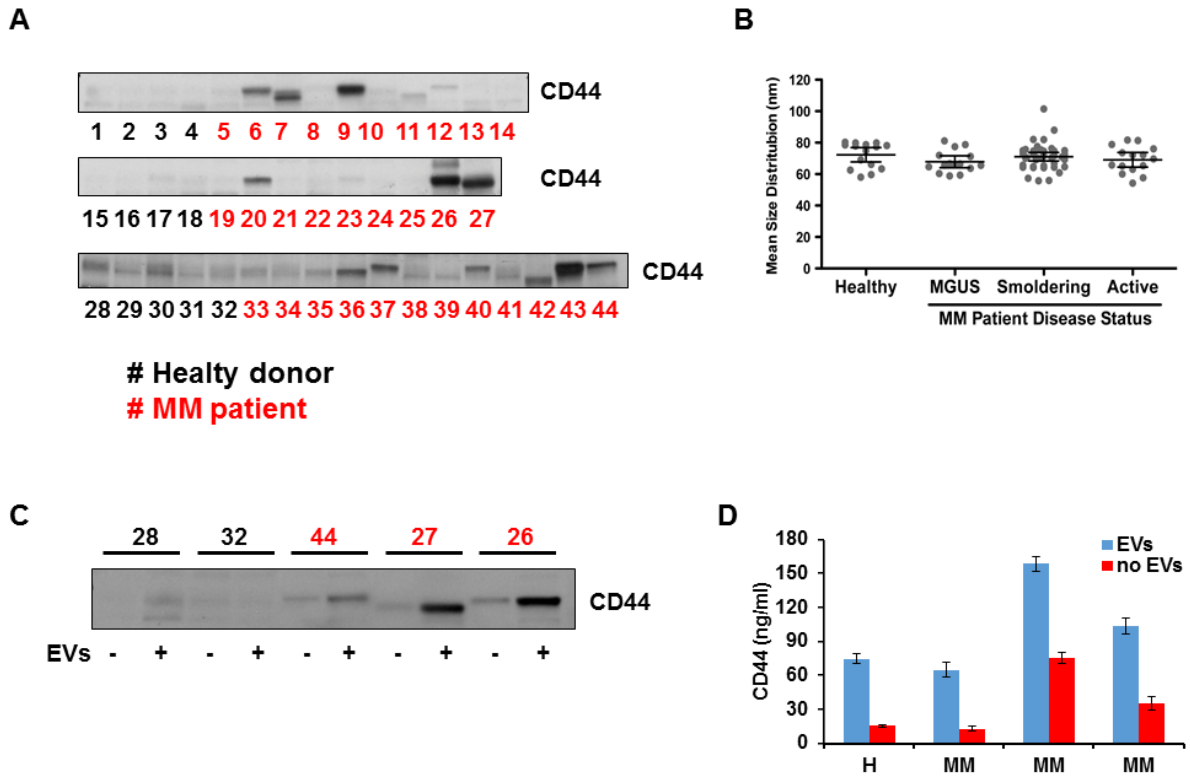

Fig. 17. Circulating CD44 in MM and Healthy donors. *A) Western blotting analysis of the CD44 expression in 13 healthy (Black) and 31 MM patients (Red) serum samples. B) Determination of EVs size in Heathy, MGUS, SMM and Active MM patients by nanosight technology. C) Immunoblotting assay of CD44 expression in serum samples collected from 2 healthy donors (Black) and 3 MM patients (red) before and after EVs depletion. D) CD44 quantitation by Elisa of 1 healthy donor (#28) and 3 MM (#44, 27, 26) patient samples before and after EVs depletion.*

The quantification of the circulating CD44 was then preformed in 202 newly diagnosed MM serum samples and 13 healthy controls (data not shown). The results (Fig. 18) showed a high variability of circulating CD44 in MM patients, with no visible trend as compared to the analyzed 13 healthy controls. Also, the differences in average of CD44 levels between MM patients (143.0 ng/ml) and healthy donor (166.8 ng/ml) was deficient in statistical significance. However, MM patients showed a wider range of CD44 levels (6.43-637.51ng/ml) as compared to the range of the normal controls (235.69-122.32 ng/ml).

Matching the results on CD44 with the clinical data of the patients, the circulating CD44 in serum isolated from the peripheral blood, for the majority carried by the EVs, correlated with the ISS stage (p=0.0049), the percentage of bone marrow plasmacells

(p=0.038), and 2 prognostic factors: β_2-microglobulin (p=0.0136) and creatinine (p <0.0001) [239].

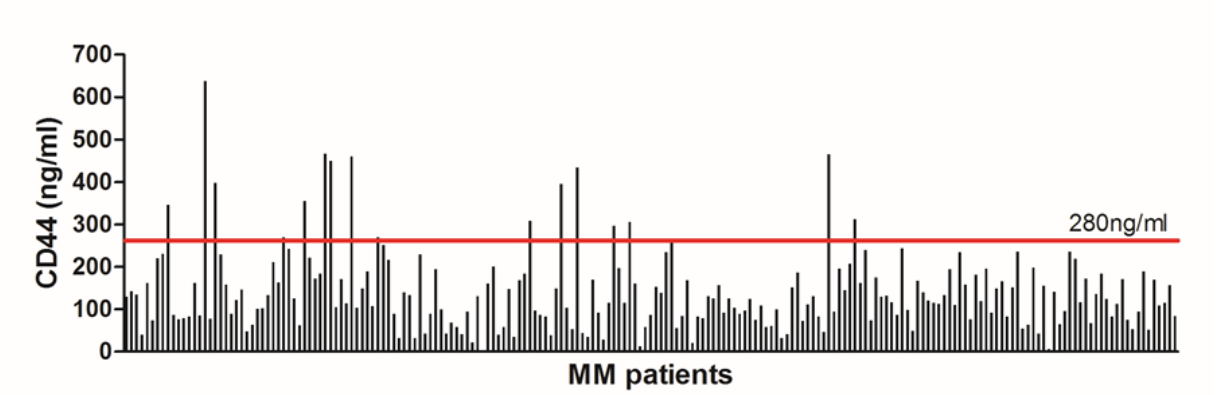

	ISS Stage	β_2-microglobulin	Creatinin	% BM plasmacells
Number of XY Pairs	163	170	202	161
p value (two-tailed)	0.0049	0.0136	<0.0001	0.038
p value summary	**	*	***	*

Fig. 18. Circulating CD44 in peripheral blood of newly diagnosed Multiple Myeloma patients. *Above) measurement of CD44 in plasma samples collected from 202 MM newly diagnosed patients. Below) statistical correlations between circulating CD44 and clinical data.*

Outcome prediction is mostly based on the International Staging System (ISS) and the presence of specific fluorescent *in-situ* hybridization abnormalities. However, additional biomarkers are necessary for a better estimation. To address this question, we extended the measurement of the serum CD44 levels to a larger cohort of newly diagnosed 233 patients who were uniformly treated and followed, correlating serum CD44 levels with clinical outcome to test their prognostic impact in a multivariate model [240]. We classified these patients in two groups, with higher (or equal) and lower than 280ng/ml CD44 levels. Among the newly diagnosed patients analyzed in a multivariate model for CD44, 87 died during the follow up with a five-year overall survival of 56.6% (95% CI: 44.8%-66.8%). Moreover, an increased risk of death was associated with augmented ISS stage, elevated β_2-microglobulin and high CD44 levels in serum. Additionally, the risk of death increased significantly when CD44 was greater than the maximum value of 280ng/mL after adjusting for age and stage (ratio: 3.00, 95% CI: 1.36-6.45). (Fig. 19). These data indicate the potential of MM-EVs as biomarkers cargo,

the role of the circulating CD44 as a new prognostic factor in MM and its importance for tumor survival.

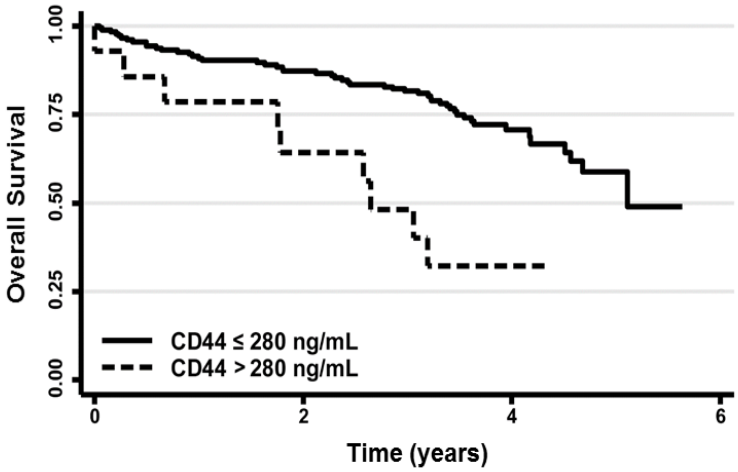

Baseline Characteristic	HR	95% CI	p-value
ISS Stage			0.020
I	1.00		
II	2.16	0.92-5.09	
III	3.38	1.42-8.04	
Isotype			0.305
BJ	1.00		
IgA	1.73	0.72-4.15	
IgG	1.16	0.51-2.63	
FISH Risk			0.382
high	1.00		
low	0.77	0.44-1.38	
β_2-microglobulin			0.048
< 3.5	1.00		
3.55-5.5	1.51	0.74-3.11	
≥ 5.5	2.33	1.19-4.58	
CD44			< 0.001
≤ 280 ng/mL	1.00		
> 280 ng/mL	3.82	1.85-7.91	
Creatinine			0.252
< 1.4	1.00		
≥ 1.4	1.41	0.78-2.55	

Fig. 19. Circulating CD44 and Overall Survival in MM. *Kaplan and Meyer representation of the OS in MM patients shared between low (<280ng/ml) and high (≥280ng/ml) circulating CD44. Table represent the statistical multivariate analysis for the overall survival.*

4.5 In vitro CD44 expression in MM

To support the importance of the CD44 in Multiple Myeloma, in 2014 Bjorklund et al. published a paper where the strong association between Dexamethasone-Lenalidomide resistance and CD44 expression in MM has been clearly demonstrated for the first time [241].

In preparation to the investigation of drugs combination for improving the drug resistance sensitivity in MM, I screened by flow cytometry the CD44 expression on the surface of twelve MM cell lines. The results showed a heterogeneous CD44 expression between different cell lines (Fig. 20). In particular, RPMI8226 and L363 have only traces of superficial CD44 while MM.1S, H929 and MM.1R were the cell lines showing the highest expression of CD44. Notably, the majority of the MM cell lines tested are sensitive to Dexamethasone, and MM.1R, which is the most resistant is also the one with the highest CD44 expression.

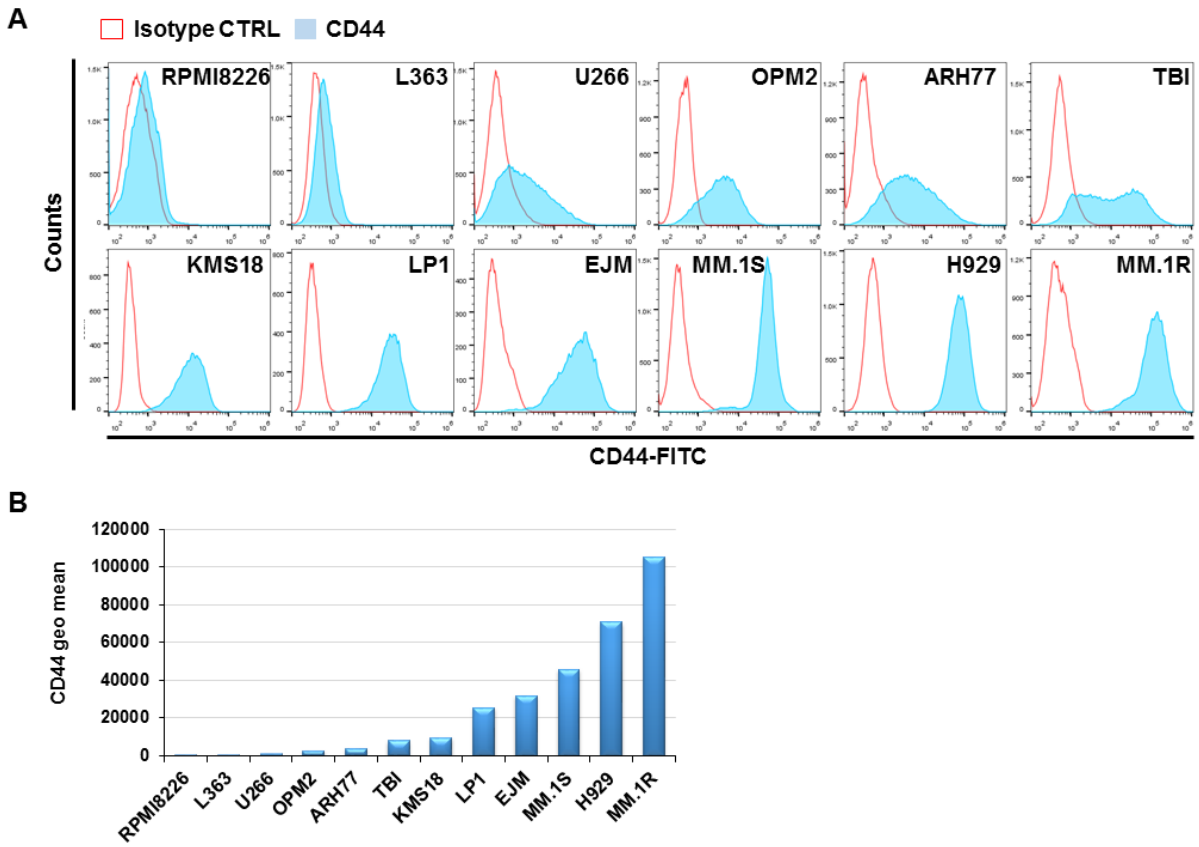

Fig. 20. CD44 expression in MM cell lines. *A) Flow cytometry analysis of the CD44 expression in 12 different MM cell lines. B) CD44 geo mean normalized by the isotype control.*

4.6 HDACi AR42 promotes histone acetylation and apoptosis in MM

To test *in vitro* the efficacy of the pan-HDAC inhibitor AR42 in Multiple Myeloma, I used sub lethal and clinically achievable concentrations of AR42 (0.1-0.2μM for up to 24h) to study the changes in Histone acetylation and the apoptosis inducement in MM.1S cells. Under these conditions, hyperacetylation of histones 3 and 4 was detected (Fig. 21A), but apoptosis after 24h of treatment (measured by AnnexinV-PI staining and flow cytometry) was not relevant (Fig. 21B). The experiment was then repeated on several MM cells lines with different concentrations of AR42 and 48 hour of incubation. As already reported for other cancers, including B-cell malignancies [242], an *in vitro* apoptotic activity was observed in MM cells treated with AR42 (as compared to SAHA) after 48h of treatment (Figure 21C) and the amount of apoptosis in other MM cell lines showed a dose dependent apoptotic activity after 48h of treatment (Fig. 21D).

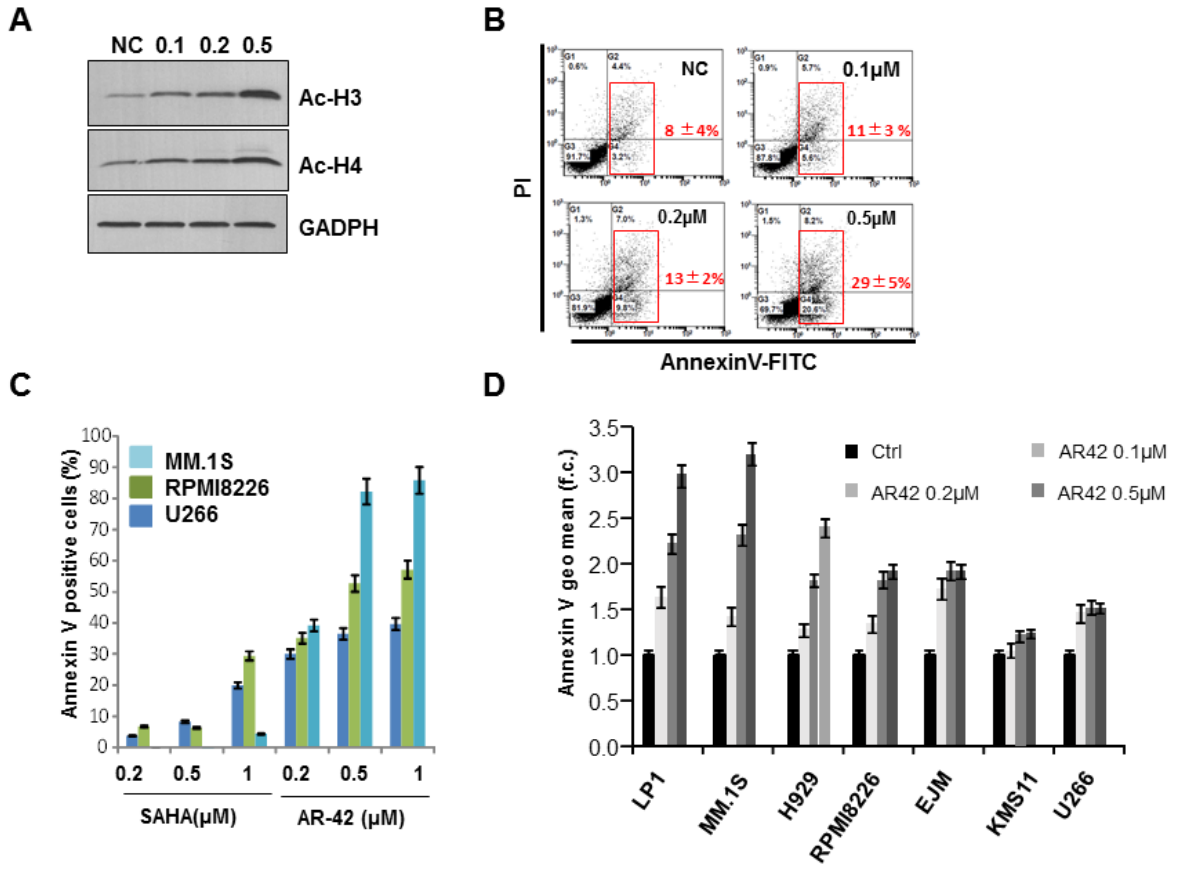

Fig. 21. AR42 induces Histone hyper-acetylation and apoptosis in MM. *A) Acetylated H3 and H4 protein form assessed by western blotting in MM.1S cells after 24h of treatment with AR42. GAPDH was used al loading control. B) AnnexinV-PI measure by flow cytometry on MM.1S cells treated with AR42 for 24h. C) Percentage of MM cells positive to AnnexinV after treatment with AR42 for 48h. D) AnnexinV expression assessed by flow cytometry in different MM cell lines after 48h of AR42 treatment as indicated. Data are expressed as fold change compared to the untreated control.*

4.7 In vitro and in vivo CD44 downregulation by HDACi AR42 in Multiple Myeloma

Based on the strong immunomodulatory activity associated with classical pan-HDACi [243], we investigated if AR42 treatment was also able to alter immunology-related gene networks in MM cells. The expression of 511 human genes was analyzed in MM.1S cells after 24h of treatment with AR42, using nCounter technology. Unsupervised hierarchical clustering analysis identified two distinct branches corresponding to treated and untreated cells (Fig. 22), and the expression of several immunology-related genes were strongly altered by AR42 (genes with altered expression after AR42 treatment and p value <0.0001 are listed in Table 2).

Interestingly, CD44 was one of the most significantly downregulated gene upon treatment ($p<0.001$). As already discussed, we decided to focus our investigation on the regulation of the CD44 expression based on its involvement in cell adhesion mediated drug resistance (CAM-DR) [151,244,245], in particular to Lenalidomide [241] in MM. The result obtained with nCounter was validated by q-RT-PCR, confirming that CD44 mRNA levels were significantly downregulated by AR42 in a dose-dependent manner as compared to vehicle control (DMSO) (figure 22B). The downregulation of CD44 was also demonstrated by Western blotting (Fig. 22C) and flow cytometry (Fig. 22D) in different MM cell lines with detectable CD44 levels. Furthermore, as shown in Figure 22E and F, we found that AR42 has a stronger capacity to downregulate CD44 as compared to Vorinostat (SAHA, first pan-HDACi FDA approved), when the drugs were used at comparable IC_{50} concentrations (AR42 0.2μM, SAHA 1.0μM).

To investigate if the AR42 treatment could affect CD44 expression *in vivo*, our group has created a xenograft MM mouse model by subcutaneous injection of $1x10^7$ MM.1S viable cells into the right flank of 12 NOD-SCID mice. After three weeks, 8 mice that developed a tumor of comparable size (250±60 mm^3) were selected and randomly divided into 2 groups. One group of mice (n=4) was intra-peritoneally injected with 25mg/kg AR42, while the second group (n=4) was treated in the same way with vehicle control (8% DMSO in PBS, NC). The treatment was performed twice within one week (on Monday and Wednesday). As AR42 efficacy in cancer has been previously reported in preclinical mouse studies [242], to avoid tumor size reduction, mice were euthanized 2 days after the second injection. At this stage the tumors, still comparable in size between experimental animal groups (Fig. 23A), were excised and used for CD44 immunohistochemistry (IHC) analysis, while the serum was collected and used for CD44 ELISA assays. IHC of tumor sections revealed that the mice treated with AR42 exhibited lower CD44 staining compared with the control group (Fig. 23B) and the circulating CD44 measured in serum samples reduced after AR42 treatment (Fig. 23C). Taken together, these data demonstrate that AR42 induces CD44 downregulation in MM either *in vitro or in vivo*.

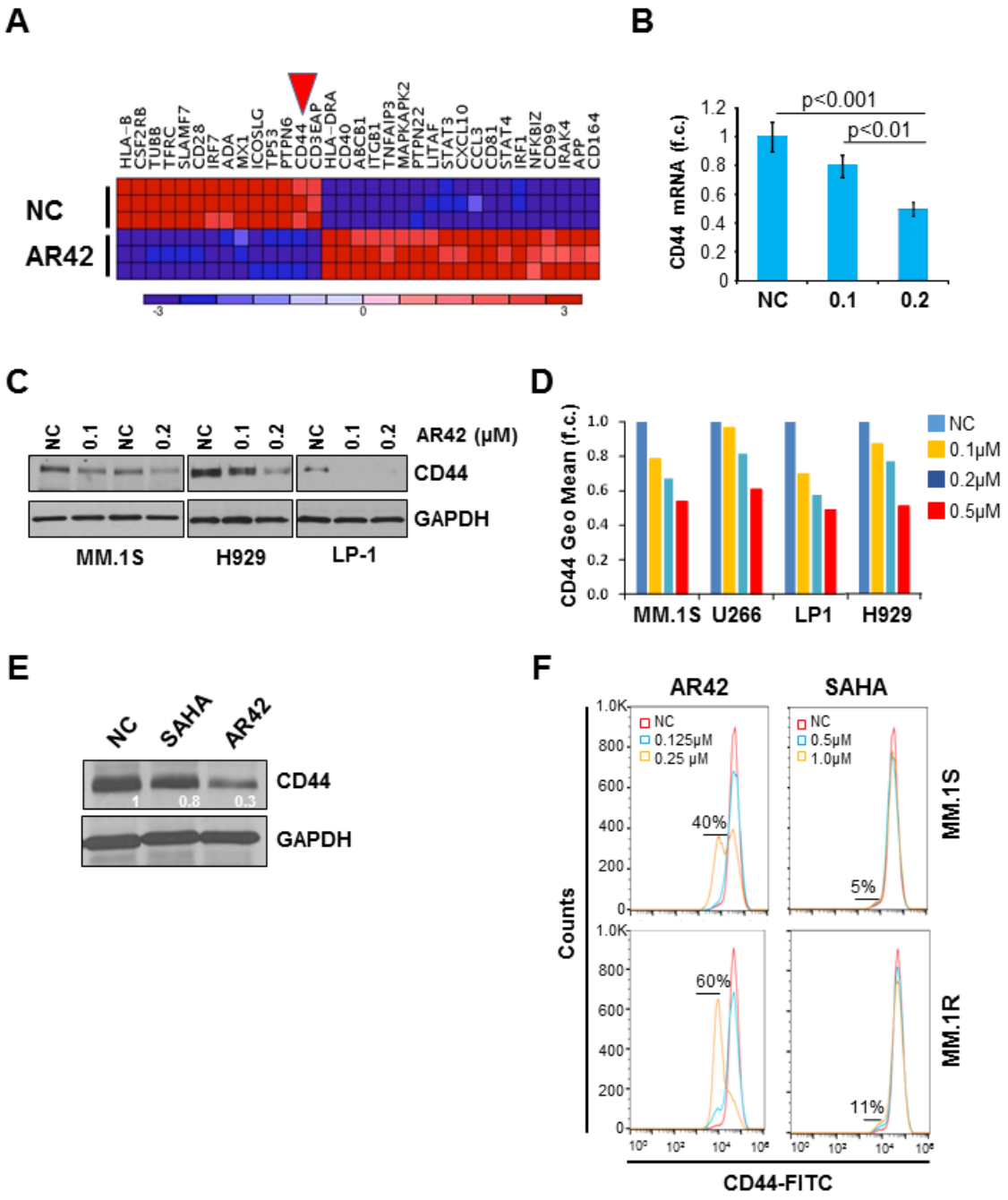

Fig. 22. AR42 induces CD44 downregulation in vitro in MM. *A) Dendrogram of the unsupervised Hierarchical clustering analysis of nCounter® GX Human Immunology assays in MM.1S cells treated with 0.1μM AR42 for 24h. B) CD44 mRNA expression measured by qRT-PCR in RNA from MM.1S cells treated for 24h with 0.1 or 0.2μM AR42. C) CD44 protein expression in MM.1S, H929, and LP1 cells treated with AR42 at 0.1 and 0.2μM for 24h. D) CD44 downregulation analyzed by flow cytometry in MM cell lines after 0.1, 0.2, and 0.5μM AR42 treatment for 48h. Data are expressed as geo mean fold change compared to the untreated control. E) CD44 expression evaluated by immunoblotting in MM.1S cells treated with 1μM SAHA or 0.2μM AR42 for 48h. White numbers indicate fold change of the densitometric analysis of the CD44 expression compared to the untreated control (NC). F) CD44 expression measured by flow cytometry in MM.1S and MM.1R cell lines after treatment with 0.125, 0.25μM AR42 or 0.5, 1μM SAHA for 48h. C) E) GAPDH was used as a loading control.*

Gene ID	log2_Fold Change AR-42 vs. Ctrl
IRF7	-4.15
CD3EAP	-3.60
ICOSLG	-2.09
TFRC	-1.12
MX1	-1.04
CSF2RB	-1.02
PTPN6	-0.93
ADA	-0.75
TUBB	-0.73
TP53	-0.63
SLAMF7	-0.60
CD44	-0.50
CD28	-0.38
HLA-B	-0.10
HLA-DRA	0.14
APP	0.17
CD164	0.33
CD99	0.41
IRF1	0.51
STAT3	0.53
TNFAIP3	0.60
LITAF	0.64
ITGB1	0.79
MAPKAPK2	0.85
IRAK4	0.89
CCL3	1.19
NFKBIZ	1.43
STAT4	1.95
PTPN22	2.20
CD40	2.32
CXCL10	2.49
CD81	5.44
ABCB1	5.57

Table 2. Immunology-related genes differentially expressed in MM.1S cells after AR-42 treatment. *Unsupervised hierarchical clustering analysis of nCounter® GX Human Immunology assays on MM.1S cells treated with AR42 0.1μM for 24h. Data are represented as immunology-related gene-expression fold change over control with p value <0.0001.*

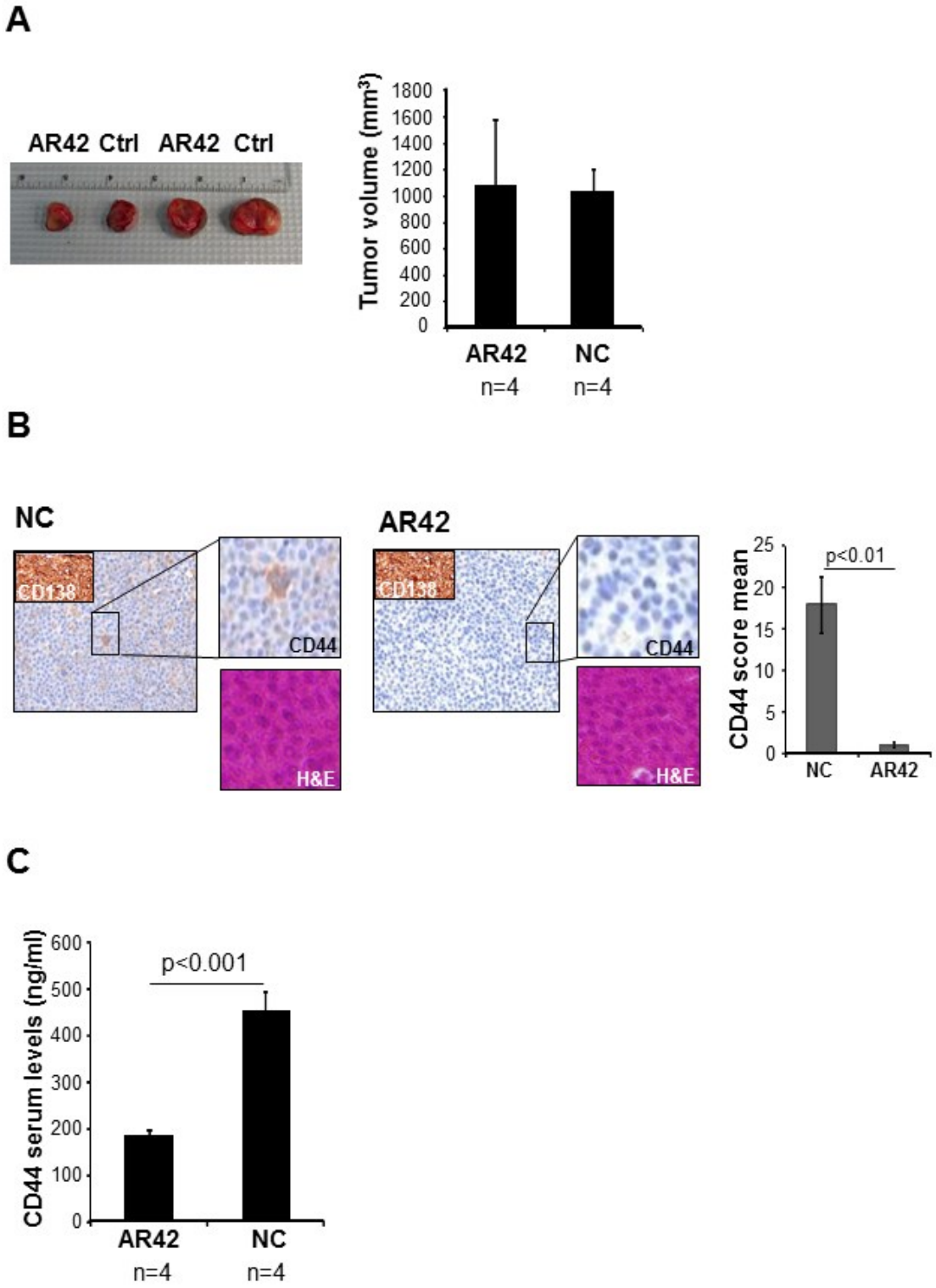

Fig. 23. AR42 downregulates CD44 in vivo. *A) 4 mice/group with comparable subcutaneous tumor size (250±60 mm³) were treated 2 times (every 48h) with 25mg/kg AR42 or DMSO by IP injection: after 2 days tumors were collected and measured. B) CD44, CD138 and H&E staining of tumor sections after AR42 or vehicle treatment. On the right side CD44 score based on the brown intensity. C) Circulating CD44 measurement in serum sample collected from mice after AR42 or vehicle treatment.*

4.8 AR42 induces CD44 downregulation through miR-9-5p and IGF2BP3

We hypothesized that AR42 could transcriptionally activate the promoter(s) of miRNAs that regulate CD44 expression. To address that, we used a reporter construct in which the 3' untranslated region (UTR) of CD44 (1.3 kb) was cloned downstream of the SV40 promoter-driven luciferase gene and we transiently transfected the resulting reporter plasmid into MM.1S cells. Additionally, an empty reporter construct was used (EV) as negative control (NC). We demonstrated that incubation with 0.2μM AR42 for 24 hours promoted nearly 35% of decrease in luciferase activity, as compared with untreated controls (figure 24A). Since RNA ribonuclease Drosha is extremely important and necessary during the initial steps of microRNA processing [246], we tested the effect of Drosha knock-down on CD44 expression using specific siRNA. CD44 protein expression augmented almost 2-fold when the microprocessor protein Drosha was silenced in MM cells (figure 24B). Therefore, these results support the hypothesis that the CD44 downregulation induced by AR42 is mediated by CD44 3'UTR and it may involve upregulation of microRNA(s).

To identify the miRNAs potentially influenced by the AR42 treatment in MM, we performed a full-spectrum analysis of miRNA levels using NanoString technology [247] with a set of probes to test the expression of more than 800 human miRNAs. The array analysis of global miRNA expression was performed on RNA from MM.1S cells grown in the presence or absence of AR42 at different concentrations (0.1 and 0.2μM) for 24 hours. Data were then used to generate an unsupervised hierarchical clustering analysis that produced a dendrogram of segregated miRNAs based on treatment and dose (figure 24C). We found that 45 miRNAs were significantly differentially expressed between AR42 treated and untreated cells, and between them, 25 were downregulated more than 2-fold and 20 were upregulated (Table 3). Since we were interested in defining the mechanism by which AR42 was able to reduce CD44 expression via microRNA(s), we focused our attention on the miRs upregulated by the treatment. Stem-loop qRT-PCR (qRT-PCR) analyses on RNA isolated from various MM cell lines (MM.1S and LP1) revealed that *miR-9-5p* was significantly upregulated in a dose-dependent manner (figure 24D).

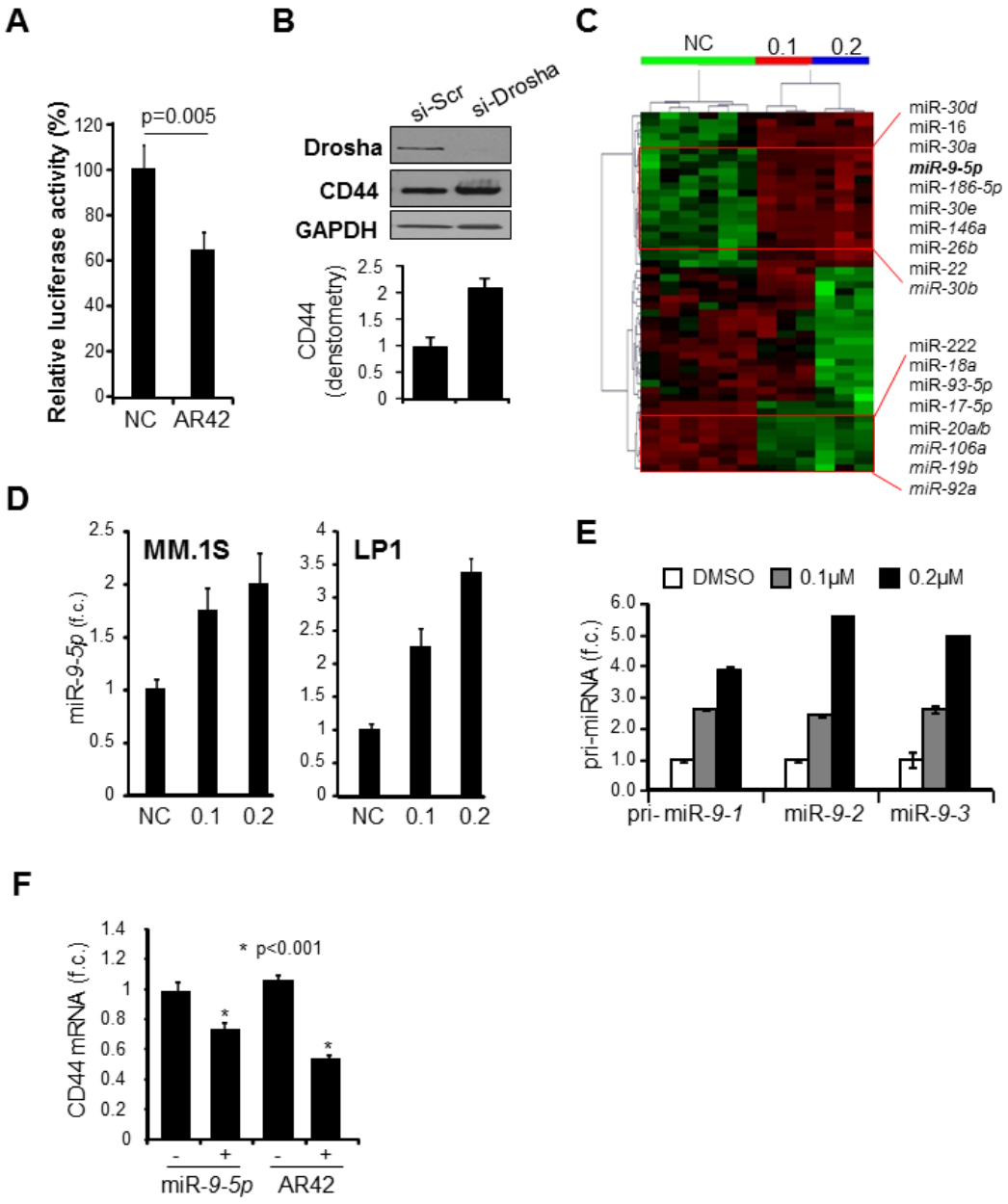

Fig. 24. AR42 treatment induce miR-9-5p upregulation. *A) Luciferase gene reported assay in MM.1S cells transiently transfected with pGL3-CD44 3'UTR construct and treated with 0.2μM AR42 for 24h, or vehicle (NC). B) RNA silencing for Drosha (si-Drosha) in MM.1S cells for 48h. Drosha and CD44 expression has been assessed by immunoblotting. GAPDH was used as loading control. C) Unsupervised hierarchical clustering analysis of miRNA expression in MM.1S cells treated with 0.1 and 0.2μM AR42 for 24h using NanoString technology. Indicated are a selection of most up- (upper) and down- (lower) regulated miRNAs. D) miR-9-5p expression by qRT-PCR in MM.1S and LP1 cells after treatment with AR42 (μM) for 24h. E) qRT-PCR of pri-miR-9-1, 9-2, 9-3 after AR42 treatment (μM) for 24h on MM.1S cells. F) U266 cells transfected with miR-9-5p, or negative control miR precursor, for 48h and the expression of CD44 mRNA assessed by qRT-PCR. U266 treated for 48h with 0.2μM AR42, or negative control were also included.*

Human *miR-9-5p* is encoded by three distinct genomic loci, primary *(pri) -miR-9-1* on chromosome 1 (q22), *pri-miR-9-2* on chromosome 5 (q14.3), and *pri-miR-9-3* on chromosome 15 (q26.1). First of all I wanted to assess if there was a specific locus accountable for *miR-9-5p* up-regulation in response to AR42. Quantitative RT-PCR showed dose dependent changes in all primary transcripts of *miR-9-5p* in MM.1S cells treated with AR42, compared to the untreated control, indicating that all *pri-miR-9* loci contribute to the increase of *miR-9-5p* expression after AR42 treatment in MM cells (Fig. 24E). Based on these findings, we hypothesized that AR42 might regulate the CD44 expression through the upregulation of *miR-9-5p.* To address this question we performed a bioinformatic search throughout the most common target prediction algorithms (Target Scan [248], Pictar [249], and miRDB) to determine the presence of *miR-9-5p* binding site(s) in CD44 3'UTR, but there were no evidences supporting the targeting. Also, none of the microRNAs upregulated by AR42 identified in our NanoString assay were predicted to bind to CD44 3'UTR. Consequently, we considered that *miR-9-5p* might downregulate CD44 expression in an indirect manner. To test this hypothesis, we transiently transfected U266 cells with *miR-9-5p* precursor, or scramble control, and measured CD44 mRNA expression by qRT-PCR after 48 hours. Figure 24F shows that in U266 cells transfected with *miR-9-5p* the CD44 mRNA expression was around 30% lower than the control. Although the downregulation was modest, it was statistically significant with a p value <0.001. As positive control, cells treated with AR42 0.2μM for 48 hours showed a significant reduction of CD44 mRNA expression, compared to the untreated control.

Subsequently, we tested the hypothesis that CD44 downregulation induced by AR42 might involve other molecules such as RNA-binding proteins. In fact, it has been previously reported that CD44 mRNA stability can be regulated by the RNA-binding proteins IGF2BP1 and IGF2BP3 [250] and their expression is strongly related to CD44 levels in other forms of cancer [251].

Despite the preliminary studies on RNA binding proteins and CD44, using the $STRING_{10}$ bioinformatic tool (browser for known and predicted protein-protein Interactions) we found that CD44 strongly interacts with IGF2BP3 (Fig. 25A), but there were no evidences of interaction with IGF2BP1.

microRNA_ID	*0.1μM* vs. *NC*	*Adjusted p-values (0.1μM vs. NC)*	*0.2μM* vs. *NC*	*Adjusted p-values (0.2μM vs. NC)*
hsa-miR-1973	11.45	1.13E-04	4.87	1.41E-04
hsa-miR-342-3p	9.74	1.75E-03	9.08	1.20E-04
hsa-miR-4516	8.09	1.94E-03	9.30	6.48E-05
hsa-miR-4284	7.29	2.20E-02	2.96	4.25E-02
hsa-miR-664-3p	6.06	6.53E-03	8.00	1.48E-04
hsa-miR-4485	5.92	2.18E-02	4.49	4.99E-03
hsa-miR-30a-5p	5.46	1.49E-02	4.65	1.91E-03
hsa-miR-575	5.28	1.51E-02	5.28	1.09E-03
hsa-miR-22-3p	5.22	9.03E-04	4.98	5.73E-05
hsa-miR-494	4.44	1.51E-02	5.22	5.08E-04
hsa-miR-630	4.19	1.64E-04	2.58	1.93E-04
hsa-miR-30d-5p	3.65	1.43E-03	2.83	3.98E-04
hsa-miR-146a-5p	2.70	1.13E-04	2.83	3.18E-06
hsa-miR-26b-5p	2.67	1.28E-05	2.73	2.42E-07
hsa-miR-320e	2.58	2.14E-02	2.14	6.35E-03
hsa-miR-361-3p	2.43	4.27E-03	2.67	1.31E-04
hsa-miR-30e-5p	2.27	1.30E-03	2.12	1.32E-04
hsa-miR-186-5p	1.95	1.30E-02	2.58	6.35E-05
hsa-miR-9-5p	1.82	4.93E-02	2.00	1.84E-03
hsa-miR-30b-5p	1.68	3.43E-03	1.43	2.84E-03
hsa-miR-548aa	0.46	1.09E-02	1.52	2.75E-02
hsa-miR-1244	0.45	3.45E-02	1.25	3.08E-01
hsa-miR-93-5p	0.44	1.12E-04	0.39	1.16E-06
hsa-miR-19b-3p	0.44	7.53E-05	0.49	6.25E-06
hsa-miR-20a-5p+20b-5p	0.41	1.13E-04	0.45	1.16E-05
hsa-miR-200c-3p	0.40	3.26E-03	0.91	5.73E-01
hsa-miR-365a-3p	0.39	3.26E-03	0.94	7.27E-01
hsa-miR-301a-3p	0.36	2.72E-04	0.49	2.04E-04
hsa-miR-18a-5p	0.36	7.75E-05	0.47	2.91E-05
hsa-miR-644a	0.35	2.58E-02	1.59	1.01E-01
hsa-miR-548ah-5p	0.33	3.06E-02	2.32	1.21E-02
hsa-miR-106a-5p+17-5p	0.33	5.10E-07	0.36	3.46E-08
hsa-miR-423-3p	0.33	1.51E-02	1.20	4.64E-01
hsa-miR-92a-3p	0.28	2.03E-04	0.33	2.77E-05
hsa-miR-4455	0.27	3.07E-02	1.18	6.35E-01

hsa-miR-223-3p	0.24	2.66E-02	1.22	5.83E-01
hsa-miR-335-5p	0.24	2.12E-02	1.57	2.05E-01
hsa-miR-4454	0.23	2.82E-02	0.78	5.24E-01
hsa-miR-720	0.21	3.45E-02	0.74	4.66E-01
hsa-miR-193b-3p	0.20	3.40E-04	1.43	1.07E-01
hsa-miR-450a-5p	0.18	3.26E-03	0.93	8.17E-01
hsa-miR-411-5p	0.17	5.84E-04	1.46	1.35E-01
hsa-miR-221-3p	0.13	2.76E-04	0.53	3.16E-02
hsa-miR-3676-3p	0.07	1.69E-05	0.60	3.89E-02
hsa-miR-126-3p	0.07	2.10E-07	0.30	3.77E-06

Table 3. mRNAs deregulated by AR42 treatment in MM cell lines. *Unsupervised hierarchical clustering analysis of mRNAs expression in MM.1S after 24h of treatment with 0.1 and 0.2μM compared to control cells treated with DMSO.*

To support the String$_{10}$ prediction, a microarray with a human genome U133 GeneChip was run on MM.1S samples treated with AR42 0.2μM for 48 hours. After bioinformatic analysis, 7903 gene expressions resulted significantly altered ($p<0.05$) after AR42 treatment. Among the most significant genes differentially expressed (4701 genes with $p<0.0001$, 1792 upregulated and 2678 downregulated), the downregulation of IGF2BP3 was confirmed (Fig. 25B) but no evidence of changes in IGB2BP1 gene expression was observed. Although there were no proof on the involvement of IGF2BP1, we decided to include it in our further investigations.

To evaluate if *miR-9-5p* could perhaps target both RNA binding proteins, we used Targetscan [248], Pictar [249], and RNA22 [252] web tools and we identified a highly conserved consensus sequence for *miR-9-5p* in the 3'UTR of IGF2BP3, and a lower target score site in the 3'UTR of IGF2BP1 (Fig. 25C). Transient expression of *miR-9-5p* precursor into L363 cells was used to validate the capacity of *miR-9-5p* to target the two RNA binding proteins, as compared to miR-16 precursor used as control (upregulated after AR42 treatment in MM.1S cells). Western blotting analysis of CD44, IGF2BP1 and IGF2BP3 expression indicated that *miR-9-5p* successfully targeted CD44 and IGF2BP3 but not IGF2BP1, while *miR-16* had no influence on the investigated protein expressions, as showed in Figure 25D.

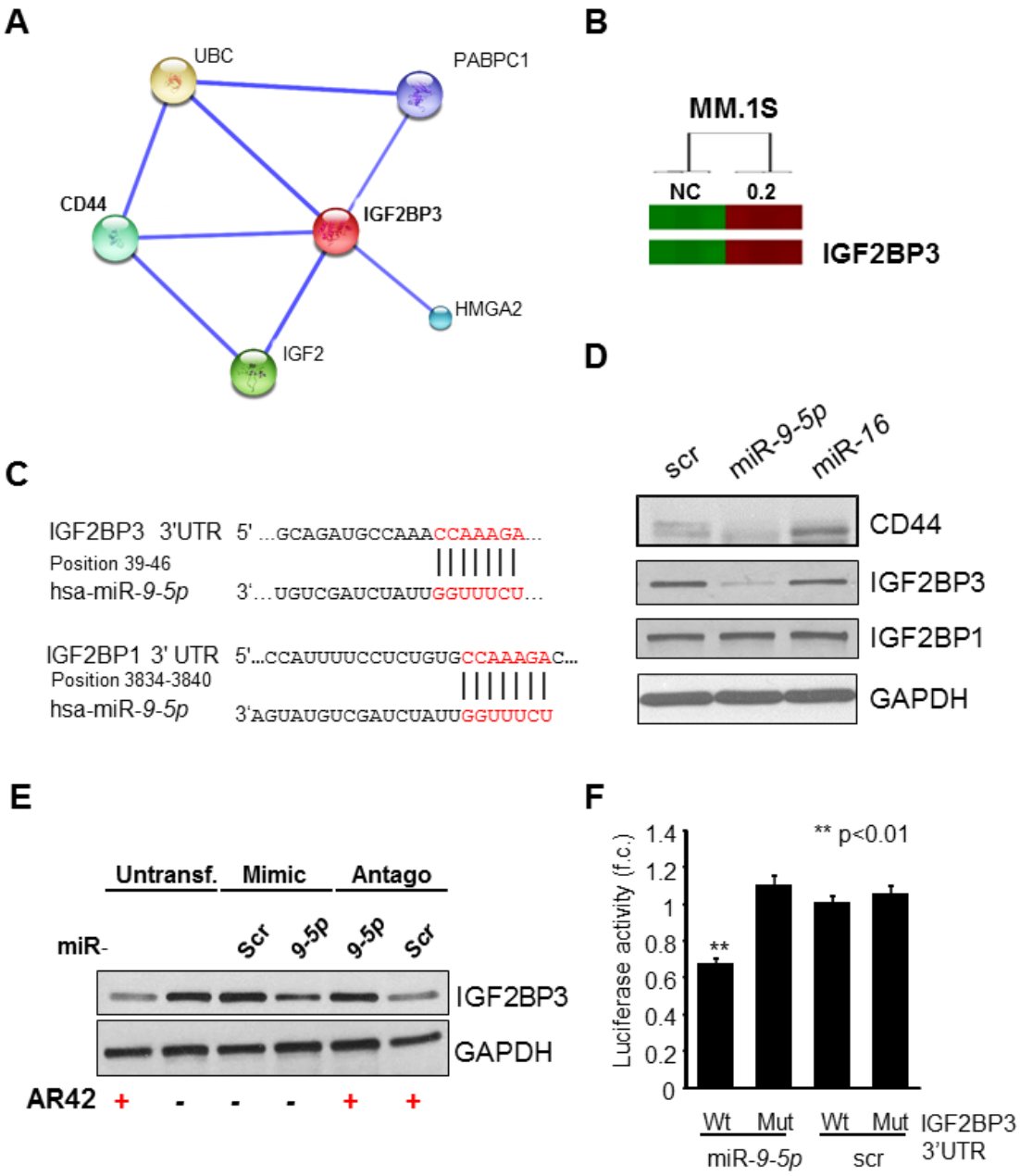

Fig. 25. miR-9-5p targets IGF2BP3, the main CD44-RNA stabilizer. *A) Image generated by the STRING$_{10}$ analysis of the functional interaction network between CD44 and IGF2BP3. B) Human 2.0ST microarray conducted on MM.1S samples after 48h of treatment with AR42 0.2μM and IGF2PB3 heatmap. p<0.0001. C) IGF2BP3 and IGF2BP1 3'UTR contains seed sequence for miR-9-5p (indicated in red). D) Transient expression of miR-Scr, -9-5p or -16 in L363 cells and immunoblotting analysis of the CD44, IGF2BP3 and IGF2BP1 expression after 48h. E) Transient expression of mimic mir-Scr and miR-9-5p or anti-miR-Scr and anti-miR-9-5p in L363 cells and IGF2BP3 expression by western blotting after treatment with AR42. D) E) GAPDH was used as loading control. F) Luciferase gene reporter assay in HeLa cells transiently cotransfected with Wt or mutant pGL3-IGF2BP3 3'UTR construct and mimic miR-9-5p or mimic miR-Scr. Luciferase assay was performed 24h later and the results are expressed as fold change of Wt construct co-transfected with miR-Scr.*

To validate if the overexpression of *miR-9-5p* due to the AR42 treatment was leading to IGF2BP3 downregulation, we proceeded with the analysis of the IGF2BP3 expression in L363 cells after ectopic overexpression of mimic and *antago miR-9-5p* or *miR-Scr* (as control) and AR42 treatment. We found that L363 MM cells treated with AR42 (0.2μM) displayed lower level of IGF2BP3 [Figure 25E (line 1-2)] and *miR-9-5p* RNA mimic decreased IGF2BP3 compared to the control sequences [Figure 25E (line 3-4)]. Moreover, knockdown of *miR-9-5p* by *anti-miR-9-5p* after 24 hours of AR42 treatment increased the level of IGF2BP3 protein as compared to anti-scramble sequence (AS-Scr) and untransfected control (untransf.) [Figure 25E (lines 5-6)].

Data were further corroborated with Luciferase reporter assay. A portion of the IGF2BP3 3'UTR containing either the wild type (Wt) or mutated (Mut) *miR-9-5p* seed sequence was cloned into a pGL3-control luciferase vector. A significantly reduction of Luciferase activity was obtained only with the Wt 3' UTR in the presence of *mir-9-5p* (Fig. 25F), showing the high specificity of *miR-9-5p* for the targeting of the IGF2BP3 gene. Hence, our data showed unequivocally that IGF2BP3 was the direct target of *miR-9-5p*, and the downregulation of IGF2BP3 induced CD44 mRNA instability and subsequent degradation.

4.9 AR42 sensitize MM to Lenalidomide in vitro

Lenalidomide (Revlimid) is an immunomodulatory drug highly effective on MM [253] and other kinds of solid and hematological malignancies. *In vitro* Lenalidomide is able to induce apoptosis in cancer, to inhibit the bone marrow support mediated by the stromal cells and the angiogenesis. Moreover, in a recent milestone publication it has been also demonstrated the Revlimid ability to specifically promote the ubiquitination, mediated by ubiquitin E3 ligase Cereblon (CRBN) and degradation of the transcription factors Ikaros (IKZF1) and Ailos (IKZF3), two of the most important mediators of the proliferation in MM [254].

As stated before, CD44 has been associated to Lenalidomide-resistance mechanism in Multiple Myeloma [241]. Due to the capacity of the pan-HDACi AR42 to downregulate the expression of this important adhesion molecule (Fig. 22-25), we hypothesized that AR42 could also reduce the resistance to Lenalidomide in MM. To determine the combinatorial index between Lenalidomide and AR42, MM.1S cells were treated with

AR42 (0.1 or 0.2μM) in combination with different concentrations of Lenalidomide (Len 2.5 or 5μM) and the cell death rate of every combination was used for the determination of the combinatorial index (CI) with the Chou-Talalay method [255]. The obtained CI<1 indicated the synergism between the two drugs (Table 4) in killing the MM cells. Consequently, we decided to analyze the inducement of apoptosis in MM.1S cells after treatment with Lenalidomide, AR42 or the two drugs together (Fig. 26A). The combinatorial use of the two drugs increased apoptosis respectively of 4.9-fold (0.1μM AR42 and 2.5μM Lenalidomide) and 5.8-fold (0.1μM AR42 and 5μM Lenalidomide) after 48 hours of treatment with a boost every 24 hours, compared to the Lenalidomide alone (2.5 and 5μM). Based on the promising results on MM.1S, we focused our attention on the BM microenvironment, and bone marrow samples collected from 5 Lenalidomide-refractory (#1, 2, 3, 4,and 7) and 3 newly diagnosed MM patients (# 5, 6, and 8) were treated with 0.2μM AR42, 5μM Lenalidomide or with the combination of both drugs for 48 hours. After treatment, the samples were analyzed with a multiparametric flow analysis (illustrated in Fig. 26B). The results, showed in Figure 24C, substantially confirmed a synergistic effect on apoptosis inducement of the combination treatment rather than single agents on the subpopulation $CD38^{high}$-$CD138^{+}$ with statistical significance (p value <0.0001) in the combined drugs compared to the untreated samples (Fig. 26C). Notably, the BM subpopulation CD38-$CD138^{-}$ treated in the same way did not show any significant difference (Fig. 26D), to indicate the specificity of the treatment restricted to the BM subpopulation containing the majority of the MM plasmacells.

CI	AR42 (μM)	Len (μM)
0.52	0.1	2.5
0.45	0.1	5.0
0.48	0.2	2.5
0.43	0.2	5.0

Table 4. Combinatorial index. *WST-1 assay on MM.1S cells treated with the AR42, Lenalidomide (Len) or the combination of both drugs for 48h. The measure of the combinatorial index was determined using the Chou-Talalay method.*

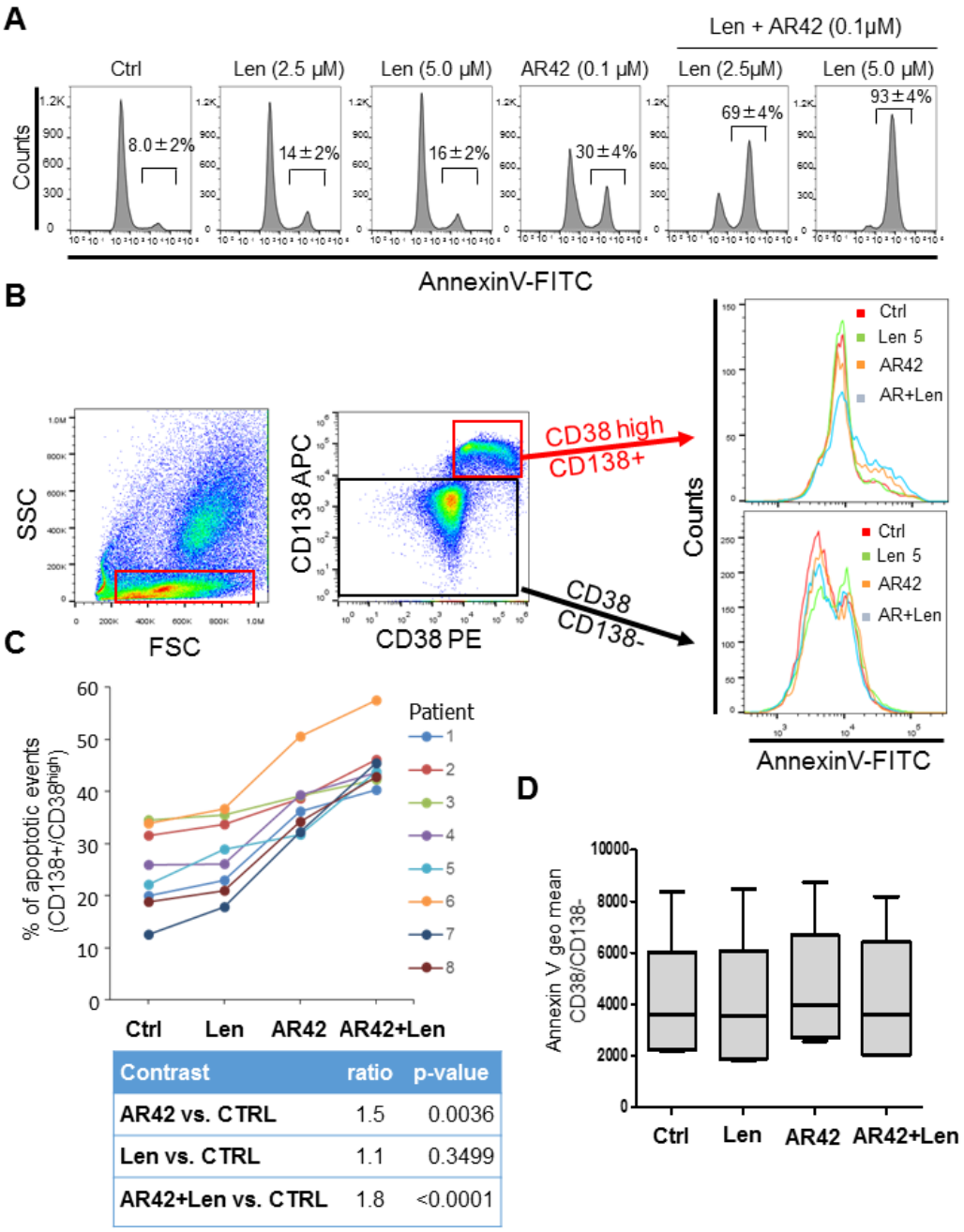

Contrast	ratio	p-value
AR42 vs. CTRL	1.5	0.0036
Len vs. CTRL	1.1	0.3499
AR42+Len vs. CTRL	1.8	<0.0001

Fig. 26. In vitro synergistic effect of AR42 in combination with Lenalidomide in MM. *A) AnnexinV expression by flow cytometry in MM.1S cells treated two times (every 24 hours), with Len (2.5 or 5.0μM), AR42 (0.1μM), or combination Len+AR42, as indicated. Values represent the average percentages of positive events ± SD. B) Scheme of analysis on BM samples by Flow Cytometry. BM cells from 8 MM patients were treated with vehicle control (Ctrl), 5μM Len, 0.25μM AR42, or the combination of both drugs for 48h. The percentage of apoptotic events were assessed into 2 subpopulations: CD38^{high}/CD138^{+} (MM plasmacells) and CD38/CD138^{-}. C) AnnexinV induction in CD38^{high}/CD138^{+} MM cells treated as described in (B). Data are expressed as % of AnnexinV positive events. D) Flow Cytometry evaluation of apoptosis in CD38/CD138^{-} BM population from the same MM patients, as in (C). Data are expressed as AnnexinV geo mean.*

Additionally, PBMCs collected from 3 healthy donors in the same experimental conditions did not show any significant induction of apoptosis, as shown in figure 27A. Finally, part of the whole BM samples were also analyzed for the CD44 expression by Flow Cytometry after 24 hours of AR42 treatment and the downregulation of CD44 was confirmed (Fig. 27B).

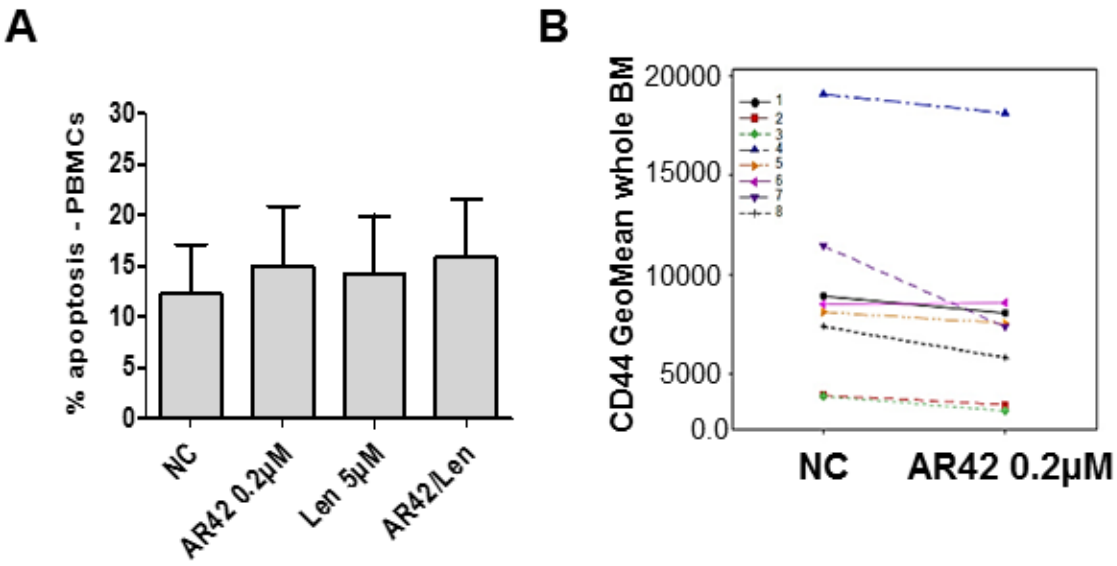

Fig. 27. Effect of AR42 in combination with Lenalidomide in Healthy and MM patients. *A) AnnexinV expression by flow cytometry in PBMCs collected from 3 healthy donors treated two times (every 24 hours), with Len (2.5 or 5.0µM), AR42 (0.1µM), or combination Len+AR42, as indicated. Values represent the average of percentages of positive events ± SD. B) Flow Cytometry analysis of the CD44 downregulation in whole BM collected from 8 MM patients (previously analyzed for apoptosis) treated for 24h with 0.2µM AR42. Results are expressed in CD44 Geo mean.*

4.10 AR42 sensitizes MM to Lenalidomide in vivo

To validate the *in vitro* efficacy of the combinatorial therapy on Multiple Myeloma, we decided to move to an *in vivo* MM mouse model. In synthesis, NOD-SCID mice (n=40) were intravenously injected with $5x10^6$ MM.1S-GFP$^+$/Luc$^+$ cells. After three weeks, mice with comparable tumor size were identified and distributed into 4 groups (5 animal/group): AR42, Lenalidomide, AR42/Len, and vehicle control (8% DMSO in PBS; VE).

To reduce the toxicity and mimic the clinical protocol (AR42 is in a Phase I clinical trial involving MM patients), mice were treated with Len (50mg/kg) or Vehicle (VE) by intraperitoneal injections daily, and AR42 (25mg/kg) or VE 3 times per week, for 3 weeks. Following the treatments, tumors appeared to be significantly shrinked or almost suppressed in all AR42/Len treated mice compared to the untreated control or single drugs (Fig. 28A and B). The amount of malignant plasma cells infiltrating the BM was measured by flow cytometry using a human anti-CD138 antibody. Data showed that the amount of malignant PCs were greatly reduced in the animals treated with the combination of AR42 and Lenalidomide, compared with the control group and the animals treated with the single drugs (Fig. 28C). Finally, to support our hypothesis, the survival study performed on 5 animals per group of treatment indicated a better survival (graph in Fig. 28D) with statistical significance (table in Fig, 28D) in those animals treated with the combination of AR42 and Lenalidomide compared to all the other treatments. Notably, the group of animals that benefited from the most effective pharmacological treatment, the combination AR42/Lenalidomide, were healthy with no sign of paralysis at the end of the study (Fig. 28D).

Taken together, the data from the *in vivo* study clearly demonstrated the AR42 ability to improve Multiple Myeloma sensitivity to the Lenalidomide, suggesting the use of drug combination AR42/Lenalidomide as a novel promising therapeutic strategy to overcome the MM drug-resistance especially in the bone marrow microenvironment.

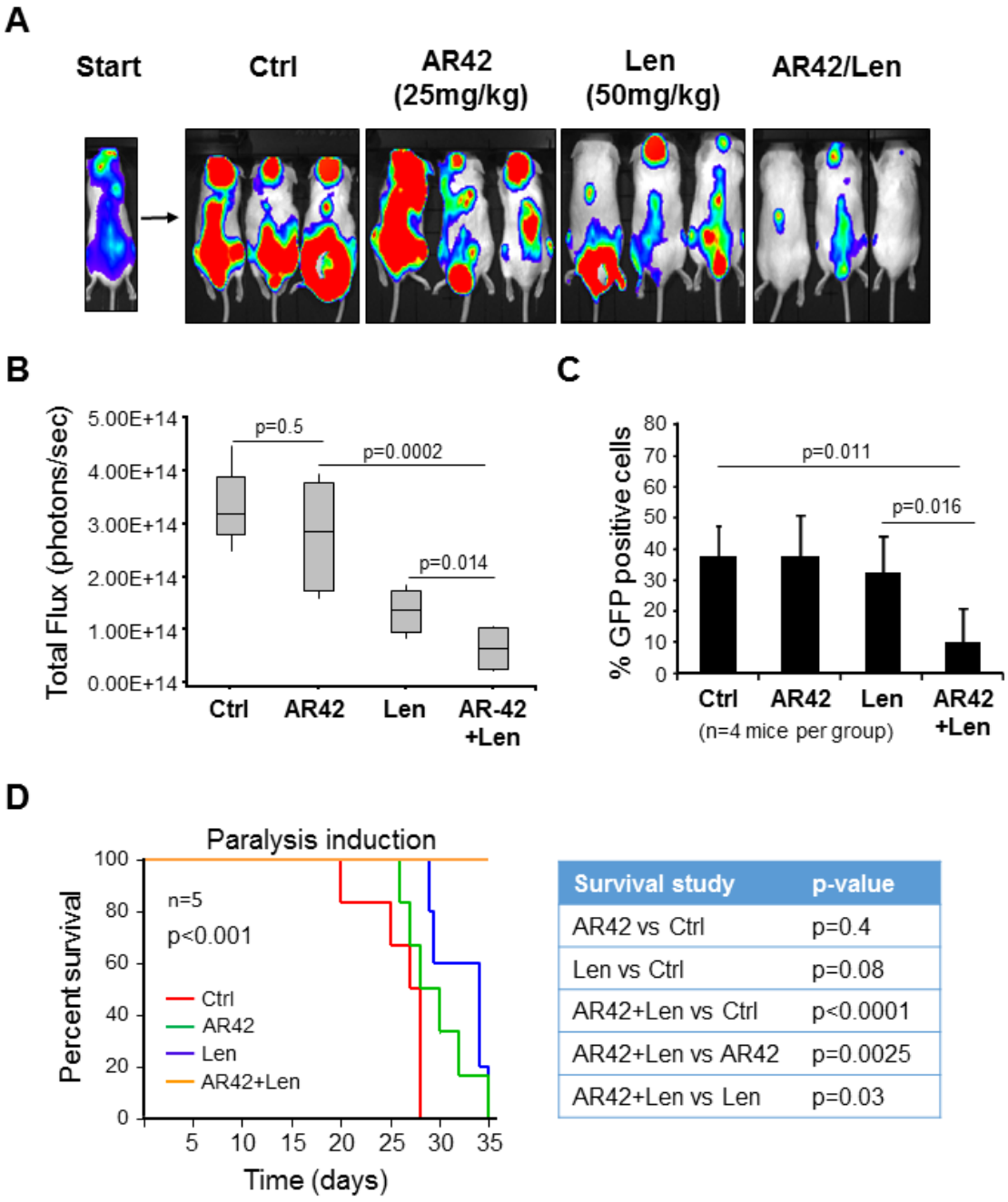

Survival study	p-value
AR42 vs Ctrl	p=0.4
Len vs Ctrl	p=0.08
AR42+Len vs Ctrl	p<0.0001
AR42+Len vs AR42	p=0.0025
AR42+Len vs Len	p=0.03

Fig. 28. In vivo synergistic effect of AR42 in combination with Lenalidomide in MM. *A) NOD-SCID mice engrafted with 5x10^6 MM.1S-GFP$^+$/Luc$^+$ cells and treated for 3 weeks with vehicle control (Ctrl), AR42 three times/week, Lenalidomide (Len) daily, or AR42/Len combination. Representative luminescence images are shown. B) The evaluation of the tumor progression in vivo has been assessed by Luminescence quantitation, data are expressed as average of tumor intensity/group. C) Flow cytometry analysis of the GFP intensity expressed by the MM cells in BM samples collected from the animals. Data expressed as percentage of GFP$^+$-MM cells in the BM sample. D) Kaplan-Meyer representative curves of the in vivo survival study; p values between different treatments are indicated in the table on the right side.*

CHAPTER 5. CONCLUSIONS

Given the poor outcome of MM, it is critical to intensify the efforts for defining molecular mechanisms of MM pathogenesis in order to find novel and more effective therapeutic strategies to treat this disease. Recently, beside the classical and well investigated inter-cellular interactions such as integrins and cytokines, cell-to-cell communication via extracellular vesicles, microvesicles, or exosomes has been widely recognized. A growing body of evidence points to EVs as possible prognostic biomarkers and potential therapeutics.

The primary purpose of this study was the characterization of multiple myeloma-derived extracellular vesiscles (EVs) in terms of size, protein contents and activity. All the MM-EVs analyzed, isolated either *in vitro* from different cell lines or *in vivo* from patients, appeared as a single, monodisperse population of vesicles, with a comparable size. The MM.1S vesicles were somewhat larger (average diameter of 177 nm) and had a slightly broader size distribution (standard deviation of 6.2 nm) compared to the U266 vesicles (average diameter of 138 nm and a standard deviation of 5.6 nm). Using the nanosight technology, we confirmed these results and we were also able to evaluate the size of circulating EVs in peripheral blood samples collected from healthy donors, and patients diagnosed for MGUS, SMM and active Multiple Myeloma. Likewise to the results obtained *in vitro*, in these set of samples the EVs size were very similar, but smaller compared to what obtained from the MM cell lines (the average of size was around 75nm).

Of extremely interest was the content of the Extracellular Vesicles secreted by MM. We made a complete proteomic analysis of the *in vitro* EVs and we found 356 different proteins in MM.1S-EVs and 337 in U266-EVs. The overlap of these data revealed 324 common proteins, 32 contained exclusively in MM.1S EVs and 13 in U266 EVs. The analysis of the common proteins carried by the two different kinds of MM-EVs indicated that the majority of them were involved in catalytic activity, structural activity, binding and metabolic processes. Based on these data, we hypothesized that the protein cargo carried by the EVs could have activity and biological effects on cellular targets. I showed

in this thesis that MM-EVs can promote MM proliferation and IL6 release in bone marrow stromal fibroblasts. IL6 is one of the most important cytokine for MM growth and survival in the BM microenvironment [28-32], suggesting one more time the supportive role of the tumor microenvironment in cancer. Moreover, we identified a cohort of enriched proteins in MM-EVs compared to the parent cells. Among them, we decided to focus our investigations on CD44, which was overexpressed in EVs. CD44 is an adhesion molecule already known for its fundamental role in keeping the cancer cells anchored to the extracellular matrix of the tumor microenvironment through the binding with Hyaluronic acid (HA) [116] and it has been largely associated to drug resistance mechanisms (CAM-DR) in several kinds of solid tumors [119-121]. One of the most important results were the demonstration of the strong presence of circulating CD44 in MM patients and the indication that CD44 was carried essentially by the circulating EVs. Remarkably, I also determined that CD44 levels were correlated with ISS stage and with the prognostic factor β2-microglobulin, thus proving that CD44 is a biomarker and a prognostic factor in MM. Of note, by selecting a cutoff of 280ng/ml, patients with CD44 levels lower than the cutoff showed a better overall survival than patients with higher CD44 levels. The importance of CD44 expression for drug resistance in MM has been highlighted in the past by the demonstration that CD44/HA interaction resulted in protecting dexamethasone-induced apoptosis [148] and recently, Bjorklund et al. [241] showed in myeloma the important role of the CD44 in resistance to Lenalidomide. Therefore, the adhesive interactions of multiple myeloma cells are important potential therapeutic targets. CD44 surface expression in several MM cell lines was extremely variable, but it is important to underline that the cell line most resistant to dexamethasone, MM.1R, was the one expressing the major number of CD44 molecules on the surface. These data prompted us to investigate deeply the mechanism of drug resistance mediated by CD44 and try to find an effecting strategy to overcome this resistance. AR42 is a novel pan-HDACi inhibitor that shows better capacity to induce apoptosis in MM cells compared to the FDA approved pan-HDACi vorinostat (SAHA). Despite the AR42 demonstrated efficacy in MM, treatment of MM patients with the therapeutic dose of AR42 as unique treatment is responsible for heavy side effects such as fatigue, diarrhea, and thrombocytopenia, which clearly constitute a limitation for its clinical use.

MM cells treated with sub lethal doses of AR42 and then subjected to nanostring analysis, showed a clear downregulation of CD44. We then hypothesized that CD44 downregulation was directly mediated by *miR-9-5p* upregulation (which was one of the most upregulated miRNA upon treatment), but we were not able to confirm this hypothesis. Although bioinformatics analysis of the predicted *miR-9-5p* targets indicated IGF2BP3 and IGF2BP1 as potential targets, microarray analysis of the MM cells after AR42 treatment showed that IGF2BP3 was the only one of the two RNA binding proteins to be highly downregulated, with statistical significance, after treatment. This RNA binding protein has a seed sequence complementary to *miR-9-5p* and it is a strong partner of the CD44, essentially serving as mRNA stabilizer.

We proved that IGF2BP3 (but nor IGF2BP1) was targeted by *miR-9-5p*, also demonstrating for the first time that treatment with AR42 provoked *miR-9-5p* upregulation, triggering a mechanism that ultimately led to IGF2BP3 degradation. The absence of the IGF2BP3 increased CD44 mRNA instability and further induced its degradation. Two possible strategies may be utilized to include anti-adhesion agents into MM therapeutic treatment. The first is the incorporation of anti-adhesion substances into current treatment protocols, based on their ability to enhance the chemosensitivity of MM cells, while targeting minimal residual MM cells by combinations of anti-adhesion molecules and anti-MM drugs is the basis of the second therapeutic approach. The discovery of the AR42 biological therapeutic mechanism, which involves the downregulation of the adhesion molecule CD44, suggested the evaluation of AR42 in combination with Lenalidomide to overcome the CD44-mediated drug resistance in MM and to increase the tumor death. *In vitro*, the combination AR42/Lenalidomide showed a synergistic effect with a reduction of MM proliferation and an enhanced inducement of apoptosis as compared to the apoptosis levels obtained with the single agents. Additionally, in bone marrow samples collected from 8 Multiple Myeloma patients, the CD38/CD138^{+} subpopulation showed higher level of apoptosis than the rest of the BM populations after AR42 treatment, to reinforce the specific anti-tumor activity against MM plasmacells. Also, AR42 treatment showed CD44 downregulation in MM-BM samples. These results were corroborated by our *in vivo* MM mouse xenograft model, in which AR42 treatment induced the CD44 downregulation in subcutaneous MM tumor mass. Furthermore, the combination

AR42/Lenalidomide on MM mouse model induced tumor shrink and better overall survival, compared to the single agents.

In conclusion, we demonstrated that Extracellular Vesicles secreted by Multiple Myeloma cells had biological activity on promoting the proliferation of MM cells, and the IL6 release from bone marrow stromal cells. Both effects are fundamental for the tumor growth and survival. Additionally, MM-EVs were enriched in CD44, an adhesion molecule highly expressed in MM cells resistant to the drug treatment. Remarkably, we discovered that the circulating CD44 was an important prognostic factor and MM patients carrying high levels of CD44 had a negative prognosis and adverse overall survival.

Treating the MM cells with sub lethal doses of AR42 allowed us to discover a therapeutic mechanism that led to the CD44 downregulation through *miR-9-5p* upregulation, IGF2BP3 downregulation, CD44 mRNA instability and degradation.

Finally, the use of AR42 in combination with Lenalidomide improved the multiple myeloma drug sensitivity either *in vitro* or *in vivo*, induced *in vivo* tumor reduction and a more favorable survival.

Data obtained in this thesis might support the therapeutic potential of the incorporation of anti-adhesion molecules into the clinical standard of care. Successful results in MM may pave the way to their use in other hematological malignancies, as well as other types of cancer, and open up new treatment directions focused on cellular adhesion.

.

CHAPTER 6. PUBLICATIONS DURING THE PhD

Part of the introduction, results, methods and conclusions of this thesis have been inspired or quoted verbatim from the following articles

1. Harshman S.W.*, **Canella A. ***, Ciarlariello P.D., Agarwal K., Branson O.E., Rocci A., Cordero H., Phelps M.A., Hade E.M., Dubovsky J.A., Palumbo A., Rosko A., Byrd J.C., Hofmeister C.C., Benson D.M., Paulaitis M.E., Freitas M.A.[¥], Pichiorri F.[¥] *Proteomic Characterization of Circulating Extracellular Vesicles Identifies Novel Serum Myeloma Associated Markers.* J. Proteomics. 2016 Jan 13. [Epub ahead of print]. Accepted in Dec. 2015. doi: 10.1016/j.jprot.2015.12.016.
*** These authors contributed equally to this work.**

2. **Canella A**., Harshman S.W., Radomska H.S., Freitas M. and Pichiorri F. *The potential diagnostic power of extracellular vesicle analysis for multiple myeloma.* Expert Review of Molecular Diagnostics. 2015 Dec 15; DOI: 10.1586/14737159.2016.1132627. Epub 2016 Jan 28.

3. **Canella A.*,** Cordero Nieves H.*, Sborov D.W., Cascione L., Radomska H.S., Smith E., Stiff A., Consiglio J., Caserta E., Rizzotto L., Zanesi N., Volinia S., Kaur B., Mo X., Byrd J.C., Efebera Y.A., Hofmeister C.C. and Pichiorri F. *HDAC inhibitor AR-42 decreases CD44 expression and sensitizes myeloma cells to lenalidomide.* Oncotarget. 2015 Oct 13;6(31):31134-50.
*** These authors contributed equally to this work.**

4. Harshman S.W.*, **Canella, A.*,** Ciarlariello, P.D., Rocci A., Agarwal K., Smith E.M., Talabere T., Efebera Y.A., Hofmeister C.C., Benson Jr. D.M., Paulaitis M.E., Freitas M. and Pichiorri F. *Characterization of Multiple Myeloma Vesicles by Label-Free Relative Quantitation.* Proteomics. 2013. 13. 3013-3029.
*** These authors contributed equally to this work.**

The following articles are the result of collaboration with other projects or scientific groups, and they are not part of this thesis

5. Stiff A, Caserta E, Sborov DW, Nuovo GJ, Mo X, Schlotter SY, **Canella A**, Smith E, Badway J, Old M, Jaime-Ramirez AC, Yan P, Benson DM Jr, Byrd JC, Baiocchi R, Kaur B, Hofmeister CC, Pichiorri F. *Histone Deacetylase Inhibitors Enhance the Therapeutic Potential of Reovirus in Multiple Myeloma.* Molecular Cancer Therapeutics. 2016 Jan 25. pii: molcanther.0240.2015. [Epub ahead of print]

6. He, W. A.*, Calore, F.*, Londhe, P., **Canella, A**., Guttridge D.C., and Croce, C.M. *Microvesicles containing miRNAs Promote Muscle Cell Death in Cancer Cachexia via TLR7*. PNAS. 2014. Mar 25;111(12):4525-9.

7. Manfrini M., Di Bona C., **Canella A.**, Lucarelli E., D'Agostino A., Barbanti-Brodano G., Pellati A. and Tognon M. *Mesenchymal stem cells from patients to assay bone graft substitutes.* Journal of Cellular Physiology. 2013. Jun;228(6):1229-37.

Acknowledgments

I started this insane adventure three years ago leaving my permanent position at the University of Ferrara, my Italian life and moving my family abroad, in the United States. It has not been easy, I've had to grow a lot and learn many lessons in this field, fighting with the language, managing stress and frustrations, competing with colleagues and facing critics, but I made it.

First, I would like to express my sincere gratitude to my supportive wife, Lara, who was almost always on my side, she believed in me and helped a lot providing scientific suggestions and English editing.

I'm grateful to my mentor, Prof. Stefano Volinia for the support and the chance he gave to me, to the Director of the PhD course, Dr. Antonio Cuneo and to the University of Ferrara, for letting me spend the majority of the course abroad.

I'm highly indebted to the Hematology Department of The Ohio State University, in particular I'm very thankful to Dr. Flavia Pichiorri. I started this track because she has been the first one to encourage me and most of the scientific publications during this experience were obtained thanks to her support, expertise and commitment of her scientific group. I cannot forget to mention the valuable proteomic analysis made by Dr. Sean Harshman and Prof. Michael Freitas and the support of Dr. Kitty Agarwal for the electronic microscopy.

I have to say thanks also to Dr. Vincenzo Coppola, despite his busy schedule, he spent time, especially during weekend days, for training me from scratch to handling mice, doing surgery and working *in vivo.*

My thanks and appreciations also go to my former colleagues and people who have willingly helped me out with their abilities: Alberto Rocci, Tiffany Talabere, Paolo Fadda, Luciano Cascione, Carolyn Cheney, Emily Smith, Andrew Stiff, Hector Cordero, Foued Amari, Ming Lu, Yu-Yu Liu, Hans Meisen, Ji Young Yoo, and Hanna Radomska. I learned a lot from you guys.

I'll never forget the support of Italian friends and former colleagues such as Carlo Cervellati, Federica Arlotti, Alberto Merlotti, Matteo Campioni and Dario Balestra.

FL.

BIBLIOGRAPHY

1. Ferlay J SI, Ervik M et al. GLOBOCAN 2012 v1.0, Cancer Incidence and Mortality Worldwide. *IARC Cancer Base No. 11. 1–10 (2012).* 11, 1-10 (2012).
2. Glavey SV, Ghobrial IM. American Society of Hematology Annual Meeting 2014: highlights in multiple myeloma. *Expert review of hematology*, 8(3), 273-275 (2015).
3. Alexander DD, Mink PJ, Adami HO *et al.* Multiple myeloma: a review of the epidemiologic literature. *International journal of cancer. Journal international du cancer*, 120 Suppl 12, 40-61 (2007).
4. Kyle RA, Rajkumar SV. Monoclonal gammopathy of undetermined significance and smoldering multiple myeloma. *Current hematologic malignancy reports*, 5(2), 62-69 (2010).
5. Kyle RA, Durie BG, Rajkumar SV *et al.* Monoclonal gammopathy of undetermined significance (MGUS) and smoldering (asymptomatic) multiple myeloma: IMWG consensus perspectives risk factors for progression and guidelines for monitoring and management. *Leukemia*, 24(6), 1121-1127 (2010).
6. Kyle RA, Rajkumar SV. Monoclonal gammopathy of undetermined significance. *British journal of haematology*, 134(6), 573-589 (2006).
7. Rajkumar SV, Kyle RA, Buadi FK. Advances in the diagnosis, classification, risk stratification, and management of monoclonal gammopathy of undetermined significance: implications for recategorizing disease entities in the presence of evolving scientific evidence. *Mayo Clinic proceedings*, 85(10), 945-948 (2010).
8. Kyle RA, Rajkumar SV. Criteria for diagnosis, staging, risk stratification and response assessment of multiple myeloma. *Leukemia*, 23(1), 3-9 (2009).
9. Osgood EE. The survival time of patients with plasmocytic myeloma. *Cancer chemotherapy reports. Part 1*, 9, 1-10 (1960).
10. Greipp PR, San Miguel J, Durie BG *et al.* International staging system for multiple myeloma. *Journal of clinical oncology : official journal of the American Society of Clinical Oncology*, 23(15), 3412-3420 (2005).
11. Rajkumar SV. Multiple myeloma: 2012 update on diagnosis, risk-stratification, and management. *American journal of hematology*, 87(1), 78-88 (2012).
12. Fonseca R, Bergsagel PL, Drach J *et al.* International Myeloma Working Group molecular classification of multiple myeloma: spotlight review. *Leukemia*, 23(12), 2210-2221 (2009).
13. Keats JJ, Reiman T, Maxwell CA *et al.* In multiple myeloma, t(4;14)(p16;q32) is an adverse prognostic factor irrespective of FGFR3 expression. *Blood*, 101(4), 1520-1529 (2003).
14. Zhan F, Huang Y, Colla S *et al.* The molecular classification of multiple myeloma. *Blood*, 108(6), 2020-2028 (2006).
15. Kumar A, Loughran T, Alsina M, Durie BG, Djulbegovic B. Management of multiple myeloma: a systematic review and critical appraisal of published studies. *The Lancet. Oncology*, 4(5), 293-304 (2003).
16. McCarthy PL, Hahn T. Strategies for induction, autologous hematopoietic stem cell transplantation, consolidation, and maintenance for transplantation-eligible multiple myeloma patients. *Hematology / the Education Program of the American Society of Hematology. American Society of Hematology. Education Program*, 2013, 496-503 (2013).
17. Kyle RA. New strategies for MGUS and smoldering multiple myeloma. *Clinical advances in hematology & oncology : H&O*, 2(8), 507, 509 (2004).
18. Kuehl WM, Bergsagel PL. Multiple myeloma: evolving genetic events and host interactions. *Nature reviews. Cancer*, 2(3), 175-187 (2002).
19. Bergsagel PL, Kuehl WM. Chromosome translocations in multiple myeloma. *Oncogene*, 20(40), 5611-5622 (2001).

20. Hideshima T, Bergsagel PL, Kuehl WM, Anderson KC. Advances in biology of multiple myeloma: clinical applications. *Blood*, 104(3), 607-618 (2004).
21. Billadeau D, Liu P, Jelinek D, Shah N, LeBien TW, Van Ness B. Activating mutations in the N- and K-ras oncogenes differentially affect the growth properties of the IL-6-dependent myeloma cell line ANBL6. *Cancer research*, 57(11), 2268-2275 (1997).
22. Hideshima T, Anderson KC. Molecular mechanisms of novel therapeutic approaches for multiple myeloma. *Nature reviews. Cancer*, 2(12), 927-937 (2002).
23. Holt RU, Baykov V, Ro TB *et al.* Human myeloma cells adhere to fibronectin in response to hepatocyte growth factor. *Haematologica*, 90(4), 479-488 (2005).
24. Uchiyama H, Barut BA, Mohrbacher AF, Chauhan D, Anderson KC. Adhesion of human myeloma-derived cell lines to bone marrow stromal cells stimulates interleukin-6 secretion. *Blood*, 82(12), 3712-3720 (1993).
25. Chauhan D, Uchiyama H, Akbarali Y *et al.* Multiple myeloma cell adhesion-induced interleukin-6 expression in bone marrow stromal cells involves activation of NF-kappa B. *Blood*, 87(3), 1104-1112 (1996).
26. Dankbar B, Padro T, Leo R *et al.* Vascular endothelial growth factor and interleukin-6 in paracrine tumor-stromal cell interactions in multiple myeloma. *Blood*, 95(8), 2630-2636 (2000).
27. Urashima M, Ogata A, Chauhan D *et al.* Transforming growth factor-beta1: differential effects on multiple myeloma versus normal B cells. *Blood*, 87(5), 1928-1938 (1996).
28. Klein B, Zhang XG, Lu ZY, Bataille R. Interleukin-6 in human multiple myeloma. *Blood*, 85(4), 863-872 (1995).
29. Klein B, Zhang XG, Jourdan M *et al.* Paracrine rather than autocrine regulation of myeloma-cell growth and differentiation by interleukin-6. *Blood*, 73(2), 517-526 (1989).
30. Catlett-Falcone R, Landowski TH, Oshiro MM *et al.* Constitutive activation of Stat3 signaling confers resistance to apoptosis in human U266 myeloma cells. *Immunity*, 10(1), 105-115 (1999).
31. Kurth I, Horsten U, Pflanz S *et al.* Activation of the signal transducer glycoprotein 130 by both IL-6 and IL-11 requires two distinct binding epitopes. *Journal of immunology*, 162(3), 1480-1487 (1999).
32. Ogata A, Chauhan D, Teoh G *et al.* IL-6 triggers cell growth via the Ras-dependent mitogen-activated protein kinase cascade. *Journal of immunology*, 159(5), 2212-2221 (1997).
33. Akiyama M, Hideshima T, Hayashi T *et al.* Cytokines modulate telomerase activity in a human multiple myeloma cell line. *Cancer research*, 62(13), 3876-3882 (2002).
34. Mitsiades CS, Mitsiades NS, McMullan CJ *et al.* Inhibition of the insulin-like growth factor receptor-1 tyrosine kinase activity as a therapeutic strategy for multiple myeloma, other hematologic malignancies, and solid tumors. *Cancer cell*, 5(3), 221-230 (2004).
35. Otsuki T, Yamada O, Yata K *et al.* Expression of fibroblast growth factor and FGF-receptor family genes in human myeloma cells, including lines possessing t(4;14)(q16.3;q32. 3) and FGFR3 translocation. *International journal of oncology*, 15(6), 1205-1212 (1999).
36. Podar K, Tai YT, Davies FE *et al.* Vascular endothelial growth factor triggers signaling cascades mediating multiple myeloma cell growth and migration. *Blood*, 98(2), 428-435 (2001).
37. Chauhan D, Li G, Hideshima T *et al.* Blockade of ubiquitin-conjugating enzyme CDC34 enhances anti-myeloma activity of Bortezomib/Proteasome inhibitor PS-341. *Oncogene*, 23(20), 3597-3602 (2004).
38. Lichtenstein A, Tu Y, Fady C, Vescio R, Berenson J. Interleukin-6 inhibits apoptosis of malignant plasma cells. *Cellular immunology*, 162(2), 248-255 (1995).
39. Hideshima T, Mitsiades C, Tonon G, Richardson PG, Anderson KC. Understanding multiple myeloma pathogenesis in the bone marrow to identify new therapeutic targets. *Nature reviews. Cancer*, 7(8), 585-598 (2007).

40. Trams EG, Lauter CJ, Salem N, Jr., Heine U. Exfoliation of membrane ecto-enzymes in the form of micro-vesicles. *Biochimica et biophysica acta*, 645(1), 63-70 (1981).
41. Raposo G, Nijman HW, Stoorvogel W *et al.* B lymphocytes secrete antigen-presenting vesicles. *The Journal of experimental medicine*, 183(3), 1161-1172 (1996).
42. Thery C. Exosomes: secreted vesicles and intercellular communications. *F1000 biology reports*, 3, 15 (2011).
43. Thery C, Ostrowski M, Segura E. Membrane vesicles as conveyors of immune responses. *Nature reviews. Immunology*, 9(8), 581-593 (2009).
44. van der Pol E, Boing AN, Harrison P, Sturk A, Nieuwland R. Classification, functions, and clinical relevance of extracellular vesicles. *Pharmacological reviews*, 64(3), 676-705 (2012).
45. Mathivanan S, Fahner CJ, Reid GE, Simpson RJ. ExoCarta 2012: database of exosomal proteins, RNA and lipids. *Nucleic acids research*, 40(Database issue), D1241-1244 (2012).
46. S ELA, Mager I, Breakefield XO, Wood MJ. Extracellular vesicles: biology and emerging therapeutic opportunities. *Nature reviews. Drug discovery*, 12(5), 347-357 (2013).
47. Camussi G, Deregibus MC, Bruno S, Grange C, Fonsato V, Tetta C. Exosome/microvesicle-mediated epigenetic reprogramming of cells. *American journal of cancer research*, 1(1), 98-110 (2011).
48. Peinado H, Aleckovic M, Lavotshkin S *et al.* Melanoma exosomes educate bone marrow progenitor cells toward a pro-metastatic phenotype through MET. *Nature medicine*, 18(6), 883-891 (2012).
49. Rak J, Guha A. Extracellular vesicles--vehicles that spread cancer genes. *BioEssays : news and reviews in molecular, cellular and developmental biology*, 34(6), 489-497 (2012).
50. Quail DF, Joyce JA. Microenvironmental regulation of tumor progression and metastasis. *Nature medicine*, 19(11), 1423-1437 (2013).
51. Barcellos-Hoff MH, Lyden D, Wang TC. The evolution of the cancer niche during multistage carcinogenesis. *Nature reviews. Cancer*, 13(7), 511-518 (2013).
52. Fong MY, Zhou W, Liu L *et al.* Breast-cancer-secreted miR-122 reprograms glucose metabolism in premetastatic niche to promote metastasis. *Nature cell biology*, 17(2), 183-194 (2015).
53. Hunter MC, O'Hagan KL, Kenyon A, Dhanani KC, Prinsloo E, Edkins AL. Hsp90 binds directly to fibronectin (FN) and inhibition reduces the extracellular fibronectin matrix in breast cancer cells. *PloS one*, 9(1), e86842 (2014).
54. Kim J, Morley S, Le M *et al.* Enhanced shedding of extracellular vesicles from amoeboid prostate cancer cells: potential effects on the tumor microenvironment. *Cancer biology & therapy*, 15(4), 409-418 (2014).
55. Bronisz A, Wang Y, Nowicki MO *et al.* Extracellular vesicles modulate the glioblastoma microenvironment via a tumor suppression signaling network directed by miR-1. *Cancer research*, 74(3), 738-750 (2014).
56. Zhai H, Acharya S, Gravanis I *et al.* Annexin A2 promotes glioma cell invasion and tumor progression. *The Journal of neuroscience : the official journal of the Society for Neuroscience*, 31(40), 14346-14360 (2011).
57. Luga V, Zhang L, Viloria-Petit AM *et al.* Exosomes mediate stromal mobilization of autocrine Wnt-PCP signaling in breast cancer cell migration. *Cell*, 151(7), 1542-1556 (2012).
58. Lugini L, Cecchetti S, Huber V *et al.* Immune surveillance properties of human NK cell-derived exosomes. *Journal of immunology*, 189(6), 2833-2842 (2012).
59. Morse MA, Garst J, Osada T *et al.* A phase I study of dexosome immunotherapy in patients with advanced non-small cell lung cancer. *Journal of translational medicine*, 3(1), 9 (2005).
60. Escudier B, Dorval T, Chaput N *et al.* Vaccination of metastatic melanoma patients with autologous dendritic cell (DC) derived-exosomes: results of thefirst phase I clinical trial. *Journal of translational medicine*, 3(1), 10 (2005).

61. Naslund TI, Gehrmann U, Qazi KR, Karlsson MC, Gabrielsson S. Dendritic cell-derived exosomes need to activate both T and B cells to induce antitumor immunity. *Journal of immunology*, 190(6), 2712-2719 (2013).
62. Cai J, Wu G, Tan X *et al.* Transferred BCR/ABL DNA from K562 extracellular vesicles causes chronic myeloid leukemia in immunodeficient mice. *PloS one*, 9(8), e105200 (2014).
63. Le MT, Hamar P, Guo C *et al.* miR-200-containing extracellular vesicles promote breast cancer cell metastasis. *The Journal of clinical investigation*, 124(12), 5109-5128 (2014).
64. Fabbri M, Paone A, Calore F *et al.* MicroRNAs bind to Toll-like receptors to induce prometastatic inflammatory response. *Proceedings of the National Academy of Sciences of the United States of America*, 109(31), E2110-2116 (2012).
65. He WA, Calore F, Londhe P, Canella A, Guttridge DC, Croce CM. Microvesicles containing miRNAs promote muscle cell death in cancer cachexia via TLR7. *Proceedings of the National Academy of Sciences of the United States of America*, 111(12), 4525-4529 (2014).
66. Xiao X, Yu S, Li S *et al.* Exosomes: decreased sensitivity of lung cancer A549 cells to cisplatin. *PloS one*, 9(2), e89534 (2014).
67. Federici C, Petrucci F, Caimi S *et al.* Exosome release and low pH belong to a framework of resistance of human melanoma cells to cisplatin. *PloS one*, 9(2), e88193 (2014).
68. Ma X, Chen Z, Hua D *et al.* Essential role for TrpC5-containing extracellular vesicles in breast cancer with chemotherapeutic resistance. *Proceedings of the National Academy of Sciences of the United States of America*, 111(17), 6389-6394 (2014).
69. Lundholm M, Schroder M, Nagaeva O *et al.* Prostate tumor-derived exosomes down-regulate NKG2D expression on natural killer cells and CD8+ T cells: mechanism of immune evasion. *PloS one*, 9(9), e108925 (2014).
70. Clayton A, Mitchell JP, Court J, Mason MD, Tabi Z. Human tumor-derived exosomes selectively impair lymphocyte responses to interleukin-2. *Cancer research*, 67(15), 7458-7466 (2007).
71. Klibi J, Niki T, Riedel A *et al.* Blood diffusion and Th1-suppressive effects of galectin-9-containing exosomes released by Epstein-Barr virus-infected nasopharyngeal carcinoma cells. *Blood*, 113(9), 1957-1966 (2009).
72. Andreola G, Rivoltini L, Castelli C *et al.* Induction of lymphocyte apoptosis by tumor cell secretion of FasL-bearing microvesicles. *The Journal of experimental medicine*, 195(10), 1303-1316 (2002).
73. Scholer N, Langer C, Dohner H, Buske C, Kuchenbauer F. Serum microRNAs as a novel class of biomarkers: a comprehensive review of the literature. *Experimental hematology*, 38(12), 1126-1130 (2010).
74. Miguet L, Pacaud K, Felden C *et al.* Proteomic analysis of malignant lymphocyte membrane microparticles using double ionization coverage optimization. *Proteomics*, 6(1), 153-171 (2006).
75. Staubach S, Razawi H, Hanisch FG. Proteomics of MUC1-containing lipid rafts from plasma membranes and exosomes of human breast carcinoma cells MCF-7. *Proteomics*, 9(10), 2820-2835 (2009).
76. Choi DS, Lee JM, Park GW *et al.* Proteomic analysis of microvesicles derived from human colorectal cancer cells. *Journal of proteome research*, 6(12), 4646-4655 (2007).
77. Mears R, Craven RA, Hanrahan S *et al.* Proteomic analysis of melanoma-derived exosomes by two-dimensional polyacrylamide gel electrophoresis and mass spectrometry. *Proteomics*, 4(12), 4019-4031 (2004).
78. Mathivanan S, Ji H, Simpson RJ. Exosomes: extracellular organelles important in intercellular communication. *Journal of proteomics*, 73(10), 1907-1920 (2010).
79. Welton JL, Khanna S, Giles PJ *et al.* Proteomics analysis of bladder cancer exosomes. *Molecular & cellular proteomics : MCP*, 9(6), 1324-1338 (2010).

80. Pisitkun T, Shen RF, Knepper MA. Identification and proteomic profiling of exosomes in human urine. *Proceedings of the National Academy of Sciences of the United States of America*, 101(36), 13368-13373 (2004).
81. Adamczyk KA, Klein-Scory S, Tehrani MM *et al.* Characterization of soluble and exosomal forms of the EGFR released from pancreatic cancer cells. *Life sciences*, 89(9-10), 304-312 (2011).
82. Epple LM, Griffiths SG, Dechkovskaia AM *et al.* Medulloblastoma exosome proteomics yield functional roles for extracellular vesicles. *PloS one*, 7(7), e42064 (2012).
83. Harshman SW, Canella A, Ciarlariello PD *et al.* Characterization of multiple myeloma vesicles by label-free relative quantitation. *Proteomics*, 13(20), 3013-3029 (2013).
84. Yang J, Wei F, Schafer C, Wong DT. Detection of tumor cell-specific mRNA and protein in exosome-like microvesicles from blood and saliva. *PloS one*, 9(11), e110641 (2014).
85. Kruger S, Abd Elmageed ZY, Hawke DH *et al.* Molecular characterization of exosome-like vesicles from breast cancer cells. *BMC cancer*, 14, 44 (2014).
86. Liao J, Liu R, Yin L, Pu Y. Expression profiling of exosomal miRNAs derived from human esophageal cancer cells by Solexa high-throughput sequencing. *International journal of molecular sciences*, 15(9), 15530-15551 (2014).
87. Thery C, Zitvogel L, Amigorena S. Exosomes: composition, biogenesis and function. *Nature reviews. Immunology*, 2(8), 569-579 (2002).
88. Taylor DD, Gercel-Taylor C. MicroRNA signatures of tumor-derived exosomes as diagnostic biomarkers of ovarian cancer. *Gynecologic oncology*, 110(1), 13-21 (2008).
89. Tanaka Y, Kamohara H, Kinoshita K *et al.* Clinical impact of serum exosomal microRNA-21 as a clinical biomarker in human esophageal squamous cell carcinoma. *Cancer*, 119(6), 1159-1167 (2013).
90. Wang ZX, Bian HB, Wang JR, Cheng ZX, Wang KM, De W. Prognostic significance of serum miRNA-21 expression in human non-small cell lung cancer. *Journal of surgical oncology*, 104(7), 847-851 (2011).
91. Boeri M, Verri C, Conte D *et al.* MicroRNA signatures in tissues and plasma predict development and prognosis of computed tomography detected lung cancer. *Proceedings of the National Academy of Sciences of the United States of America*, 108(9), 3713-3718 (2011).
92. Hu Z, Chen X, Zhao Y *et al.* Serum microRNA signatures identified in a genome-wide serum microRNA expression profiling predict survival of non-small-cell lung cancer. *Journal of clinical oncology : official journal of the American Society of Clinical Oncology*, 28(10), 1721-1726 (2010).
93. Lazaro-Ibanez E, Sanz-Garcia A, Visakorpi T *et al.* Different gDNA content in the subpopulations of prostate cancer extracellular vesicles: apoptotic bodies, microvesicles, and exosomes. *The Prostate*, 74(14), 1379-1390 (2014).
94. Povero D, Eguchi A, Li H *et al.* Circulating extracellular vesicles with specific proteome and liver microRNAs are potential biomarkers for liver injury in experimental fatty liver disease. *PloS one*, 9(12), e113651 (2014).
95. Tamura H, Ishibashi M, Yamashita T *et al.* Marrow stromal cells induce B7-H1 expression on myeloma cells, generating aggressive characteristics in multiple myeloma. *Leukemia*, 27(2), 464-472 (2013).
96. Manier S, Sacco A, Leleu X, Ghobrial IM, Roccaro AM. Bone marrow microenvironment in multiple myeloma progression. *Journal of biomedicine & biotechnology*, 2012, 157496 (2012).
97. Kumar S, Witzig TE, Timm M *et al.* Bone marrow angiogenic ability and expression of angiogenic cytokines in myeloma: evidence favoring loss of marrow angiogenesis inhibitory activity with disease progression. *Blood*, 104(4), 1159-1165 (2004).
98. Thompson CA, Purushothaman A, Ramani VC, Vlodavsky I, Sanderson RD. Heparanase regulates secretion, composition, and function of tumor cell-derived exosomes. *The Journal of biological chemistry*, 288(14), 10093-10099 (2013).

99. Raimondi L, De Luca A, Amodio N *et al.* Involvement of multiple myeloma cell-derived exosomes in osteoclast differentiation. *Oncotarget*, 6(15), 13772-13789 (2015).
100. Xu S, Cecilia Santini G, De Veirman K *et al.* Upregulation of miR-135b is involved in the impaired osteogenic differentiation of mesenchymal stem cells derived from multiple myeloma patients. *PloS one*, 8(11), e79752 (2013).
101. Umezu T, Tadokoro H, Azuma K, Yoshizawa S, Ohyashiki K, Ohyashiki JH. Exosomal miR-135b shed from hypoxic multiple myeloma cells enhances angiogenesis by targeting factor-inhibiting HIF-1. *Blood*, 124(25), 3748-3757 (2014).
102. Fan GC. Hypoxic exosomes promote angiogenesis. *Blood*, 124(25), 3669-3670 (2014).
103. Wu W, Wang Z, Yang P *et al.* MicroRNA-135b regulates metastasis suppressor 1 expression and promotes migration and invasion in colorectal cancer. *Molecular and cellular biochemistry*, 388(1-2), 249-259 (2014).
104. Lulla RR, Costa FF, Bischof JM *et al.* Identification of Differentially Expressed MicroRNAs in Osteosarcoma. *Sarcoma*, 2011, 732690 (2011).
105. Lin CW, Chang YL, Chang YC *et al.* MicroRNA-135b promotes lung cancer metastasis by regulating multiple targets in the Hippo pathway and LZTS1. *Nature communications*, 4, 1877 (2013).
106. Liu Y, Zhu XJ, Zeng C *et al.* Microvesicles secreted from human multiple myeloma cells promote angiogenesis. *Acta pharmacologica Sinica*, 35(2), 230-238 (2014).
107. Arendt BK, Walters DK, Wu X, Tschumper RC, Jelinek DF. Multiple myeloma dell-derived microvesicles are enriched in CD147 expression and enhance tumor cell proliferation. *Oncotarget*, 5(14), 5686-5699 (2014).
108. Sun L, Wang HX, Zhu XJ *et al.* Serum deprivation elevates the levels of microvesicles with different size distributions and selectively enriched proteins in human myeloma cells in vitro. *Acta pharmacologica Sinica*, 35(3), 381-393 (2014).
109. Roccaro AM, Sacco A, Maiso P *et al.* BM mesenchymal stromal cell-derived exosomes facilitate multiple myeloma progression. *The Journal of clinical investigation*, 123(4), 1542-1555 (2013).
110. Rocci A, Hofmeister CC, Geyer S *et al.* Circulating miRNA markers show promise as new prognosticators for multiple myeloma. *Leukemia*, 28(9), 1922-1926 (2014).
111. Wang J, Hendrix A, Hernot S *et al.* Bone marrow stromal cell-derived exosomes as communicators in drug resistance in multiple myeloma cells. *Blood*, 124(4), 555-566 (2014).
112. Di Noto G, Paolini L, Zendrini A, Radeghieri A, Caimi L, Ricotta D. C-src enriched serum microvesicles are generated in malignant plasma cell dyscrasia. *PloS one*, 8(8), e70811 (2013).
113. Xie Y, Bai O, Zhang H *et al.* Membrane-bound HSP70-engineered myeloma cell-derived exosomes stimulate more efficient CD8(+) CTL- and NK-mediated antitumour immunity than exosomes released from heat-shocked tumour cells expressing cytoplasmic HSP70. *Journal of cellular and molecular medicine*, 14(11), 2655-2666 (2010).
114. Caivano A, Laurenzana I, De Luca L *et al.* High serum levels of extracellular vesicles expressing malignancy-related markers are released in patients with various types of hematological neoplastic disorders. *Tumour biology : the journal of the International Society for Oncodevelopmental Biology and Medicine*, 36(12), 9739-9752 (2015).
115. Aruffo A, Stamenkovic I, Melnick M, Underhill CB, Seed B. CD44 is the principal cell surface receptor for hyaluronate. *Cell*, 61(7), 1303-1313 (1990).
116. Zoller M. CD44: can a cancer-initiating cell profit from an abundantly expressed molecule? *Nature reviews. Cancer*, 11(4), 254-267 (2011).
117. Ghatak S, Misra S, Toole BP. Hyaluronan oligosaccharides inhibit anchorage-independent growth of tumor cells by suppressing the phosphoinositide 3-kinase/Akt cell survival pathway. *The Journal of biological chemistry*, 277(41), 38013-38020 (2002).

118. Subramaniam V, Vincent IR, Gilakjan M, Jothy S. Suppression of human colon cancer tumors in nude mice by siRNA CD44 gene therapy. *Experimental and molecular pathology*, 83(3), 332-340 (2007).
119. Mulder JW, Kruyt PM, Sewnath M *et al.* Colorectal cancer prognosis and expression of exon-v6-containing CD44 proteins. *Lancet*, 344(8935), 1470-1472 (1994).
120. Marangoni E, Lecomte N, Durand L *et al.* CD44 targeting reduces tumour growth and prevents post-chemotherapy relapse of human breast cancers xenografts. *British journal of cancer*, 100(6), 918-922 (2009).
121. Bourguignon LY, Peyrollier K, Xia W, Gilad E. Hyaluronan-CD44 interaction activates stem cell marker Nanog, Stat-3-mediated MDR1 gene expression, and ankyrin-regulated multidrug efflux in breast and ovarian tumor cells. *The Journal of biological chemistry*, 283(25), 17635-17651 (2008).
122. Ohashi R, Takahashi F, Cui R *et al.* Interaction between CD44 and hyaluronate induces chemoresistance in non-small cell lung cancer cell. *Cancer letters*, 252(2), 225-234 (2007).
123. Shigeishi H, Biddle A, Gammon L *et al.* Maintenance of stem cell self-renewal in head and neck cancers requires actions of GSK3beta influenced by CD44 and RHAMM. *Stem cells*, 31(10), 2073-2083 (2013).
124. Xu Y, Stamenkovic I, Yu Q. CD44 attenuates activation of the hippo signaling pathway and is a prime therapeutic target for glioblastoma. *Cancer research*, 70(6), 2455-2464 (2010).
125. Ghatak S, Misra S, Toole BP. Hyaluronan constitutively regulates ErbB2 phosphorylation and signaling complex formation in carcinoma cells. *The Journal of biological chemistry*, 280(10), 8875-8883 (2005).
126. Lakshman M, Subramaniam V, Rubenthiran U, Jothy S. CD44 promotes resistance to apoptosis in human colon cancer cells. *Experimental and molecular pathology*, 77(1), 18-25 (2004).
127. Park YS, Huh JW, Lee JH, Kim HR. shRNA against CD44 inhibits cell proliferation, invasion and migration, and promotes apoptosis of colon carcinoma cells. *Oncology reports*, 27(2), 339-346 (2012).
128. Fedorchenko O, Stiefelhagen M, Peer-Zada AA *et al.* CD44 regulates the apoptotic response and promotes disease development in chronic lymphocytic leukemia. *Blood*, 121(20), 4126-4136 (2013).
129. Orian-Rousseau V, Chen L, Sleeman JP, Herrlich P, Ponta H. CD44 is required for two consecutive steps in HGF/c-Met signaling. *Genes & development*, 16(23), 3074-3086 (2002).
130. Yasuda M, Tanaka Y, Fujii K, Yasumoto K. CD44 stimulation down-regulates Fas expression and Fas-mediated apoptosis of lung cancer cells. *International immunology*, 13(10), 1309-1319 (2001).
131. Katz BZ. Adhesion molecules--The lifelines of multiple myeloma cells. *Seminars in cancer biology*, 20(3), 186-195 (2010).
132. Pallotta I, Lovett M, Rice W, Kaplan DL, Balduini A. Bone marrow osteoblastic niche: a new model to study physiological regulation of megakaryopoiesis. *PloS one*, 4(12), e8359 (2009).
133. Fraser JR, Laurent TC, Laurent UB. Hyaluronan: its nature, distribution, functions and turnover. *Journal of internal medicine*, 242(1), 27-33 (1997).
134. Tokoyoda K, Hauser AE, Nakayama T, Radbruch A. Organization of immunological memory by bone marrow stroma. *Nature reviews. Immunology*, 10(3), 193-200 (2010).
135. Tancred TM, Belch AR, Reiman T, Pilarski LM, Kirshner J. Altered expression of fibronectin and collagens I and IV in multiple myeloma and monoclonal gammopathy of undetermined significance. *The journal of histochemistry and cytochemistry : official journal of the Histochemistry Society*, 57(3), 239-247 (2009).
136. Wight TN, Kinsella MG, Keating A, Singer JW. Proteoglycans in human long-term bone marrow cultures: biochemical and ultrastructural analyses. *Blood*, 67(5), 1333-1343 (1986).

137. Toole BP, Slomiany MG. Hyaluronan: a constitutive regulator of chemoresistance and malignancy in cancer cells. *Seminars in cancer biology*, 18(4), 244-250 (2008).
138. Avigdor A, Goichberg P, Shivtiel S *et al.* CD44 and hyaluronic acid cooperate with SDF-1 in the trafficking of human CD34+ stem/progenitor cells to bone marrow. *Blood*, 103(8), 2981-2989 (2004).
139. van Driel M, Gunthert U, Stauder R, Joling P, Lokhorst HM, Bloem AC. CD44 isoforms distinguish between bone marrow plasma cells from normal individuals and patients with multiple myeloma at different stages of disease. *Leukemia*, 12(11), 1821-1828 (1998).
140. Turley EA, Belch AJ, Poppema S, Pilarski LM. Expression and function of a receptor for hyaluronan-mediated motility on normal and malignant B lymphocytes. *Blood*, 81(2), 446-453 (1993).
141. Crainie M, Belch AR, Mant MJ, Pilarski LM. Overexpression of the receptor for hyaluronan-mediated motility (RHAMM) characterizes the malignant clone in multiple myeloma: identification of three distinct RHAMM variants. *Blood*, 93(5), 1684-1696 (1999).
142. Eisterer W, Bechter O, Hilbe W *et al.* CD44 isoforms are differentially regulated in plasma cell dyscrasias and CD44v9 represents a new independent prognostic parameter in multiple myeloma. *Leukemia research*, 25(12), 1051-1057 (2001).
143. Stauder R, Van Driel M, Schwarzler C *et al.* Different CD44 splicing patterns define prognostic subgroups in multiple myeloma. *Blood*, 88(8), 3101-3108 (1996).
144. Liebisch P, Eppinger S, Schopflin C *et al.* CD44v6, a target for novel antibody treatment approaches, is frequently expressed in multiple myeloma and associated with deletion of chromosome arm 13q. *Haematologica*, 90(4), 489-493 (2005).
145. Guedez L, Martinez A, Zhao S *et al.* Tissue inhibitor of metalloproteinase 1 (TIMP-1) promotes plasmablastic differentiation of a Burkitt lymphoma cell line: implications in the pathogenesis of plasmacytic/plasmablastic tumors. *Blood*, 105(4), 1660-1668 (2005).
146. Vincent T, Mechti N. IL-6 regulates CD44 cell surface expression on human myeloma cells. *Leukemia*, 18(5), 967-975 (2004).
147. Caers J, Gunthert U, De Raeve H *et al.* The involvement of osteopontin and its receptors in multiple myeloma cell survival, migration and invasion in the murine 5T33MM model. *British journal of haematology*, 132(4), 469-477 (2006).
148. Ohwada C, Nakaseko C, Koizumi M *et al.* CD44 and hyaluronan engagement promotes dexamethasone resistance in human myeloma cells. *European journal of haematology*, 80(3), 245-250 (2008).
149. Van Driel M, Gunthert U, van Kessel AC *et al.* CD44 variant isoforms are involved in plasma cell adhesion to bone marrow stromal cells. *Leukemia*, 16(1), 135-143 (2002).
150. Asosingh K, Gunthert U, De Raeve H, Van Riet I, Van Camp B, Vanderkerken K. A unique pathway in the homing of murine multiple myeloma cells: CD44v10 mediates binding to bone marrow endothelium. *Cancer research*, 61(7), 2862-2865 (2001).
151. Damiano JS, Cress AE, Hazlehurst LA, Shtil AA, Dalton WS. Cell adhesion mediated drug resistance (CAM-DR): role of integrins and resistance to apoptosis in human myeloma cell lines. *Blood*, 93(5), 1658-1667 (1999).
152. Hazlehurst LA, Damiano JS, Buyuksal I, Pledger WJ, Dalton WS. Adhesion to fibronectin via beta1 integrins regulates p27kip1 levels and contributes to cell adhesion mediated drug resistance (CAM-DR). *Oncogene*, 19(38), 4319-4327 (2000).
153. Matsunaga T, Fukai F, Miura S *et al.* Combination therapy of an anticancer drug with the FNIII14 peptide of fibronectin effectively overcomes cell adhesion-mediated drug resistance of acute myelogenous leukemia. *Leukemia*, 22(2), 353-360 (2008).
154. Li ZW, Dalton WS. Tumor microenvironment and drug resistance in hematologic malignancies. *Blood reviews*, 20(6), 333-342 (2006).

155. Noborio-Hatano K, Kikuchi J, Takatoku M *et al.* Bortezomib overcomes cell-adhesion-mediated drug resistance through downregulation of VLA-4 expression in multiple myeloma. *Oncogene*, 28(2), 231-242 (2009).
156. Landowski TH, Olashaw NE, Agrawal D, Dalton WS. Cell adhesion-mediated drug resistance (CAM-DR) is associated with activation of NF-kappa B (RelB/p50) in myeloma cells. *Oncogene*, 22(16), 2417-2421 (2003).
157. Hazlehurst LA, Enkemann SA, Beam CA *et al.* Genotypic and phenotypic comparisons of de novo and acquired melphalan resistance in an isogenic multiple myeloma cell line model. *Cancer research*, 63(22), 7900-7906 (2003).
158. Garcia-Gila M, Lopez-Martin EM, Garcia-Pardo A. Adhesion to fibronectin via alpha4 integrin (CD49d) protects B cells from apoptosis induced by serum deprivation but not via IgM or Fas/Apo-1 receptors. *Clinical and experimental immunology*, 127(3), 455-462 (2002).
159. Auphan N, DiDonato JA, Rosette C, Helmberg A, Karin M. Immunosuppression by glucocorticoids: inhibition of NF-kappa B activity through induction of I kappa B synthesis. *Science*, 270(5234), 286-290 (1995).
160. Chauhan D, Auclair D, Robinson EK *et al.* Identification of genes regulated by dexamethasone in multiple myeloma cells using oligonucleotide arrays. *Oncogene*, 21(9), 1346-1358 (2002).
161. DiDonato JA, Hayakawa M, Rothwarf DM, Zandi E, Karin M. A cytokine-responsive IkappaB kinase that activates the transcription factor NF-kappaB. *Nature*, 388(6642), 548-554 (1997).
162. Riechelmann H, Sauter A, Golze W *et al.* Phase I trial with the CD44v6-targeting immunoconjugate bivatuzumab mertansine in head and neck squamous cell carcinoma. *Oral oncology*, 44(9), 823-829 (2008).
163. Rupp U, Schoendorf-Holland E, Eichbaum M *et al.* Safety and pharmacokinetics of bivatuzumab mertansine in patients with CD44v6-positive metastatic breast cancer: final results of a phase I study. *Anti-cancer drugs*, 18(4), 477-485 (2007).
164. Barnes PJ, Adcock IM, Ito K. Histone acetylation and deacetylation: importance in inflammatory lung diseases. *The European respiratory journal*, 25(3), 552-563 (2005).
165. Haery L, Thompson RC, Gilmore TD. Histone acetyltransferases and histone deacetylases in B- and T-cell development, physiology and malignancy. *Genes & cancer*, 6(5-6), 184-213 (2015).
166. Rundlett SE, Carmen AA, Suka N, Turner BM, Grunstein M. Transcriptional repression by UME6 involves deacetylation of lysine 5 of histone H4 by RPD3. *Nature*, 392(6678), 831-835 (1998).
167. Brownell JE, Zhou J, Ranalli T *et al.* Tetrahymena histone acetyltransferase A: a homolog to yeast Gcn5p linking histone acetylation to gene activation. *Cell*, 84(6), 843-851 (1996).
168. Taunton J, Hassig CA, Schreiber SL. A mammalian histone deacetylase related to the yeast transcriptional regulator Rpd3p. *Science*, 272(5260), 408-411 (1996).
169. Glozak MA, Sengupta N, Zhang X, Seto E. Acetylation and deacetylation of non-histone proteins. *Gene*, 363, 15-23 (2005).
170. de Ruijter AJ, van Gennip AH, Caron HN, Kemp S, van Kuilenburg AB. Histone deacetylases (HDACs): characterization of the classical HDAC family. *The Biochemical journal*, 370(Pt 3), 737-749 (2003).
171. Yang XJ, Gregoire S. Class II histone deacetylases: from sequence to function, regulation, and clinical implication. *Molecular and cellular biology*, 25(8), 2873-2884 (2005).
172. Blander G, Guarente L. The Sir2 family of protein deacetylases. *Annual review of biochemistry*, 73, 417-435 (2004).
173. Grozinger CM, Schreiber SL. Deacetylase enzymes: biological functions and the use of small-molecule inhibitors. *Chemistry & biology*, 9(1), 3-16 (2002).
174. Min J, Landry J, Sternglanz R, Xu RM. Crystal structure of a SIR2 homolog-NAD complex. *Cell*, 105(2), 269-279 (2001).

175. Shi T, Wang F, Stieren E, Tong Q. SIRT3, a mitochondrial sirtuin deacetylase, regulates mitochondrial function and thermogenesis in brown adipocytes. *The Journal of biological chemistry*, 280(14), 13560-13567 (2005).
176. Yao Y, Yang Y, Zhu WG. Sirtuins: nodes connecting aging, metabolism and tumorigenesis. *Current pharmaceutical design*, 20(11), 1614-1624 (2014).
177. Gao L, Cueto MA, Asselbergs F, Atadja P. Cloning and functional characterization of HDAC11, a novel member of the human histone deacetylase family. *The Journal of biological chemistry*, 277(28), 25748-25755 (2002).
178. Guenther MG, Barak O, Lazar MA. The SMRT and N-CoR corepressors are activating cofactors for histone deacetylase 3. *Molecular and cellular biology*, 21(18), 6091-6101 (2001).
179. Ashburner BP, Westerheide SD, Baldwin AS, Jr. The p65 (RelA) subunit of NF-kappaB interacts with the histone deacetylase (HDAC) corepressors HDAC1 and HDAC2 to negatively regulate gene expression. *Molecular and cellular biology*, 21(20), 7065-7077 (2001).
180. Chen L, Fischle W, Verdin E, Greene WC. Duration of nuclear NF-kappaB action regulated by reversible acetylation. *Science*, 293(5535), 1653-1657 (2001).
181. Zhong H, May MJ, Jimi E, Ghosh S. The phosphorylation status of nuclear NF-kappa B determines its association with CBP/p300 or HDAC-1. *Molecular cell*, 9(3), 625-636 (2002).
182. Fraga MF, Ballestar E, Villar-Garea A *et al.* Loss of acetylation at Lys16 and trimethylation at Lys20 of histone H4 is a common hallmark of human cancer. *Nature genetics*, 37(4), 391-400 (2005).
183. Ozdag H, Teschendorff AE, Ahmed AA *et al.* Differential expression of selected histone modifier genes in human solid cancers. *BMC genomics*, 7, 90 (2006).
184. Weichert W, Roske A, Gekeler V *et al.* Histone deacetylases 1, 2 and 3 are highly expressed in prostate cancer and HDAC2 expression is associated with shorter PSA relapse time after radical prostatectomy. *British journal of cancer*, 98(3), 604-610 (2008).
185. Weichert W, Roske A, Niesporek S *et al.* Class I histone deacetylase expression has independent prognostic impact in human colorectal cancer: specific role of class I histone deacetylases in vitro and in vivo. *Clinical cancer research : an official journal of the American Association for Cancer Research*, 14(6), 1669-1677 (2008).
186. Krusche CA, Wulfing P, Kersting C *et al.* Histone deacetylase-1 and -3 protein expression in human breast cancer: a tissue microarray analysis. *Breast cancer research and treatment*, 90(1), 15-23 (2005).
187. Minamiya Y, Ono T, Saito H *et al.* Expression of histone deacetylase 1 correlates with a poor prognosis in patients with adenocarcinoma of the lung. *Lung cancer*, 74(2), 300-304 (2011).
188. Osada H, Tatematsu Y, Saito H, Yatabe Y, Mitsudomi T, Takahashi T. Reduced expression of class II histone deacetylase genes is associated with poor prognosis in lung cancer patients. *International journal of cancer. Journal international du cancer*, 112(1), 26-32 (2004).
189. Rikimaru T, Taketomi A, Yamashita Y *et al.* Clinical significance of histone deacetylase 1 expression in patients with hepatocellular carcinoma. *Oncology*, 72(1-2), 69-74 (2007).
190. Weichert W, Roske A, Gekeler V *et al.* Association of patterns of class I histone deacetylase expression with patient prognosis in gastric cancer: a retrospective analysis. *The Lancet. Oncology*, 9(2), 139-148 (2008).
191. Glozak MA, Seto E. Histone deacetylases and cancer. *Oncogene*, 26(37), 5420-5432 (2007).
192. Eot-Houllier G, Fulcrand G, Magnaghi-Jaulin L, Jaulin C. Histone deacetylase inhibitors and genomic instability. *Cancer letters*, 274(2), 169-176 (2009).
193. Duan H, Heckman CA, Boxer LM. Histone deacetylase inhibitors down-regulate bcl-2 expression and induce apoptosis in t(14;18) lymphomas. *Molecular and cellular biology*, 25(5), 1608-1619 (2005).
194. Luo J, Su F, Chen D, Shiloh A, Gu W. Deacetylation of p53 modulates its effect on cell growth and apoptosis. *Nature*, 408(6810), 377-381 (2000).

195. Archer SY, Meng S, Shei A, Hodin RA. p21(WAF1) is required for butyrate-mediated growth inhibition of human colon cancer cells. *Proceedings of the National Academy of Sciences of the United States of America*, 95(12), 6791-6796 (1998).
196. Richon VM, Sandhoff TW, Rifkind RA, Marks PA. Histone deacetylase inhibitor selectively induces p21WAF1 expression and gene-associated histone acetylation. *Proceedings of the National Academy of Sciences of the United States of America*, 97(18), 10014-10019 (2000).
197. Sasakawa Y, Naoe Y, Inoue T *et al.* Effects of FK228, a novel histone deacetylase inhibitor, on human lymphoma U-937 cells in vitro and in vivo. *Biochemical pharmacology*, 64(7), 1079-1090 (2002).
198. Wang LG, Ossowski L, Ferrari AC. Androgen receptor level controlled by a suppressor complex lost in an androgen-independent prostate cancer cell line. *Oncogene*, 23(30), 5175-5184 (2004).
199. Insinga A, Monestiroli S, Ronzoni S *et al.* Inhibitors of histone deacetylases induce tumor-selective apoptosis through activation of the death receptor pathway. *Nature medicine*, 11(1), 71-76 (2005).
200. Nakata S, Yoshida T, Horinaka M, Shiraishi T, Wakada M, Sakai T. Histone deacetylase inhibitors upregulate death receptor 5/TRAIL-R2 and sensitize apoptosis induced by TRAIL/APO2-L in human malignant tumor cells. *Oncogene*, 23(37), 6261-6271 (2004).
201. Bolden JE, Peart MJ, Johnstone RW. Anticancer activities of histone deacetylase inhibitors. *Nature reviews. Drug discovery*, 5(9), 769-784 (2006).
202. Shao Y, Gao Z, Marks PA, Jiang X. Apoptotic and autophagic cell death induced by histone deacetylase inhibitors. *Proceedings of the National Academy of Sciences of the United States of America*, 101(52), 18030-18035 (2004).
203. Rosato RR, Almenara JA, Grant S. The histone deacetylase inhibitor MS-275 promotes differentiation or apoptosis in human leukemia cells through a process regulated by generation of reactive oxygen species and induction of p21CIP1/WAF1 1. *Cancer research*, 63(13), 3637-3645 (2003).
204. Xu W, Ngo L, Perez G, Dokmanovic M, Marks PA. Intrinsic apoptotic and thioredoxin pathways in human prostate cancer cell response to histone deacetylase inhibitor. *Proceedings of the National Academy of Sciences of the United States of America*, 103(42), 15540-15545 (2006).
205. Bali P, Pranpat M, Bradner J *et al.* Inhibition of histone deacetylase 6 acetylates and disrupts the chaperone function of heat shock protein 90: a novel basis for antileukemia activity of histone deacetylase inhibitors. *The Journal of biological chemistry*, 280(29), 26729-26734 (2005).
206. Liang D, Kong X, Sang N. Effects of histone deacetylase inhibitors on HIF-1. *Cell cycle*, 5(21), 2430-2435 (2006).
207. Nebbioso A, Clarke N, Voltz E *et al.* Tumor-selective action of HDAC inhibitors involves TRAIL induction in acute myeloid leukemia cells. *Nature medicine*, 11(1), 77-84 (2005).
208. Hagelkruys A, Sawicka A, Rennmayr M, Seiser C. The biology of HDAC in cancer: the nuclear and epigenetic components. *Handbook of experimental pharmacology*, 206, 13-37 (2011).
209. Zain J, O'Connor OA. Targeting histone deacetyalses in the treatment of B- and T-cell malignancies. *Investigational new drugs*, 28 Suppl 1, S58-78 (2010).
210. Chen S, Dai Y, Pei XY, Grant S. Bim upregulation by histone deacetylase inhibitors mediates interactions with the Bcl-2 antagonist ABT-737: evidence for distinct roles for Bcl-2, Bcl-xL, and Mcl-1. *Molecular and cellular biology*, 29(23), 6149-6169 (2009).
211. Vannini A, Volpari C, Filocamo G *et al.* Crystal structure of a eukaryotic zinc-dependent histone deacetylase, human HDAC8, complexed with a hydroxamic acid inhibitor. *Proceedings of the National Academy of Sciences of the United States of America*, 101(42), 15064-15069 (2004).
212. Lee JH, Choy ML, Marks PA. Mechanisms of resistance to histone deacetylase inhibitors. *Advances in cancer research*, 116, 39-86 (2012).

213. Lee HZ, Kwitkowski VE, Del Valle PL *et al.* FDA Approval: Belinostat for the Treatment of Patients with Relapsed or Refractory Peripheral T-cell Lymphoma. *Clinical cancer research : an official journal of the American Association for Cancer Research*, 21(12), 2666-2670 (2015).
214. Peart MJ, Tainton KM, Ruefli AA *et al.* Novel mechanisms of apoptosis induced by histone deacetylase inhibitors. *Cancer research*, 63(15), 4460-4471 (2003).
215. Kelly-Sell MJ, Kim YH, Straus S *et al.* The histone deacetylase inhibitor, romidepsin, suppresses cellular immune functions of cutaneous T-cell lymphoma patients. *American journal of hematology*, 87(4), 354-360 (2012).
216. Smith EM, Boyd K, Davies FE. The potential role of epigenetic therapy in multiple myeloma. *British journal of haematology*, 148(5), 702-713 (2010).
217. Kaiser MF, Johnson DC, Wu P *et al.* Global methylation analysis identifies prognostically important epigenetically inactivated tumor suppressor genes in multiple myeloma. *Blood*, 122(2), 219-226 (2013).
218. Walker BA, Wardell CP, Chiecchio L *et al.* Aberrant global methylation patterns affect the molecular pathogenesis and prognosis of multiple myeloma. *Blood*, 117(2), 553-562 (2011).
219. Mitsiades CS, Mitsiades NS, McMullan CJ *et al.* Transcriptional signature of histone deacetylase inhibition in multiple myeloma: biological and clinical implications. *Proceedings of the National Academy of Sciences of the United States of America*, 101(2), 540-545 (2004).
220. Catley L, Weisberg E, Kiziltepe T *et al.* Aggresome induction by proteasome inhibitor bortezomib and alpha-tubulin hyperacetylation by tubulin deacetylase (TDAC) inhibitor LBH589 are synergistic in myeloma cells. *Blood*, 108(10), 3441-3449 (2006).
221. Maiso P, Carvajal-Vergara X, Ocio EM *et al.* The histone deacetylase inhibitor LBH589 is a potent antimyeloma agent that overcomes drug resistance. *Cancer research*, 66(11), 5781-5789 (2006).
222. Feng R, Oton A, Mapara MY, Anderson G, Belani C, Lentzsch S. The histone deacetylase inhibitor, PXD101, potentiates bortezomib-induced anti-multiple myeloma effect by induction of oxidative stress and DNA damage. *British journal of haematology*, 139(3), 385-397 (2007).
223. Khan SB, Maududi T, Barton K, Ayers J, Alkan S. Analysis of histone deacetylase inhibitor, depsipeptide (FR901228), effect on multiple myeloma. *British journal of haematology*, 125(2), 156-161 (2004).
224. Dimopoulos M, Siegel DS, Lonial S *et al.* Vorinostat or placebo in combination with bortezomib in patients with multiple myeloma (VANTAGE 088): a multicentre, randomised, double-blind study. *The Lancet. Oncology*, 14(11), 1129-1140 (2013).
225. Richardson PG, Hungria VT, Yoon SS *et al.* Panobinostat plus bortezomib and dexamethasone in relapsed/relapsed and refractory myeloma: outcomes by prior treatment. *Blood*, (2015).
226. Hideshima T, Bradner JE, Wong J *et al.* Small-molecule inhibition of proteasome and aggresome function induces synergistic antitumor activity in multiple myeloma. *Proceedings of the National Academy of Sciences of the United States of America*, 102(24), 8567-8572 (2005).
227. Santo L, Hideshima T, Kung AL *et al.* Preclinical activity, pharmacodynamic, and pharmacokinetic properties of a selective HDAC6 inhibitor, ACY-1215, in combination with bortezomib in multiple myeloma. *Blood*, 119(11), 2579-2589 (2012).
228. Vogl DT, Stadtmauer EA, Tan KS *et al.* Combined autophagy and proteasome inhibition: a phase 1 trial of hydroxychloroquine and bortezomib in patients with relapsed/refractory myeloma. *Autophagy*, 10(8), 1380-1390 (2014).
229. Yee AJ, Hari P, Marcheselli R *et al.* Outcomes in patients with relapsed or refractory multiple myeloma in a phase I study of everolimus in combination with lenalidomide. *British journal of haematology*, 166(3), 401-409 (2014).
230. Hideshima T, Mazitschek R, Santo L *et al.* Induction of differential apoptotic pathways in multiple myeloma cells by class-selective histone deacetylase inhibitors. *Leukemia*, 28(2), 457-460 (2014).

231. Kulp SK, Chen CS, Wang DS, Chen CY, Chen CS. Antitumor effects of a novel phenylbutyrate-based histone deacetylase inhibitor, (S)-HDAC-42, in prostate cancer. *Clinical cancer research : an official journal of the American Association for Cancer Research*, 12(17), 5199-5206 (2006).
232. Bush ML, Oblinger J, Brendel V *et al.* AR42, a novel histone deacetylase inhibitor, as a potential therapy for vestibular schwannomas and meningiomas. *Neuro-oncology*, 13(9), 983-999 (2011).
233. Lin TY, Fenger J, Murahari S *et al.* AR-42, a novel HDAC inhibitor, exhibits biologic activity against malignant mast cell lines via down-regulation of constitutively activated Kit. *Blood*, 115(21), 4217-4225 (2010).
234. Benjamini Y, Fonio E, Galili T, Havkin GZ, Golani I. Quantifying the buildup in extent and complexity of free exploration in mice. *Proceedings of the National Academy of Sciences of the United States of America*, 108 Suppl 3, 15580-15587 (2011).
235. Godar S, Ince TA, Bell GW *et al.* Growth-inhibitory and tumor- suppressive functions of p53 depend on its repression of CD44 expression. *Cell*, 134(1), 62-73 (2008).
236. Fevrier B, Raposo G. Exosomes: endosomal-derived vesicles shipping extracellular messages. *Current opinion in cell biology*, 16(4), 415-421 (2004).
237. Hertweck MK, Erdfelder F, Kreuzer KA. CD44 in hematological neoplasias. *Annals of hematology*, 90(5), 493-508 (2011).
238. Yan Y, Zuo X, Wei D. Concise Review: Emerging Role of CD44 in Cancer Stem Cells: A Promising Biomarker and Therapeutic Target. *Stem cells translational medicine*, 4(9), 1033-1043 (2015).
239. Bataille R, Durie BG, Grenier J. Serum beta2 microglobulin and survival duration in multiple myeloma: a simple reliable marker for staging. *British journal of haematology*, 55(3), 439-447 (1983).
240. Palumbo A, Bringhen S, Rossi D *et al.* Bortezomib-melphalan-prednisone-thalidomide followed by maintenance with bortezomib-thalidomide compared with bortezomib-melphalan-prednisone for initial treatment of multiple myeloma: a randomized controlled trial. *Journal of clinical oncology : official journal of the American Society of Clinical Oncology*, 28(34), 5101-5109 (2010).
241. Bjorklund CC, Baladandayuthapani V, Lin HY *et al.* Evidence of a role for CD44 and cell adhesion in mediating resistance to lenalidomide in multiple myeloma: therapeutic implications. *Leukemia*, 28(2), 373-383 (2014).
242. Lucas DM, Alinari L, West DA *et al.* The novel deacetylase inhibitor AR-42 demonstrates pre-clinical activity in B-cell malignancies in vitro and in vivo. *PLoS One*, 5(6), e10941 (2010).
243. Woan KV, Sahakian E, Sotomayor EM, Seto E, Villagra A. Modulation of antigen-presenting cells by HDAC inhibitors: implications in autoimmunity and cancer. *Immunology and cell biology*, 90(1), 55-65 (2012).
244. Bourguignon LY, Spevak CC, Wong G, Xia W, Gilad E. Hyaluronan-CD44 interaction with protein kinase C(epsilon) promotes oncogenic signaling by the stem cell marker Nanog and the Production of microRNA-21, leading to down-regulation of the tumor suppressor protein PDCD4, anti-apoptosis, and chemotherapy resistance in breast tumor cells. *The Journal of biological chemistry*, 284(39), 26533-26546 (2009).
245. Chikamatsu K, Ishii H, Murata T *et al.* Alteration of cancer stem cell-like phenotype by histone deacetylase inhibitors in squamous cell carcinoma of the head and neck. *Cancer science*, 104(11), 1468-1475 (2013).
246. Lee Y, Ahn C, Han J *et al.* The nuclear RNase III Drosha initiates microRNA processing. *Nature*, 425(6956), 415-419 (2003).
247. Fortina P, Surrey S. Digital mRNA profiling. *Nat Biotechnol*, 26(3), 293-294 (2008).
248. Lewis BP, Shih IH, Jones-Rhoades MW, Bartel DP, Burge CB. Prediction of mammalian microRNA targets. *Cell*, 115(7), 787-798 (2003).

249. Krek A, Grün D, Poy MN *et al.* Combinatorial microRNA target predictions. *Nat Genet*, 37(5), 495-500 (2005).
250. Vikesaa J, Hansen TV, Jonson L *et al.* RNA-binding IMPs promote cell adhesion and invadopodia formation. *The EMBO journal*, 25(7), 1456-1468 (2006).
251. Schaeffer DF, Owen DR, Lim HJ *et al.* Insulin-like growth factor 2 mRNA binding protein 3 (IGF2BP3) overexpression in pancreatic ductal adenocarcinoma correlates with poor survival. *BMC cancer*, 10, 59 (2010).
252. Miranda KC, Huynh T, Tay Y *et al.* A pattern-based method for the identification of MicroRNA binding sites and their corresponding heteroduplexes. *Cell*, 126(6), 1203-1217 (2006).
253. Rajkumar SV, Hayman SR, Lacy MQ *et al.* Combination therapy with lenalidomide plus dexamethasone (Rev/Dex) for newly diagnosed myeloma. *Blood*, 106(13), 4050-4053 (2005).
254. Kronke J, Udeshi ND, Narla A *et al.* Lenalidomide causes selective degradation of IKZF1 and IKZF3 in multiple myeloma cells. *Science*, 343(6168), 301-305 (2014).
255. Chou TC. Drug combination studies and their synergy quantification using the Chou-Talalay method. *Cancer Res*, 70(2), 440-446 (2010).

APPENDIX

Uniprot Accession	MM.1S Global Spectral Count			U266 Global Spectral Count			Statistics			Uniprot Accession	MM.1S Vesicle Spectral Count			U266 Vesicle Spectral Count			Statistics		
	Replicate 1	Replicate 2	Replicate 3	Replicate 1	Replicate 2	Replicate 3	logFC	logCPM	PValue		Replicate 1	Replicate 2	Replicate 3	Replicate 1	Replicate 2	Replicate 3	logFC	logCPM	PValue
P84077	11	8	2	12	20	18	0.69653	10.54203	0.07428	P84077	33	32	32	20	16	16	-0.46669	11.61439	0.15909
P27824	14	19	8	45	53	44	1.23841	11.90030	0.00000	P27824	11	0	0	19	4	0	1.47141	9.50308	0.01524
P14324	3	4	10	0	0	0	-6.40544	8.48645	0.00000	P14324	7	4	5	0	0	0	-5.82613	8.39380	0.00018
P55327	1	0	1	2	3	9	2.14854	8.39344	0.03604	P55327	1	2	1	13	5	0	2.51805	8.88016	0.00089
Q9H0U4	6	5	7	5	10	10	-0.07488	9.82157	0.87927	Q9H0U4	13	8	2	3	5	3	-0.62321	9.48703	0.33162
Q15233	2	9	7	19	22	24	1.29317	10.76477	0.00052	Q15233	6	0	0	1	0	0	-1.94275	7.20855	0.22536
P30086	5	7	8	7	11	11	-0.01348	10.00987	1.00000	P30086	6	3	6	4	5	5	0.32604	9.26798	0.72859
Q13501	0	0	0	5	8	6	6.02149	8.64045	0.00003	-	-	-	-	-	-	-	-	-	-
P35637	4	4	2	9	5	13	0.87009	9.60291	0.13706	-	-	-	-	-	-	-	-	-	-
Q14764	1	3	1	0	0	1	-2.55376	6.98109	0.12586	Q14764	16	5	14	22	76	37	2.36917	11.87795	0.00000
P18621	0	6	0	8	6	5	1.08768	9.03773	0.09560	P18621	0	2	3	5	0	0	0.41077	7.73129	0.75956
Q00610	17	14	22	38	45	43	0.69757	11.87290	0.00567	Q00610	76	86	84	78	110	60	0.44239	13.37439	0.07628
P04439	6	5	6	11	9	9	0.21843	9.91849	0.76931	P04439	43	37	37	41	46	49	0.64697	12.42018	0.01666
P49368	6	8	5	7	9	23	0.48342	10.25101	0.28919	P49368	5	4	5	2	5	5	0.20485	9.11007	0.85380
P07737	39	39	43	19	18	24	-1.53321	11.91834	0.00000	P07737	38	27	33	22	25	22	-0.07481	11.78774	0.86077
P14317	9	8	5	1	2	2	-2.61716	9.15401	0.00003	-	-	-	-	-	-	-	-	-	-
O43169	0	0	0	1	7	5	5.48422	8.09362	0.00101	-	-	-	-	-	-	-	-	-	-
-	-	-	-	-	-	-	-	-	-	P24844	2	6	9	6	5	3	0.14866	9.36393	1.00000
Q13576	0	1	0	2	2	0	1.28711	6.71694	0.62549	Q13576	5	9	15	0	1	0	-4.16256	9.29495	0.00001
-	-	-	-	-	-	-	-	-	-	P23634	0	0	0	10	17	13	7.56121	9.76863	0.00000
P43307	3	3	0	3	7	3	0.55041	8.64254	0.48330	-	-	-	-	-	-	-	-	-	-
P11021	69	72	74	236	201	224	1.06993	14.13926	0.00000	P11021	16	7	10	26	9	8	0.80765	10.66802	0.04982
P26010	7	4	5	0	0	0	-6.31904	8.39875	0.00001	P26010	3	1	4	0	0	6	0.01556	8.21771	1.00000
Q9Y6B6	0	0	0	8	10	9	6.52186	9.14631	0.00000	-	-	-	-	-	-	-	-	-	-
P51572	2	3	3	8	8	13	1.28687	9.60213	0.02589	-	-	-	-	-	-	-	-	-	-
P05386	3	8	8	10	10	6	-0.09610	9.88759	0.88209	P05386	11	10	11	5	6	3	-0.75260	9.92080	0.13013
P0CV98	0	0	0	17	18	21	7.56617	10.19473	0.00000	P0CV98	0	0	0	3	7	2	5.84196	8.00365	0.00035
Q8TCT9	6	2	3	0	0	0	-5.78666	7.85714	0.00026	-	-	-	-	-	-	-	-	-	-
P43243	7	8	3	11	6	9	-0.01894	9.85492	1.00000	-	-	-	-	-	-	-	-	-	-
O43390	8	11	7	24	23	17	0.74535	10.88393	0.02694	-	-	-	-	-	-	-	-	-	-
Q92522	4	5	6	8	7	8	0.06612	9.64316	1.00000	-	-	-	-	-	-	-	-	-	-
-	-	-	-	-	-	-	-	-	-	P80723	30	27	36	0	0	0	-8.34408	10.89128	0.00000
P09211	43	41	44	37	30	38	-0.83364	12.27030	0.00006	P09211	47	50	45	28	17	14	-0.83367	12.03167	0.00522
-	-	-	-	-	-	-	-	-	-	O95466	20	20	25	10	16	7	-0.54390	11.00805	0.14403
Q15651	7	8	7	3	3	9	-1.08717	9.60695	0.03576	-	-	-	-	-	-	-	-	-	-
P78371	8	7	9	23	21	27	1.00899	10.96029	0.00274	P78371	10	11	15	19	26	5	0.89976	10.84596	0.02203
Q9BSJ8	0	0	0	17	27	14	7.61654	10.24525	0.00000	-	-	-	-	-	-	-	-	-	-
Q16543	2	0	0	6	6	10	2.78968	8.97743	0.00093	Q16543	0	0	0	7	7	0	6.06075	8.22663	0.00010
P62269	15	13	14	3	3	8	-2.11130	10.20921	0.00000	P62269	8	3	5	3	7	1	-0.10741	9.15739	0.85380
P55209	10	10	4	11	7	15	-0.08946	10.22836	0.89576	P55209	6	10	15	8	5	4	-0.43092	9.98805	0.42923
P15153	6	5	6	0	0	0	-6.40544	8.48639	0.00000	P15153	18	19	18	2	7	3	-1.74738	10.44809	0.00028
P43490	2	3	4	8	6	9	0.79031	9.39395	0.20491	P43490	6	4	3	1	3	0	-1.22598	8.48703	0.22707
P40227	9	8	17	19	17	30	0.40515	11.03680	0.23730	P40227	4	9	5	10	10	0	0.57561	9.65936	0.36327
O60361	9	12	21	13	9	17	-0.65260	10.73836	0.06672	O60361	10	11	16	6	6	6	-0.60256	10.18131	0.21897
Q00839	27	28	31	27	25	32	-0.58193	11.81025	0.01607	Q00839	6	6	6	19	3	6	1.05668	9.94597	0.03315
P30510	4	5	3	11	12	10	0.89849	9.88503	0.06981	P30510	46	37	37	20	21	23	-0.47439	11.91664	0.13558
P17987	2	2	3	21	18	27	2.65261	10.57732	0.00000	P17987	1	3	2	1	4	0	0.16085	7.86666	1.00000
-	-	-	-	-	-	-	-	-	-	P08195	57	32	32	51	64	67	1.01835	12.69672	0.00009
P31942	0	0	0	3	5	2	5.11534	7.71582	0.00400	-	-	-	-	-	-	-	-	-	-
P41250	0	0	1	12	12	16	4.51636	9.74732	0.00000	P41250	5	2	1	2	3	0	-0.23762	8.10445	1.00000
P06576	30	45	30	90	90	79	0.75176	12.89111	0.00003	P06576	0	0	2	6	0	0	1.87292	7.41204	0.18892
P30456	6	5	6	6	6	6	-0.46072	9.52564	0.50446	P30456	34	30	31	26	24	23	0.05097	11.80235	0.90812
P41219	8	7	10	13	16	14	0.23100	10.48194	0.63283	P41219	10	7	6	1	0	0	-3.83182	8.97495	0.00024
P22492	9	12	9	18	25	19	0.49480	10.91628	0.14873	P22492	0	0	2	2	3	1	1.87292	7.41168	0.18892
-	-	-	-	-	-	-	-	-	-	O14818	5	2	3	2	0	0	-5.16323	7.72016	0.00460
O60506	19	20	12	14	17	13	-0.75869	10.96933	0.01638	O60506	1	1	3	2	4	0	0.66395	7.86763	0.55920
-	-	-	-	-	-	-	-	-	-	Q16720	0	0	1	3	5	4	3.67739	8.12028	0.00247
P60174	4	7	9	6	0	3	-1.66939	9.25644	0.00566	P60174	28	27	32	14	8	8	-1.09945	11.25266	0.00254
O75915	6	5	4	6	11	9	0.24088	9.75213	0.64022	-	-	-	-	-	-	-	-	-	-
Q6IS14	3	6	5	0	0	0	-6.12898	8.20558	0.00003	Q6IS14	6	6	9	0	3	3	-1.34648	9.15327	0.05585
P29350	7	7	3	0	0	0	-6.40544	8.48630	0.00000	P29350	3	4	10	0	0	0	-5.91209	8.48199	0.00010
P43362	0	0	0	3	4	5	5.37143	7.97846	0.00201	P43362	0	0	0	3	2	0	4.61371	6.73397	0.06547

Uniprot Accession	MM.1S Global Spectral Count			U266 Global Spectral Count			Statistics		
	Replicate 1	Replicate 2	Replicate 3	Replicate 1	Replicate 2	Replicate 3	logFC	logCPM	PValue
Q03135	4	2	0	2	1	0	-1.46145	7.56618	0.18098
Q14240	9	7	8	14	12	13	0.14956	10.37224	0.80202
P09936	7	9	15	11	6	17	-0.41327	10.41923	0.33124
P10316	6	5	6	9	9	9	0.11642	9.85452	1.00000
P62258	12	13	16	9	9	14	-0.90102	10.58893	0.01132
O60234	5	5	5	0	0	0	-6.22714	8.30537	0.00002
P14174	6	6	6	6	6	10	-0.25699	9.71773	0.64022
Q13838	5	5	2	5	2	4	-0.66096	8.91988	0.40843
P04080	18	17	24	1	0	3	-4.33392	10.38424	0.00000
P83731	1	1	1	5	6	6	1.88338	8.71540	0.03186
P36776	1	3	0	16	22	12	3.03133	10.14410	0.00000
P50502	0	0	0	4	2	4	5.11534	7.71584	0.00400
-	-	-	-	-	-	-	-	-	-
P10599	14	13	15	7	5	9	-1.53636	10.37831	0.00007
Q9Y4L1	17	18	7	20	22	22	0.05773	11.12271	0.92449
-	-	-	-	-	-	-	-	-	-
Q9TNN7	4	4	3	6	6	6	0.15806	9.25304	0.85191
Q8N684	1	4	2	6	6	5	0.71419	8.97931	0.40843
P52209	4	7	11	5	5	4	-1.18471	9.56793	0.02158
O75526	10	5	3	0	0	0	-6.48696	8.56906	0.00000
P23528	15	17	20	23	19	35	0.01661	11.40616	1.00000
O00410	2	3	0	0	5	1	-0.27432	7.85476	1.00000
P23246	8	9	4	27	24	23	1.25937	10.95950	0.00028
P62277	1	0	0	6	4	8	3.37730	8.64085	0.00247
P25205	2	2	2	6	8	7	1.22995	9.14841	0.07800
P21796	18	18	9	30	38	38	0.68394	11.62801	0.01081
Q8WU39	25	23	21	0	0	0	-8.41362	10.51800	0.00000
P49327	14	14	9	0	0	0	-7.51820	9.61242	0.00000
P35613	0	1	0	3	3	3	2.40053	7.71614	0.03962
P08133	24	32	33	36	30	42	-0.26984	12.02023	0.25301
-	-	-	-	-	-	-	-	-	-
-	-	-	-	-	-	-	-	-	-
-	-	-	-	-	-	-	-	-	-
P62158	11	15	10	9	7	7	-1.18563	10.28217	0.00321
P39019	4	7	1	3	7	3	-0.42580	9.03965	0.69246
P10809	67	82	58	125	145	106	0.31115	13.57535	0.03096
-	-	-	-	-	-	-	-	-	-
P05204	9	12	13	6	6	12	-1.04301	10.25669	0.00996
Q71U36	49	58	64	74	73	71	-0.19909	13.00318	0.23647
-	-	-	-	-	-	-	-	-	-
P14136	0	0	0	9	10	9	6.57376	9.19870	0.00000
-	-	-	-	-	-	-	-	-	-
Q14242	3	3	0	3	0	0	-1.46145	7.56621	0.34536
P62805	77	77	90	210	221	189	0.79520	14.12692	0.00000
Q96QV6	32	39	30	90	94	63	0.73932	12.82754	0.00004
P40925	10	13	16	6	2	9	-1.73011	10.20830	0.00004
P62913	3	4	3	3	3	3	-0.68381	8.64404	0.36230
-	-	-	-	-	-	-	-	-	-
P68032	92	95	112	93	91	96	-0.64384	13.59012	0.00001
-	-	-	-	-	-	-	-	-	-
P42765	0	0	0	9	10	5	6.35389	8.97704	0.00001
P34897	4	13	5	26	24	22	1.15351	10.94454	0.00086
-	-	-	-	-	-	-	-	-	-
P16189	6	5	6	6	6	6	-0.46072	9.52564	0.50446
O00148	6	6	1	5	3	4	-0.65222	9.04019	0.42816
Q01518	5	7	9	10	5	8	-0.41379	9.85606	0.45785
Q562R1	28	30	37	44	36	38	-0.23634	12.13337	0.30196
Q9BX68	3	3	0	7	7	5	1.08768	9.03778	0.09560
-	-	-	-	-	-	-	-	-	-
P00338	26	21	35	27	39	30	-0.32137	11.87436	0.17493
P09651	28	41	27	43	59	57	0.17789	12.38655	0.41090
P54652	26	28	24	37	39	54	0.18684	12.09319	0.42898

Uniprot Accession	MM.1S Vesicle Spectral Count			U266 Vesicle Spectral Count			Statistics		
	Replicate 1	Replicate 2	Replicate 3	Replicate 1	Replicate 2	Replicate 3	logFC	logCPM	PValue
Q03135	7	4	2	3	6	0	-0.09714	8.86267	1.00000
Q14240	6	4	2	3	3	3	0.01574	8.79962	1.00000
P09936	40	19	26	13	9	15	-0.76537	11.31762	0.03688
P10316	35	36	34	34	30	25	0.19215	12.01483	0.53301
P62258	28	27	38	21	21	17	-0.22461	11.64875	0.53108
-	-	-	-	-	-	-	-	-	-
P14174	9	10	8	8	6	6	-0.00179	9.96310	1.00000
-	-	-	-	-	-	-	-	-	-
P04080	17	18	20	2	2	0	-3.28290	10.25696	0.00000
P83731	2	2	2	0	0	0	-4.45286	6.98753	0.06547
P36776	0	3	0	3	0	0	0.39823	6.99440	1.00000
P50502	0	0	0	3	2	0	4.61371	6.73397	0.06547
O00560	4	12	9	0	5	17	0.24415	9.97558	0.69662
P10599	19	15	16	1	6	8	-1.29374	10.41146	0.00457
-	-	-	-	-	-	-	-	-	-
P10114	11	6	5	0	6	3	-0.84332	9.35213	0.23113
Q9TNN7	31	27	28	20	20	20	-0.08792	11.59583	0.84744
-	-	-	-	-	-	-	-	-	-
P52209	5	5	6	1	0	0	-3.31602	8.48346	0.00139
-	-	-	-	-	-	-	-	-	-
P23528	33	41	50	24	31	22	-0.25561	12.05069	0.38232
O00410	8	9	8	0	0	0	-6.46080	9.03293	0.00000
-	-	-	-	-	-	-	-	-	-
-	-	-	-	-	-	-	-	-	-
-	-	-	-	-	-	-	-	-	-
-	-	-	-	-	-	-	-	-	-
Q8WU39	6	1	6	3	0	1	-1.22598	8.48743	0.22707
P49327	32	21	10	0	3	0	-3.86880	10.40995	0.00000
P35613	17	13	10	11	15	25	0.77734	10.93826	0.03703
P08133	147	145	140	85	57	21	-0.97408	13.56987	0.00003
P09326	27	24	20	23	26	31	0.60135	11.66848	0.04798
Q04760	9	6	5	0	0	0	-6.14296	8.71294	0.00001
Q6UWD8	0	3	0	0	3	10	2.43822	8.42503	0.00334
P62158	15	18	14	12	18	7	0.08551	10.79943	0.92550
-	-	-	-	-	-	-	-	-	-
P10809	10	0	3	5	1	0	-0.66553	8.64709	0.49877
O00161	1	3	0	9	16	5	3.24825	9.51875	0.00000
-	-	-	-	-	-	-	-	-	-
Q71U36	52	42	43	45	31	18	-0.11205	12.25051	0.67790
P63218	9	6	6	3	3	3	-0.77709	9.30717	0.29612
-	-	-	-	-	-	-	-	-	-
P19397	2	5	6	0	4	8	0.30954	9.05799	0.70636
Q14242	12	10	8	8	9	8	0.16661	10.19142	0.81065
P62805	81	95	75	76	63	39	-0.06458	13.14785	0.75762
Q96QV6	21	20	24	21	15	10	-0.06735	11.19893	0.87663
P40925	8	12	19	2	3	3	-1.82693	9.94426	0.00119
P62913	4	6	6	8	4	2	0.23463	9.31640	0.86486
P33908	0	0	0	0	11	1	5.84196	8.00161	0.00035
P68032	140	179	207	148	142	145	0.15702	14.33241	0.47723
P07948	3	0	1	1	10	2	2.05504	8.50157	0.01637
-	-	-	-	-	-	-	-	-	-
-	-	-	-	-	-	-	-	-	-
P01834	0	0	0	34	36	21	8.74279	10.98572	0.00000
P16189	33	26	29	23	21	23	0.03769	11.68600	0.90221
-	-	-	-	-	-	-	-	-	-
Q01518	19	18	29	3	6	2	-2.13241	10.64104	0.00001
Q562R1	51	64	78	52	53	52	0.13313	12.86955	0.62184
-	-	-	-	-	-	-	-	-	-
Q9Y624	6	10	10	5	6	0	-0.79804	9.60779	0.11579
P00338	43	51	67	39	29	37	-0.18517	12.46102	0.53650
P09651	16	12	20	16	10	5	-0.19834	10.70452	0.69697
P54652	29	25	36	27	23	29	0.24237	11.81966	0.42271

Uniprot Accession	MM.1S Global Spectral Count			U266 Global Spectral Count			Statistics		
	Replicate 1	Replicate 2	Replicate 3	Replicate 1	Replicate 2	Replicate 3	logFC	logCPM	PValue
Q9H8H3	6	7	8	0	0	0	-6.70705	8.79206	0.00000
P26583	14	17	16	0	0	0	-7.86166	9.95962	0.00000
-	-	-	-	-	-	-	-	-	-
P29692	13	16	14	0	0	2	-4.78295	9.89567	0.00000
P35580	5	3	0	2	2	7	-0.08794	8.64311	1.00000
P62937	60	49	74	73	74	77	-0.25771	13.06997	0.12149
-	-	-	-	-	-	-	-	-	-
P61247	3	3	2	2	2	7	-0.08794	8.64312	1.00000
P61313	3	5	5	0	7	8	-0.33728	9.20278	0.57512
-	-	-	-	-	-	-	-	-	-
P48047	4	4	3	10	5	6	0.37710	9.39489	0.60046
P30450	6	5	6	9	9	9	0.11642	9.85452	1.00000
P46783	3	1	5	7	9	7	0.79031	9.39401	0.20491
P07900	34	36	48	62	69	86	0.32873	12.77761	0.07725
Q9P0S9	0	1	2	8	11	9	2.59351	9.34611	0.00020
O60884	3	0	2	4	4	7	1.00618	8.71610	0.16971
P07237	38	51	44	113	116	100	0.75609	13.23264	0.00000
P13804	0	0	0	8	6	3	5.86364	8.48061	0.00007
Q9UQ80	8	7	6	3	0	0	-3.23469	8.98444	0.00001
P62820	5	5	8	6	10	6	-0.25699	9.71789	0.64022
P53999	16	24	18	7	14	13	-1.31268	10.92542	0.00003
P16401	1	8	3	13	12	12	1.06216	10.00725	0.02815
P04350	39	27	36	49	63	59	0.19539	12.48539	0.33625
Q29963	4	4	3	14	15	13	1.36701	10.11968	0.00304
-	-	-	-	-	-	-	-	-	-
-	-	-	-	-	-	-	-	-	-
Q7Z406	3	2	3	3	2	5	-0.22166	8.56546	0.81562
P30447	6	5	6	9	9	9	0.11642	9.85452	1.00000
P16190	7	5	6	9	9	9	0.03490	9.88717	1.00000
Q16836	7	14	9	7	12	11	-0.54519	10.30380	0.16307
-	-	-	-	-	-	-	-	-	-
P69905	15	0	5	0	0	0	-6.63735	8.72172	0.00000
P45880	3	3	4	8	14	13	1.24089	9.88406	0.02121
P52566	19	16	22	0	0	0	-8.13888	10.24012	0.00000
Q13765	3	3	4	3	3	6	-0.28035	8.85503	0.83302
-	-	-	-	-	-	-	-	-	-
P46940	3	7	5	9	12	11	0.53738	9.94833	0.30923
P30040	3	3	3	36	33	31	2.89637	11.15214	0.00000
Q15365	4	4	1	11	10	12	1.30555	9.78480	0.01802
P26038	29	29	21	39	49	48	0.23345	12.14054	0.29938
Q13509	29	26	31	49	57	59	0.38958	12.36187	0.07364
P49257	1	5	0	0	0	0	-4.93381	6.98142	0.01584
P04844	9	18	11	10	10	12	-0.79196	10.52766	0.03597
P31939	10	16	7	13	8	15	-0.42113	10.50540	0.28553
Q9ULV4	6	4	5	10	7	8	0.18494	9.71703	0.75233
P02768	12	10	3	0	0	0	-6.95638	9.04433	0.00000
P32119	11	14	18	4	4	6	-2.14509	10.23507	0.00000
P00403	4	4	0	15	9	9	1.47151	9.75020	0.00565
-	-	-	-	-	-	-	-	-	-
P04222	1	2	0	8	9	9	2.48776	9.25015	0.00059
Q95365	0	0	0	12	14	12	7.01035	9.63788	0.00000
P04075	50	45	65	67	59	84	-0.15715	12.92976	0.37262
-	-	-	-	-	-	-	-	-	-
P32969	1	2	0	9	7	3	2.04124	8.85293	0.01236
P09382	2	3	3	11	13	13	1.63517	9.88353	0.00328
P07195	47	39	45	3	5	11	-3.31502	11.64714	0.00000
Q13813	8	4	3	3	3	2	-1.42335	8.92097	0.02371
P11233	0	0	0	1	4	0	4.15638	6.71652	0.12549
P0CG48	255	300	273	443	381	447	0.06857	15.42794	0.47144
-	-	-	-	-	-	-	-	-	-
-	-	-	-	-	-	-	-	-	-
P08107	6	8	9	14	17	22	0.65007	10.64027	0.10877

Uniprot Accession	MM.1S Vesicle Spectral Count			U266 Vesicle Spectral Count			Statistics		
	Replicate 1	Replicate 2	Replicate 3	Replicate 1	Replicate 2	Replicate 3	logFC	logCPM	PValue
-	-	-	-	-	-	-	-	-	-
-	-	-	-	-	-	-	-	-	-
O15247	4	10	15	0	0	0	-6.67266	9.24608	0.00000
P29692	13	9	18	3	0	0	-3.21721	9.80696	0.00000
P35580	3	7	11	6	10	4	0.35645	9.76879	0.56842
P62937	25	49	53	28	34	24	-0.13096	12.14125	0.66068
P16520	7	8	7	6	9	6	0.35989	9.83827	0.57906
P61247	6	11	6	3	3	0	-1.47503	9.25498	0.02722
P61313	5	9	11	0	8	3	-0.74209	9.57016	0.20969
Q08431	34	34	34	9	9	13	-1.28126	11.43408	0.00036
-	-	-	-	-	-	-	-	-	-
P30450	38	33	37	35	30	30	0.24552	12.08297	0.39298
P46783	3	2	3	2	0	0	-1.47376	7.72460	0.18892
P07900	56	50	53	66	60	43	0.51836	12.78593	0.04933
-	-	-	-	-	-	-	-	-	-
-	-	-	-	-	-	-	-	-	-
P07237	8	1	3	10	0	1	0.29917	8.93057	0.83998
-	-	-	-	-	-	-	-	-	-
Q9UQ80	7	2	1	1	0	0	-2.65313	7.85797	0.02447
P62820	15	7	2	3	5	5	-0.44709	9.61042	0.44187
P53999	5	6	4	3	3	2	-0.46519	8.92809	0.54407
-	-	-	-	-	-	-	-	-	-
P04350	61	62	42	40	39	30	-0.16668	12.49904	0.54365
Q29963	50	39	39	30	31	32	-0.02962	12.19535	0.96219
P15121	10	10	6	1	0	0	-4.00665	9.14400	0.00005
P21926	8	11	13	0	0	0	-6.81336	9.38514	0.00000
Q7Z406	3	6	8	7	3	3	0.04341	9.31599	1.00000
P30447	67	65	65	27	34	35	-0.60484	12.58074	0.02887
P16190	37	29	35	32	27	30	0.24803	11.98762	0.39836
-	-	-	-	-	-	-	-	-	-
P05556	0	0	0	5	10	10	6.88771	9.07875	0.00000
-	-	-	-	-	-	-	-	-	-
-	-	-	-	-	-	-	-	-	-
P52566	21	24	24	0	0	0	-7.91498	10.47313	0.00000
-	-	-	-	-	-	-	-	-	-
Q16222	0	0	0	11	9	10	7.14872	9.34632	0.00000
P46940	20	13	19	20	28	7	0.50970	11.15322	0.17747
-	-	-	-	-	-	-	-	-	-
-	-	-	-	-	-	-	-	-	-
P26038	128	198	208	175	201	210	0.56496	14.58255	0.00988
Q13509	48	42	33	21	15	11	-0.95361	11.78709	0.00229
-	-	-	-	-	-	-	-	-	-
-	-	-	-	-	-	-	-	-	-
P31939	7	5	5	4	2	0	-1.04520	8.92252	0.15367
Q9ULV4	17	11	16	6	5	8	-0.77366	10.37303	0.11324
P02768	24	0	0	0	0	0	-6.40259	8.96556	0.00000
P32119	17	20	15	13	21	16	0.37276	11.09002	0.33262
-	-	-	-	-	-	-	-	-	-
P50993	27	19	14	14	24	22	0.42938	11.32603	0.21509
P04222	31	24	25	17	17	17	-0.21751	11.43512	0.57953
Q95365	52	46	47	43	49	38	0.27312	12.52134	0.31943
P04075	49	54	54	43	34	43	0.04335	12.52894	0.87395
P35609	11	6	11	6	6	7	-0.12691	9.96005	0.89402
P32969	0	0	6	0	0	0	-4.45286	6.98742	0.06547
P09382	9	8	7	9	10	11	0.74613	10.17510	0.09133
P07195	51	50	44	6	3	1	-3.39929	11.61838	0.00000
Q13813	12	16	13	4	3	5	-1.32613	10.12138	0.01083
P11233	7	2	1	6	9	6	1.47526	9.37317	0.01181
P0CG48	261	270	279	235	229	282	0.31231	15.04184	0.12623
P60763	11	10	11	0	3	3	-1.94646	9.63856	0.00266
Q969P0	0	0	2	0	1	8	2.44130	7.87954	0.04401
P08107	11	7	17	6	7	10	-0.17306	10.26396	0.81461

Uniprot Accession	MM.1S Global Spectral Count			U266 Global Spectral Count			Statistics		
	Replicate 1	Replicate 2	Replicate 3	Replicate 1	Replicate 2	Replicate 3	logFC	logCPM	PValue
Q95604	7	7	6	8	9	6	-0.34409	9.82257	0.54802
P62191	0	3	2	7	5	6	1.26454	8.91740	0.08040
-	-	-	-	-	-	-	-	-	-
Q14103	9	16	8	11	13	6	-0.68181	10.37519	0.08303
P06753	3	6	10	3	3	10	-0.78639	9.52603	0.18040
P09493	3	3	3	3	5	4	-0.13153	8.78774	1.00000
P53675	0	0	0	3	2	3	4.80378	7.39418	0.01584
P30479	0	0	0	13	16	13	7.15367	9.78171	0.00000
Q3ZCM7	12	13	11	17	23	17	0.11268	10.93386	0.83878
P18669	15	11	18	12	8	16	-0.83396	10.72131	0.01663
Q9UKY7	6	6	6	0	0	2	-3.53599	8.72066	0.00001
P61586	3	1	2	4	1	9	0.65502	8.71638	0.50627
-	-	-	-	-	-	-	-	-	-
P50990	4	2	4	5	5	9	0.36972	9.25258	0.57512
P18085	2	3	0	4	5	9	1.26454	8.91708	0.08040
Q07020	8	7	9	3	6	8	-1.03433	9.75525	0.02962
-	-	-	-	-	-	-	-	-	-
-	-	-	-	-	-	-	-	-	-
-	-	-	-	-	-	-	-	-	-
-	-	-	-	-	-	-	-	-	-
P22102	4	3	1	1	8	5	0.25183	8.85413	0.83302
Q96KP4	18	10	25	22	8	29	-0.39322	11.20556	0.17103
P51991	12	18	8	18	21	15	-0.04248	10.91906	1.00000
Q09028	6	3	3	2	0	2	-2.05548	8.39734	0.01321
Q9UBV2	2	3	2	4	8	2	0.43939	8.78711	0.66581
P13639	46	61	64	30	39	43	-1.15806	12.55661	0.00000
P16615	0	0	0	24	22	17	7.73525	10.36424	0.00000
P36578	3	9	3	6	13	11	0.44515	9.88559	0.36710
-	-	-	-	-	-	-	-	-	-
Q58FF3	7	10	9	9	9	11	-0.38865	10.17787	0.42703
P06744	8	11	15	18	22	30	0.48967	11.09260	0.14580
Q92841	5	7	5	16	8	9	0.40306	10.03846	0.39913
P62995	0	2	0	7	4	6	2.42335	8.64128	0.00788
Q06830	29	28	28	20	18	19	-1.12212	11.55429	0.00001
Q92930	2	1	3	3	3	1	-0.31531	8.09616	1.00000
Q02878	17	19	11	8	14	8	-1.18937	10.66732	0.00087
-	-	-	-	-	-	-	-	-	-
P61088	8	10	9	0	0	2	-4.11558	9.25855	0.00000
P26373	4	1	4	6	7	6	0.51854	9.20194	0.44611
P18463	0	0	0	12	14	12	7.01035	9.63788	0.00000
P14625	69	84	76	80	79	81	-0.48148	13.27956	0.00210
-	-	-	-	-	-	-	-	-	-
-	-	-	-	-	-	-	-	-	-
Q06323	6	10	11	7	4	9	-0.97217	9.95263	0.03187
P35268	2	2	5	0	0	2	-2.55198	7.85632	0.01200
-	-	-	-	-	-	-	-	-	-
Q9UBS4	0	0	0	8	13	2	6.29326	8.91581	0.00002
P31949	6	4	6	2	0	0	-3.36807	8.56851	0.00008
Q12906	2	4	3	8	12	10	1.16934	9.67819	0.04970
-	-	-	-	-	-	-	-	-	-
P30512	6	5	6	6	6	6	-0.46072	9.52564	0.50446
P10314	6	5	6	8	6	6	-0.31106	9.60565	0.62185
O75390	0	0	0	8	9	8	6.41208	9.03562	0.00001
Q09160	3	2	3	3	3	3	-0.36904	8.48321	0.63100
Q9P2J5	3	6	2	9	8	10	0.73519	9.64161	0.19308
P52565	12	9	9	3	3	2	-2.41369	9.64845	0.00001
O75947	0	3	0	19	17	21	3.61132	10.29481	0.00000
Q96EP5	0	0	0	5	3	2	5.11534	7.71598	0.00400
Q99497	7	17	15	14	13	8	-0.70109	10.60804	0.05282
-	-	-	-	-	-	-	-	-	-
-	-	-	-	-	-	-	-	-	-
P05534	6	5	6	9	9	9	0.11642	9.85452	1.00000

Uniprot Accession	MM.1S Vesicle Spectral Count			U266 Vesicle Spectral Count			Statistics		
	Replicate 1	Replicate 2	Replicate 3	Replicate 1	Replicate 2	Replicate 3	logFC	logCPM	PValue
Q95604	40	34	32	28	27	23	-0.01133	11.93033	1.00000
P62191	2	1	1	1	2	0	0.01504	7.21359	1.00000
P20648	5	5	5	3	4	3	-0.15076	9.05024	1.00000
Q14103	7	9	6	3	6	0	-0.84332	9.35276	0.16224
P06753	7	10	14	16	14	12	0.86327	10.61491	0.03444
P09493	3	2	4	5	3	3	0.70302	8.73382	0.40603
P53675	15	15	15	20	18	16	0.69069	11.05394	0.05709
P30479	45	32	43	41	50	37	0.52321	12.37988	0.05821
Q3ZCM7	21	22	17	16	13	12	-0.11760	11.06414	0.80520
P18669	23	20	35	15	15	19	-0.23858	11.39228	0.57125
-	-	-	-	-	-	-	-	-	-
P61586	22	17	13	6	18	13	-0.05950	10.88094	0.92880
P61225	15	16	12	4	9	4	-0.89929	10.30031	0.05856
P50990	0	0	1	3	7	0	3.41937	7.87394	0.00780
P18085	15	19	15	10	8	10	-0.37370	10.67036	0.37639
Q07020	6	9	6	0	1	1	-2.83480	8.91851	0.00145
Q9BY67	10	6	5	0	0	0	-6.21238	8.78227	0.00001
O15143	2	3	4	0	0	1	-2.50559	7.72424	0.04311
P22732	0	0	0	12	15	21	7.82297	10.04312	0.00000
P12814	17	14	21	16	17	12	0.22143	11.01113	0.55424
P22102	5	1	0	0	1	0	-1.94275	7.20903	0.22536
Q96KP4	39	25	23	6	1	2	-2.81288	10.94564	0.00000
-	-	-	-	-	-	-	-	-	-
-	-	-	-	-	-	-	-	-	-
-	-	-	-	-	-	-	-	-	-
P13639	88	89	99	19	25	18	-1.71973	12.74445	0.00000
-	-	-	-	-	-	-	-	-	-
P36578	5	5	3	3	4	1	-0.26290	8.79700	0.83163
P63092	7	12	12	11	13	15	0.75692	10.55481	0.06334
-	-	-	-	-	-	-	-	-	-
P06744	21	22	16	16	14	10	-0.12891	11.03382	0.73723
-	-	-	-	-	-	-	-	-	-
-	-	-	-	-	-	-	-	-	-
Q06830	25	17	24	12	10	4	-0.90730	10.90865	0.01802
Q92930	5	2	2	1	4	0	-0.40198	8.21024	0.79718
Q02878	12	20	15	4	12	4	-0.79502	10.46096	0.06131
Q30134	8	3	3	0	0	0	-5.63711	8.20185	0.00066
P61088	4	8	7	3	5	1	-0.63475	9.20969	0.27671
P26373	2	3	4	3	3	1	0.06651	8.40743	1.00000
P18463	51	42	46	40	46	38	0.26591	12.45672	0.34291
P14625	13	7	6	8	4	1	-0.56125	9.68345	0.36327
P20339	6	6	3	4	6	4	0.32604	9.26821	0.72859
Q9H3S1	13	0	0	0	0	1	-3.02232	8.20120	0.02656
Q06323	7	3	3	2	6	1	-0.09714	8.86291	1.00000
P35268	2	3	4	0	2	0	-1.63812	7.86144	0.11768
P20020	0	0	0	10	13	8	7.19569	9.39186	0.00000
-	-	-	-	-	-	-	-	-	-
P31949	13	11	18	1	3	4	-1.93310	10.03035	0.00040
-	-	-	-	-	-	-	-	-	-
P63096	14	12	14	7	11	11	-0.03256	10.51640	1.00000
P30512	33	26	29	24	24	26	0.18062	11.75464	0.55336
P10314	33	26	29	30	27	28	0.38002	11.85592	0.21486
-	-	-	-	-	-	-	-	-	-
Q09160	25	21	22	24	28	26	0.62695	11.61730	0.04985
Q9P2J5	3	0	0	0	3	1	0.78917	7.21497	1.00000
P52565	11	12	14	4	4	4	-1.17911	10.00874	0.03315
-	-	-	-	-	-	-	-	-	-
Q96EP5	3	1	1	0	0	0	-4.20294	6.72447	0.12855
Q99497	7	12	12	6	3	4	-0.81246	9.85994	0.16352
Q13733	10	5	5	5	11	5	0.49554	9.76772	0.39168
P62136	0	6	2	3	1	3	0.23087	8.31915	1.00000
P05534	69	72	67	31	38	38	-0.52694	12.68814	0.05220

Uniprot Accession	MM.1S Global Spectral Count			U266 Global Spectral Count			Statistics		
	Replicate 1	Replicate 2	Replicate 3	Replicate 1	Replicate 2	Replicate 3	logFC	logCPM	PValue
P61006	2	1	2	5	6	2	0.80403	8.56459	0.33502
P12956	25	27	30	24	28	35	-0.46293	11.80024	0.05738
P30466	0	0	0	9	11	9	6.62387	9.24917	0.00000
P30484	3	3	3	12	14	12	1.50739	9.94643	0.00416
-	-	-	-	-	-	-	-	-	-
P60660	6	11	10	4	6	12	-0.83658	10.01209	0.04781
P01893	3	2	3	9	9	9	1.18486	9.52250	0.03705
P09874	32	25	33	2	0	5	-4.17746	11.01257	0.00000
Q12765	0	0	0	7	11	10	6.57376	9.19852	0.00000
P08238	82	88	100	80	78	103	-0.59803	13.46236	0.00005
P61981	22	16	13	7	9	22	-0.96867	10.87554	0.00274
P27348	15	18	12	11	14	23	-0.45416	10.93635	0.15834
-	-	-	-	-	-	-	-	-	-
P35606	0	0	0	1	2	10	5.48422	8.09348	0.00101
P23497	1	2	7	0	0	0	-5.65177	7.71943	0.00101
P24534	11	9	12	3	6	2	-2.06092	9.82676	0.00002
Q99623	6	7	4	11	9	5	0.00664	9.78789	1.00000
P61224	0	0	0	18	13	11	7.15367	9.78214	0.00000
P00505	0	0	0	7	8	4	6.02149	8.64066	0.00003
-	-	-	-	-	-	-	-	-	-
P61604	27	27	27	25	27	24	-0.63958	11.69574	0.01217
-	-	-	-	-	-	-	-	-	-
-	-	-	-	-	-	-	-	-	-
-	-	-	-	-	-	-	-	-	-
P56134	0	3	4	4	6	9	0.87205	9.09426	0.23334
-	-	-	-	-	-	-	-	-	-
P63241	10	15	18	9	9	15	-0.92541	10.64721	0.00718
Q9Y3Z3	3	12	7	0	0	0	-6.77354	8.85919	0.00000
P13797	2	3	5	3	3	3	-0.68381	8.64409	0.36230
P30044	8	9	11	17	13	15	0.13390	10.58483	0.81676
Q13423	1	2	0	8	9	3	2.11413	8.91683	0.00759
P00558	31	30	34	56	63	102	0.66723	12.68790	0.00060
P62424	2	2	3	6	5	3	0.43939	8.78728	0.66581
P52272	10	12	5	32	33	34	1.31831	11.36454	0.00002
P0C0S8	56	77	55	159	156	112	0.63328	13.64542	0.00001
P30483	0	0	0	10	13	9	6.76452	9.39081	0.00000
P61769	0	0	0	10	11	11	6.76452	9.39075	0.00000
P06748	27	26	28	62	60	62	0.63275	12.43741	0.00200
O00571	1	0	0	12	13	8	4.24108	9.47852	0.00000
P18465	3	3	3	9	11	9	1.12091	9.64101	0.06841
P63104	28	28	27	29	21	36	-0.49700	11.80085	0.04063
P30049	6	5	4	3	3	4	-1.11179	9.04085	0.07800
-	-	-	-	-	-	-	-	-	-
P42167	6	5	8	7	8	9	-0.21022	9.82212	0.76403
P19338	17	28	23	46	42	51	0.48058	12.08364	0.03899
P14314	3	5	2	32	29	30	2.61191	11.04333	0.00000
P55084	0	0	0	4	4	7	5.68637	8.29993	0.00026
P16070	3	3	3	0	0	2	-2.55198	7.85627	0.01200
P15531	6	8	17	3	2	5	-2.14912	9.75797	0.00001
O43707	1	3	0	6	1	2	0.59570	8.09550	0.58270
P50395	11	10	10	9	14	18	-0.14532	10.56548	0.81676
-	-	-	-	-	-	-	-	-	-
P22314	24	20	28	21	9	15	-1.22231	11.27458	0.00002
Q00325	2	3	3	4	12	8	1.01689	9.39329	0.10204
-	-	-	-	-	-	-	-	-	-
Q71DI3	61	69	54	117	113	82	0.21195	13.34613	0.16574
P49588	0	4	1	6	5	11	1.54978	9.14784	0.01543
P01892	6	5	6	6	6	6	-0.46072	9.52564	0.50446
P01854	0	0	0	10	14	20	7.22032	9.84811	0.00000
O00299	2	1	4	4	3	3	-0.03410	8.48295	1.00000
P62263	7	7	6	8	9	10	-0.11549	9.95016	0.88473
P16188	6	5	6	9	9	9	0.11642	9.85452	1.00000

Uniprot Accession	MM.1S Vesicle Spectral Count			U266 Vesicle Spectral Count			Statistics		
	Replicate 1	Replicate 2	Replicate 3	Replicate 1	Replicate 2	Replicate 3	logFC	logCPM	PValue
P61006	13	15	6	7	5	2	-0.83931	9.98174	0.08080
P12956	2	4	4	1	4	0	-0.54952	8.31094	0.61970
P30466	49	42	43	37	46	38	0.28338	12.41319	0.31209
P30484	57	47	48	40	47	38	0.14874	12.52660	0.57857
Q99828	5	8	3	0	0	2	-2.44855	8.56950	0.01637
P60660	16	17	21	18	18	10	0.19884	11.05437	0.61941
P01893	37	30	31	30	33	35	0.43006	12.03981	0.13831
P09874	7	8	12	1	0	0	-4.06051	9.19602	0.00003
-	-	-	-	-	-	-	-	-	-
P08238	99	88	94	78	85	52	0.04487	13.35954	0.90122
P61981	28	29	30	22	21	16	-0.12870	11.59366	0.69897
P27348	19	18	27	21	19	15	0.21163	11.30756	0.60637
P27701	10	14	13	0	0	0	-7.02107	9.59186	0.00000
-	-	-	-	-	-	-	-	-	-
-	-	-	-	-	-	-	-	-	-
P24534	3	3	7	0	0	0	-5.53242	8.09754	0.00066
-	-	-	-	-	-	-	-	-	-
P61224	24	35	22	23	18	16	-0.07553	11.51727	0.84131
-	-	-	-	-	-	-	-	-	-
O94832	3	1	5	0	0	0	-5.01570	7.56927	0.00888
-	-	-	-	-	-	-	-	-	-
P05023	87	58	49	48	59	66	0.26551	12.94196	0.27088
P53985	4	4	5	7	7	10	1.29691	9.63359	0.02329
Q9BZQ8	7	0	1	6	13	5	1.97799	9.42056	0.00079
-	-	-	-	-	-	-	-	-	-
P28838	9	0	3	0	0	0	-5.41954	7.97930	0.00125
P63241	14	13	14	0	3	3	-2.30119	9.93962	0.00012
-	-	-	-	-	-	-	-	-	-
P13797	5	4	8	4	3	0	-0.82989	8.98489	0.23409
P30044	6	0	11	3	0	0	-1.99658	8.71682	0.02474
-	-	-	-	-	-	-	-	-	-
P00558	54	58	75	38	35	35	-0.36023	12.60009	0.17966
P62424	4	4	6	3	4	3	-0.05316	8.99207	1.00000
-	-	-	-	-	-	-	-	-	-
P0C0S8	57	58	67	33	39	26	-0.46107	12.51730	0.09078
P30483	39	33	38	35	43	29	0.39037	12.18114	0.18175
P61769	14	9	10	9	12	11	0.38383	10.43606	0.38599
P06748	28	18	17	25	14	3	-0.15307	11.11134	0.68492
-	-	-	-	-	-	-	-	-	-
P18465	53	44	42	37	46	31	0.14482	12.39353	0.63840
P63104	31	26	33	28	26	28	0.29600	11.84546	0.33625
-	-	-	-	-	-	-	-	-	-
Q5Y7A7	7	0	0	4	6	0	0.91814	8.49473	0.35127
-	-	-	-	-	-	-	-	-	-
P19338	17	18	20	11	5	0	-1.33865	10.53407	0.00242
-	-	-	-	-	-	-	-	-	-
-	-	-	-	-	-	-	-	-	-
P16070	35	24	30	26	24	41	0.46194	11.92153	0.10395
P15531	17	20	13	10	12	6	-0.40268	10.68479	0.32144
O43707	40	36	44	31	40	33	0.22421	12.22360	0.45551
P50395	27	36	46	17	23	12	-0.63449	11.71931	0.03724
Q9Y3L5	11	7	5	0	6	4	-0.75798	9.44360	0.24844
P22314	18	14	10	13	2	0	-1.04377	10.22328	0.01971
-	-	-	-	-	-	-	-	-	-
P27105	0	0	0	3	9	7	6.49563	8.67586	0.00000
Q71DI3	37	34	20	14	22	3	-0.78793	11.40338	0.01785
P49588	16	5	1	2	3	0	-1.66489	9.14582	0.02079
P01892	30	29	26	29	27	18	0.23050	11.72613	0.50866
-	-	-	-	-	-	-	-	-	-
O00299	21	36	32	14	27	29	0.08444	11.73033	0.81101
P62263	4	3	0	1	4	0	-0.05210	7.99024	1.00000
P16188	50	40	43	29	32	36	-0.02416	12.25451	1.00000

Uniprot Accession	MM.1S Global Spectral Count			U266 Global Spectral Count			Statistics		
	Replicate 1	Replicate 2	Replicate 3	Replicate 1	Replicate 2	Replicate 3	logFC	logCPM	PValue
P84085	4	6	4	6	8	9	0.16428	9.60423	0.86948
P35749	5	5	4	6	5	9	-0.03459	9.48275	1.00000
Q05639	44	50	52	43	37	48	-0.73816	12.50410	0.00012
P05141	13	11	13	12	13	11	-0.58524	10.58782	0.10877
Q8IUE6	19	24	20	59	67	49	0.92206	12.28014	0.00003
P10321	3	2	3	11	12	10	1.47151	9.74996	0.01039
Q13011	2	0	0	7	11	4	2.78968	8.97767	0.00093
O14979	3	3	3	5	6	3	0.08588	8.91885	1.00000
-	-	-	-	-	-	-	-	-	-
A6NHL2	0	2	1	3	6	5	1.60857	8.48124	0.07835
P25787	0	0	0	0	3	4	4.61850	7.20143	0.03156
P68363	51	59	64	74	73	71	-0.22415	13.01477	0.18869
Q13748	44	46	52	56	58	59	-0.26438	12.69899	0.14934
P48643	3	6	6	13	12	17	0.92653	10.22528	0.04378
P30480	0	0	0	15	17	16	7.34505	9.97352	0.00000
P29401	4	3	12	1	0	9	-1.44877	9.25568	0.01716
P07205	12	13	11	10	11	18	-0.43136	10.62571	0.25949
O43852	5	4	3	29	38	35	2.51779	11.21658	0.00000
Q15181	7	8	7	4	3	4	-1.52448	9.44274	0.00325
Q9BY50	4	6	3	0	0	0	-6.02365	8.09843	0.00007
Q58FF6	10	9	9	10	8	12	-0.44634	10.25485	0.29815
P30505	4	4	3	9	9	10	0.78710	9.67902	0.19308
P30085	3	6	4	4	1	6	-0.77459	8.98134	0.31127
P09429	7	8	22	0	0	0	-7.51820	9.61272	0.00000
-	-	-	-	-	-	-	-	-	-
P01891	6	5	6	9	9	9	0.11642	9.85452	1.00000
O75844	2	3	1	3	7	4	0.65502	8.71636	0.36230
P31946	26	26	23	8	10	19	-1.56140	11.21214	0.00000
Q14011	1	3	0	13	10	10	2.43625	9.60107	0.00023
P04406	75	97	115	78	56	91	-0.89992	13.41707	0.00000
P24752	7	7	6	7	9	10	-0.16934	9.91921	0.76931
P13796	42	33	51	26	26	38	-1.03267	12.16242	0.00000
Q13310	7	8	5	3	5	6	-1.04852	9.48476	0.06039
P12004	2	2	13	0	0	0	-6.40544	8.48655	0.00000
P10319	4	5	3	9	11	9	0.71385	9.75122	0.20531
P13667	35	34	48	19	22	25	-1.37167	11.92488	0.00000
P53674	5	6	4	0	0	0	-6.22714	8.30533	0.00002
P51665	3	2	0	0	0	0	-4.68019	6.71828	0.03156
P60866	0	0	3	2	3	3	0.82353	7.85422	0.55030
P35579	62	68	54	32	44	51	-1.08277	12.69259	0.00000
-	-	-	-	-	-	-	-	-	-
-	-	-	-	-	-	-	-	-	-
P20073	0	3	1	4	3	3	0.74309	8.20208	0.58270
P08670	68	82	48	181	196	192	0.97253	13.95090	0.00000
P08758	13	7	13	21	21	25	0.46956	11.03674	0.16777
P04843	11	14	4	16	9	3	-0.59514	10.23076	0.19299
Q969X5	5	7	1	9	5	5	-0.00215	9.39547	1.00000
P23526	10	6	8	7	9	16	-0.13345	10.20283	0.79138
P62829	6	5	3	5	3	3	-0.87992	9.04065	0.17226
P18464	4	5	3	12	14	12	1.10033	10.03628	0.02046
-	-	-	-	-	-	-	-	-	-
-	-	-	-	-	-	-	-	-	-
P07954	15	22	19	17	15	12	-0.89311	11.04458	0.00360
P52907	4	0	0	0	0	1	-2.24583	6.71795	0.21967
P30685	4	5	3	12	14	12	1.10033	10.03628	0.02046
P39748	4	4	10	4	5	5	-0.89813	9.39714	0.11391
Q7Z2X7	0	0	0	12	9	12	6.80851	9.43511	0.00000
P18124	12	7	8	12	6	3	-0.90278	9.98350	0.04781
P06733	37	43	69	111	103	143	0.71017	13.36297	0.00001
Q99714	7	6	4	5	10	6	-0.24168	9.64369	0.74582
-	-	-	-	-	-	-	-	-	-
Q6FI13	56	77	55	157	153	111	0.61287	13.63184	0.00002

Uniprot Accession	MM.1S Vesicle Spectral Count			U266 Vesicle Spectral Count			Statistics		
	Replicate 1	Replicate 2	Replicate 3	Replicate 1	Replicate 2	Replicate 3	logFC	logCPM	PValue
P84085	15	22	16	10	8	10	-0.48628	10.74191	0.24930
P35749	5	10	21	10	6	6	-0.27690	10.26318	0.63897
Q05639	37	36	37	30	26	31	0.09250	12.03660	0.79741
-	-	-	-	-	-	-	-	-	-
Q8IUE6	31	31	30	22	17	16	-0.30997	11.59922	0.36639
P10321	39	27	27	28	27	26	0.23119	11.85763	0.43056
-	-	-	-	-	-	-	-	-	-
O14979	6	4	0	3	3	0	-0.29634	8.40392	0.81070
Q7Z403	4	6	7	0	0	1	-3.40199	8.56660	0.00334
A6NHL2	2	4	2	3	3	2	0.41818	8.41032	0.81070
P25787	9	6	3	0	1	0	-3.48312	8.64109	0.00044
P68363	53	42	43	45	31	18	-0.12252	12.25618	0.64555
Q13748	44	38	36	39	28	15	-0.09370	12.04392	0.75716
P48643	12	8	6	7	9	4	0.05208	9.92899	1.00000
P30480	58	45	52	49	56	46	0.39280	12.68099	0.13389
P29401	42	34	44	0	2	0	-5.33323	11.27271	0.00000
P07205	9	11	15	11	10	10	0.25416	10.45801	0.59182
-	-	-	-	-	-	-	-	-	-
Q15181	17	17	21	0	0	0	-7.58934	10.15209	0.00000
-	-	-	-	-	-	-	-	-	-
Q58FF6	12	8	9	9	9	4	0.03229	10.07752	1.00000
P30505	38	30	32	23	25	23	-0.06277	11.82328	0.90890
P30085	1	0	2	0	2	1	0.39823	6.99266	1.00000
-	-	-	-	-	-	-	-	-	-
P22234	5	14	5	4	0	0	-2.09614	9.20416	0.00422
P01891	31	29	28	31	28	25	0.36299	11.84649	0.23455
-	-	-	-	-	-	-	-	-	-
P31946	24	18	22	20	19	19	0.28796	11.34635	0.42837
-	-	-	-	-	-	-	-	-	-
P04406	114	106	133	58	46	49	-0.77415	13.35485	0.00174
-	-	-	-	-	-	-	-	-	-
P13796	62	56	83	25	33	2	-1.30996	12.38037	0.00000
-	-	-	-	-	-	-	-	-	-
P12004	0	1	1	0	0	3	0.92153	6.73337	0.69187
P10319	46	44	37	31	37	27	0.01230	12.20176	1.00000
-	-	-	-	-	-	-	-	-	-
P53674	4	3	5	0	0	0	-5.41954	7.98246	0.00125
P51665	7	5	0	6	0	3	0.01574	8.80066	1.00000
P60866	3	1	0	1	2	0	0.01504	7.21320	1.00000
P35579	39	75	116	78	65	38	0.08541	13.09463	0.81709
Q10589	6	6	7	5	6	6	0.26701	9.58112	0.64489
P49720	7	1	3	0	0	0	-5.29707	7.85571	0.00240
P20073	3	1	2	10	4	2	1.79783	8.87714	0.01509
P08670	44	36	38	26	9	6	-1.08997	11.68696	0.00078
P08758	35	22	21	32	33	24	0.61963	11.80799	0.04306
-	-	-	-	-	-	-	-	-	-
Q969X5	4	1	0	0	2	0	-0.82537	7.21094	0.69187
P23526	12	10	14	10	7	6	-0.21337	10.28633	0.72778
P62829	3	3	3	0	0	0	-5.01570	7.57014	0.00888
P18464	52	46	46	34	38	34	-0.01083	12.37363	1.00000
Q8WWI5	21	10	6	0	0	0	-7.02107	9.58679	0.00000
Q15758	40	32	38	31	30	35	0.23419	12.10529	0.39990
P07954	1	2	5	0	0	0	-4.85133	7.40134	0.01721
P52907	10	8	5	6	4	0	-0.75798	9.44244	0.17855
P30685	50	47	43	34	38	34	0.02973	12.35248	0.93043
-	-	-	-	-	-	-	-	-	-
Q7Z2X7	0	0	0	3	3	0	4.86689	6.99769	0.03350
P18124	8	9	1	0	0	0	-5.99322	8.56398	0.00005
P06733	92	81	113	83	102	100	0.42573	13.59137	0.06607
-	-	-	-	-	-	-	-	-	-
P62879	12	18	20	8	19	17	0.24543	10.97095	0.54874
Q6FI13	49	51	57	27	37	20	-0.47013	12.30054	0.08545

Uniprot Accession	MM.1S Global Spectral Count			U266 Global Spectral Count			Statistics		
	Replicate 1	Replicate 2	Replicate 3	Replicate 1	Replicate 2	Replicate 3	logFC	logCPM	PValue
P15311	9	8	4	22	27	23	1.22000	10.92877	0.00054
P22392	9	12	21	14	11	18	-0.51275	10.80733	0.13896
-	-	-	-	-	-	-	-	-	-
Q16629	4	5	7	7	9	12	0.25472	9.85392	0.76403
P62979	31	36	33	51	45	55	0.04478	12.36638	0.85921
P54819	5	8	10	1	0	2	-3.36473	9.10013	0.00000
O14950	4	6	1	3	6	6	-0.10030	9.09565	1.00000
Q15084	26	33	30	62	63	66	0.55098	12.51715	0.00585
P06899	42	45	46	171	187	162	1.41604	13.71372	0.00000
-	-	-	-	-	-	-	-	-	-
-	-	-	-	-	-	-	-	-	-
P05455	5	5	5	3	2	4	-1.25918	8.98212	0.04499
Q969H8	7	5	7	6	4	2	-1.19269	9.35206	0.05250
P62266	4	3	8	5	5	6	-0.44941	9.35044	0.47762
Q04826	0	0	0	13	16	13	7.15367	9.78171	0.00000
P09622	0	0	0	6	3	0	4.96796	7.56427	0.00796
P55072	28	23	30	34	22	35	-0.38064	11.82567	0.12879
P03989	0	0	0	11	13	9	6.80851	9.43512	0.00000
-	-	-	-	-	-	-	-	-	-
P26640	6	9	6	0	0	0	-6.70705	8.79197	0.00000
Q29865	1	2	0	11	12	10	2.82825	9.56121	0.00002
O75083	5	4	4	0	0	5	-1.86727	8.56706	0.01995
P38646	20	24	27	60	70	54	0.82235	12.38006	0.00010
-	-	-	-	-	-	-	-	-	-
P01744	0	0	0	6	9	8	6.29326	8.91548	0.00002
O00567	5	8	5	6	8	6	-0.39258	9.64407	0.51647
P36542	5	3	5	12	8	6	0.44437	9.68016	0.42346
P26599	9	16	4	26	26	31	0.96248	11.19684	0.00178
P68104	67	68	68	91	95	92	-0.09597	13.30769	0.54753
Q12905	4	4	1	12	17	16	1.74958	10.14551	0.00038
Q9Y6N5	0	0	0	8	2	4	5.58883	8.20095	0.00051
A6NL28	3	3	5	2	0	6	-0.98288	8.64431	0.16971
P13010	22	19	18	32	32	36	0.21086	11.70644	0.44429
P17661	13	11	10	25	24	27	0.60783	11.17319	0.04801
-	-	-	-	-	-	-	-	-	-
P23396	12	14	16	19	24	23	0.10193	11.14948	0.77833
P50991	3	1	0	3	3	6	0.99917	8.39432	0.30416
O75955	0	0	0	4	3	2	4.96796	7.56405	0.00796
P27797	36	37	41	80	79	73	0.47470	12.82286	0.00849
P62847	5	0	4	6	6	4	0.27477	9.03901	0.84008
O43143	0	0	0	5	6	7	5.94472	8.56257	0.00007
Q9Y281	4	5	8	11	9	10	0.26685	9.94935	0.66350
Q08211	5	4	4	18	15	17	1.37994	10.36846	0.00189
Q6DN03	5	5	4	23	23	22	1.71596	10.74645	0.00002
P14550	4	4	3	0	0	0	-5.78666	7.85706	0.00026
P11142	50	64	53	63	60	85	-0.23263	12.94968	0.19234
O75396	0	0	0	3	3	4	5.11534	7.71576	0.00400
P14866	10	11	7	17	19	20	0.44754	10.78543	0.19353
P62249	0	0	2	11	15	10	3.49267	9.63862	0.00000
Q07021	0	6	0	1	10	4	0.75256	8.78632	0.26632
-	-	-	-	-	-	-	-	-	-
P59998	5	5	5	0	0	0	-6.22714	8.30537	0.00002
P31947	7	7	7	3	3	9	-1.02068	9.56725	0.04970
Q31612	3	2	3	11	12	10	1.47151	9.74996	0.01039
P13747	0	0	0	6	6	6	5.94472	8.56268	0.00007
P46778	1	0	1	2	1	6	1.52767	7.85375	0.22825
Q9NQZ3	0	0	0	24	6	14	7.22032	9.84932	0.00000
P05362	0	0	0	3	3	0	4.40586	6.97955	0.06291
P07355	14	22	14	5	10	14	-1.32669	10.70461	0.00011
P61158	2	3	3	0	0	0	-5.33700	7.39700	0.00400
-	-	-	-	-	-	-	-	-	-
-	-	-	-	-	-	-	-	-	-

Uniprot Accession	MM.1S Vesicle Spectral Count			U266 Vesicle Spectral Count			Statistics		
	Replicate 1	Replicate 2	Replicate 3	Replicate 1	Replicate 2	Replicate 3	logFC	logCPM	PValue
P15311	58	96	116	102	107	156	0.86540	13.78323	0.00016
P22392	27	28	25	13	13	6	-0.88638	11.19287	0.01099
P32942	25	32	20	9	21	21	-0.16257	11.40775	0.67452
Q16629	4	1	0	4	4	0	1.06658	8.10953	0.28138
P62979	29	30	31	27	29	35	0.44587	11.92771	0.12930
P54819	12	0	4	0	3	1	-1.51968	8.71610	0.07545
O14950	6	12	14	9	7	11	0.18449	10.29780	0.73312
Q15084	7	2	0	11	7	0	1.40282	9.16873	0.02722
P06899	52	49	43	54	31	14	-0.10919	12.32313	0.65626
P54709	23	16	10	4	14	14	-0.18242	10.74408	0.70162
P20039	10	3	3	2	3	0	-1.21241	8.78881	0.13230
P05455	3	2	2	0	0	0	-4.66581	7.20872	0.03350
-	-	-	-	-	-	-	-	-	-
P62266	0	5	4	3	2	0	-0.40198	8.21405	0.79718
Q04826	45	32	44	41	50	37	0.51127	12.38524	0.06505
-	-	-	-	-	-	-	-	-	-
P55072	46	48	56	5	0	0	-4.41833	11.61356	0.00000
P03989	45	39	43	37	43	32	0.24931	12.31673	0.39893
A8MTJ3	8	10	9	7	8	8	0.19786	10.05587	0.70354
-	-	-	-	-	-	-	-	-	-
Q29865	37	27	28	20	20	23	-0.11476	11.68118	0.80586
O75083	18	22	16	9	16	21	0.14665	11.08906	0.68492
-	-	-	-	-	-	-	-	-	-
Q01650	5	3	0	9	13	18	2.70988	10.02853	0.00000
-	-	-	-	-	-	-	-	-	-
O00567	6	4	4	3	3	4	-0.05316	8.99233	1.00000
-	-	-	-	-	-	-	-	-	-
P26599	16	9	12	8	6	0	-0.96032	10.06271	0.04900
P68104	69	54	71	54	48	45	0.03087	12.82238	0.89264
-	-	-	-	-	-	-	-	-	-
-	-	-	-	-	-	-	-	-	-
A6NL28	6	5	8	11	11	6	0.97987	9.97342	0.04900
P13010	11	5	4	0	0	0	-6.14296	8.71182	0.00001
P17661	5	3	4	3	0	0	-1.50403	8.30714	0.19380
P04899	30	25	23	26	30	27	0.51919	11.75562	0.08581
P23396	14	16	23	12	16	9	-0.08683	10.89656	0.85918
P50991	4	3	2	2	4	3	0.41959	8.57959	0.82200
O75955	7	3	3	11	8	1	1.03641	9.45763	0.10361
P27797	2	0	0	3	0	0	0.92153	6.73009	1.00000
P62847	2	4	0	0	0	0	-4.45286	6.98841	0.06547
O43143	6	3	8	0	0	0	-5.91209	8.48048	0.00010
Q9Y281	16	19	19	9	11	5	-0.67529	10.69802	0.09341
Q08211	2	0	1	0	8	0	1.75224	7.86914	0.11768
Q6DN03	3	4	1	7	2	2	0.86738	8.66114	0.38020
-	-	-	-	-	-	-	-	-	-
P11142	64	57	72	60	53	59	0.26460	12.93529	0.28161
-	-	-	-	-	-	-	-	-	-
-	-	-	-	-	-	-	-	-	-
P62249	3	4	5	10	2	1	0.53596	9.05510	0.45033
-	-	-	-	-	-	-	-	-	-
Q99959	2	2	8	5	13	19	2.02981	10.05382	0.00006
P59998	20	11	11	2	2	3	-2.12041	9.99782	0.00018
P31947	10	9	12	9	8	9	0.17586	10.24423	0.81461
Q31612	43	31	40	39	39	31	0.36563	12.22018	0.19086
P13747	22	15	21	14	19	16	0.18701	11.15259	0.57967
P46778	0	0	0	6	0	0	4.86689	6.99873	0.03350
-	-	-	-	-	-	-	-	-	-
P05362	20	12	25	18	27	29	0.80461	11.46555	0.01376
P07355	50	41	46	19	27	24	-0.53623	12.08242	0.07543
P61158	16	14	13	3	6	4	-1.28083	10.19710	0.00973
P17612	6	3	0	0	0	0	-5.01570	7.56899	0.00888
P33241	0	0	3	9	15	37	4.65011	10.47363	0.00000

Uniprot Accession	MM.1S Global Spectral Count			U266 Global Spectral Count			Statistics		
	Replicate 1	Replicate 2	Replicate 3	Replicate 1	Replicate 2	Replicate 3	logFC	logCPM	PValue
P17858	3	7	6	3	2	5	-1.20370	9.09756	0.05431
O43175	0	0	0	5	4	0	4.96796	7.56419	0.00796
P40926	35	29	33	46	40	42	-0.14926	12.21147	0.53185
Q9UNM6	4	7	2	6	6	6	-0.07892	9.34957	1.00000
Q96E39	6	6	3	3	3	5	-0.97808	9.09721	0.12538
Q15637	7	8	0	6	3	3	-0.85571	9.15169	0.25197
P39023	2	6	0	3	8	4	0.34937	8.91816	0.83302
O00764	2	3	1	0	0	0	-4.93381	6.98150	0.01584
Q01534	0	0	0	16	14	17	7.31486	9.94334	0.00000
Q99798	7	9	8	6	7	7	-0.80359	9.85683	0.10093
-	-	-	-	-	-	-	-	-	-
P25705	38	56	33	73	59	57	0.02385	12.69926	0.87664
Q9UMX0	0	1	0	4	8	10	3.66254	8.91561	0.00024
P48735	26	19	18	0	0	0	-8.28278	10.38564	0.00000
P11940	4	3	2	6	5	4	0.18341	8.98014	1.00000
Q03518	0	0	0	5	0	1	4.40586	6.97967	0.06291
-	-	-	-	-	-	-	-	-	-
P30101	20	17	22	18	17	17	-0.72861	11.19468	0.01339
Q8NBS9	45	41	52	137	124	105	0.85655	13.35644	0.00000
P67936	3	3	3	3	3	6	-0.13153	8.78769	1.00000
Q9HB71	4	0	0	2	0	2	-0.51773	7.39567	0.72728
P40939	26	28	12	33	29	20	-0.23573	11.60717	0.43105
P31040	2	3	3	6	6	8	0.75738	9.20142	0.25197
Q16891	1	2	0	9	4	6	2.04124	8.85285	0.01236
P34931	11	11	12	28	27	35	0.85088	11.34400	0.00449
P62081	19	16	16	23	18	22	-0.24376	11.23006	0.46797
P35232	14	11	6	6	13	6	-0.85239	10.20543	0.03646
Q99832	2	0	3	12	15	15	2.47348	9.94498	0.00001
P30041	9	20	14	12	5	17	-0.88272	10.66586	0.01056
O60814	47	47	48	179	200	168	1.39470	13.79033	0.00000
-	-	-	-	-	-	-	-	-	-
Q14568	4	6	9	16	15	20	0.86787	10.52133	0.03054
Q13200	3	11	5	3	2	4	-1.59616	9.20516	0.00873
P62244	2	3	1	3	4	9	0.84391	8.85341	0.38660
P0C0S5	32	43	34	73	78	54	0.36103	12.68513	0.05245
P61978	28	26	20	27	35	26	-0.29879	11.73787	0.23036
P50213	3	2	0	5	4	5	0.90864	8.64230	0.24067
P30481	0	0	0	10	13	9	6.76452	9.39081	0.00000
P39656	3	1	0	6	6	4	1.40547	8.71591	0.06520
P62826	11	13	12	9	12	9	-0.80660	10.44286	0.03054
-	-	-	-	-	-	-	-	-	-
Q58FG0	6	6	9	7	6	19	0.05746	10.12266	1.00000
-	-	-	-	-	-	-	-	-	-
P62753	4	3	7	9	10	11	0.54331	9.85343	0.28654
-	-	-	-	-	-	-	-	-	-
P62841	0	1	2	0	6	1	0.63824	7.71674	0.75471
Q86V81	0	0	0	0	10	8	5.94472	8.56216	0.00007
P37837	1	3	9	0	0	0	-6.02365	8.09858	0.00007
P57737	1	2	3	0	1	0	-2.80738	7.20378	0.07103
P00387	0	0	0	8	8	15	6.71914	9.34484	0.00000
-	-	-	-	-	-	-	-	-	-
P13929	8	13	11	29	26	25	0.76848	11.19844	0.01467
P47755	5	5	6	0	0	0	-6.31904	8.39871	0.00001
P63244	19	20	18	13	14	16	-0.95149	11.04462	0.00188
P16402	48	54	30	52	61	45	-0.28979	12.57955	0.14442
P68366	33	47	41	40	50	49	-0.34893	12.42199	0.08459
P23284	39	44	46	37	48	47	-0.51553	12.43003	0.00835
Q7KZF4	2	3	4	3	0	1	-1.64842	8.09723	0.05850
P0CW22	2	5	9	9	8	10	0.20282	9.82112	0.75839
P30613	2	3	2	9	10	10	1.47442	9.56254	0.00981
Q9NTK5	2	1	2	3	3	4	0.43516	8.30182	0.79149
P22695	7	16	2	0	0	0	-6.95638	9.04409	0.00000

Uniprot Accession	MM.1S Vesicle Spectral Count			U266 Vesicle Spectral Count			Statistics		
	Replicate 1	Replicate 2	Replicate 3	Replicate 1	Replicate 2	Replicate 3	logFC	logCPM	PValue
P17858	14	9	7	0	1	0	-4.21099	9.33857	0.00001
-	-	-	-	-	-	-	-	-	-
P40926	0	0	0	6	0	0	4.86689	6.99873	0.03350
-	-	-	-	-	-	-	-	-	-
-	-	-	-	-	-	-	-	-	-
-	-	-	-	-	-	-	-	-	-
P39023	1	2	6	3	3	0	-0.14880	8.31261	1.00000
O00764	13	16	14	0	0	0	-7.23633	9.80475	0.00000
Q01534	0	0	0	3	6	2	5.71871	7.87748	0.00066
-	-	-	-	-	-	-	-	-	-
P01111	3	0	3	3	10	8	2.18563	9.17870	0.00114
-	-	-	-	-	-	-	-	-	-
Q9UMX0	0	0	0	6	0	0	4.86689	6.99873	0.03350
-	-	-	-	-	-	-	-	-	-
-	-	-	-	-	-	-	-	-	-
-	-	-	-	-	-	-	-	-	-
P13612	12	9	6	9	15	13	0.87874	10.42274	0.04955
-	-	-	-	-	-	-	-	-	-
Q8NBS9	7	3	8	24	4	0	1.05668	9.94057	0.04335
P67936	6	2	9	9	9	7	0.97562	9.81026	0.06515
Q9HB71	12	6	10	2	4	0	-1.75565	9.47674	0.00599
-	-	-	-	-	-	-	-	-	-
-	-	-	-	-	-	-	-	-	-
-	-	-	-	-	-	-	-	-	-
P34931	14	9	16	10	10	13	0.18884	10.58208	0.68194
P62081	14	6	3	0	9	0	-0.90665	9.39339	0.12235
-	-	-	-	-	-	-	-	-	-
Q99832	3	3	6	0	4	0	-1.11310	8.40068	0.19380
P30041	13	11	21	10	17	20	0.49124	10.94507	0.16632
O60814	54	51	47	58	34	16	-0.06177	12.42239	0.80074
P62330	0	0	2	7	6	8	3.64452	8.95319	0.00000
Q14568	15	16	12	14	13	7	0.09176	10.67486	0.92183
Q13200	3	0	1	1	0	1	-0.52289	6.99069	1.00000
P62244	8	9	12	0	0	0	-6.67266	9.24433	0.00000
P0C0S5	16	18	20	17	17	11	0.16728	11.04025	0.67695
P61978	7	3	0	3	2	0	-0.54952	8.30934	0.61970
-	-	-	-	-	-	-	-	-	-
P30481	29	27	27	29	34	25	0.51405	11.84151	0.10004
-	-	-	-	-	-	-	-	-	-
P62826	13	9	11	6	8	6	-0.28853	10.13009	0.61595
P01903	12	7	3	6	7	2	-0.11976	9.61220	0.87798
Q58FG0	8	7	10	16	12	7	0.90886	10.32735	0.04095
P13760	5	0	0	2	3	0	0.41077	7.72749	0.75956
P62753	5	7	9	4	5	0	-0.77709	9.30639	0.21302
P34910	1	0	0	0	3	3	2.70232	7.22087	0.07552
-	-	-	-	-	-	-	-	-	-
Q86V81	2	0	0	0	3	2	1.61974	7.21792	0.29826
P37837	7	6	12	0	0	0	-6.46080	9.03208	0.00000
P57737	14	6	7	3	3	7	-0.61512	9.72260	0.37785
-	-	-	-	-	-	-	-	-	-
Q9H4M9	0	0	1	11	12	12	5.20508	9.61280	0.00000
P13929	21	15	21	16	10	12	-0.15300	10.97406	0.73017
P47755	14	8	5	4	9	0	-0.61512	9.71718	0.29585
P63244	6	8	7	0	0	0	-6.21238	8.78450	0.00001
P16402	0	1	5	5	4	1	1.13109	8.41241	0.22707
P68366	32	29	30	27	20	9	-0.26836	11.59562	0.39937
P23284	0	0	3	8	3	4	2.64157	8.59156	0.00116
-	-	-	-	-	-	-	-	-	-
P0CW22	4	4	3	0	0	0	-5.29707	7.85813	0.00240
P30613	0	3	2	4	4	4	1.63902	8.50548	0.03808
Q9NTK5	6	2	1	1	8	1	0.56825	8.65479	0.66180
-	-	-	-	-	-	-	-	-	-

Uniprot Accession	MM.1S Global Spectral Count			U266 Global Spectral Count			Statistics		
	Replicate 1	Replicate 2	Replicate 3	Replicate 1	Replicate 2	Replicate 3	logFC	logCPM	PValue
P37802	5	6	2	0	0	0	-6.02365	8.09842	0.00007
-	-	-	-	-	-	-	-	-	-
P07108	9	16	17	0	0	0	-7.70013	9.79632	0.00000
P63000	4	3	3	0	0	0	-5.65177	7.71937	0.00101
P16152	0	0	0	4	5	4	5.48422	8.09388	0.00101
Q8N0Y7	8	8	7	7	4	5	-1.05937	9.68338	0.04102
P29966	0	0	0	13	12	12	6.97217	9.59964	0.00000
P22626	43	30	31	69	76	68	0.48379	12.69675	0.01043
Q04917	11	11	7	3	3	9	-1.48253	9.85834	0.00191
-	-	-	-	-	-	-	-	-	-
P46782	6	0	2	5	3	5	0.14722	8.78760	1.00000
P61160	11	9	7	0	3	2	-2.91017	9.40012	0.00000
P16949	6	3	5	7	7	11	0.28311	9.68001	0.63137
P14618	31	34	39	238	221	249	2.21528	14.00838	0.00000
P62701	6	9	3	7	9	7	-0.19370	9.75322	0.75839
P61026	2	2	2	6	9	4	1.08768	9.03778	0.15481
O43681	0	0	0	3	3	8	5.58883	8.20045	0.00051
P05388	7	10	7	7	14	13	-0.04677	10.25307	1.00000
P49755	3	3	3	4	11	10	0.90913	9.48076	0.11391
-	-	-	-	-	-	-	-	-	-
P09972	3	8	12	14	12	10	0.09587	10.27791	0.89762
P30508	7	7	6	14	15	13	0.51632	10.34782	0.25424
P68371	56	45	51	76	92	81	0.16220	13.03994	0.36703
P52597	8	7	4	12	10	15	0.40806	10.20131	0.34934
Q07955	9	5	2	5	3	4	-0.94762	9.20440	0.13976
P30048	4	8	6	8	10	3	-0.32319	9.68162	0.52768
Q14974	4	6	3	6	9	11	0.44437	9.67944	0.42346
Q6S8J3	63	53	65	39	37	50	-1.07046	12.67455	0.00000
P49773	3	4	0	3	5	4	0.22198	8.64286	0.81562
P12236	5	4	4	11	7	5	0.26961	9.56505	0.73878
P46926	1	0	5	0	0	0	-4.93381	6.98164	0.01584
-	-	-	-	-	-	-	-	-	-
-	-	-	-	-	-	-	-	-	-
P09104	9	13	8	26	23	22	0.68948	11.05004	0.02973
Q99729	1	1	0	3	3	2	1.36349	7.71655	0.34536
P16104	32	39	30	82	90	62	0.66141	12.77379	0.00036
Q12907	0	4	0	9	7	3	1.64923	8.91721	0.02763
P51571	9	8	5	9	8	6	-0.48028	9.88862	0.37829
P30499	1	3	0	8	9	7	1.98164	9.20007	0.00437
P31150	1	3	3	7	12	12	1.56969	9.64003	0.00656
-	-	-	-	-	-	-	-	-	-
P31943	9	7	3	11	8	5	-0.21022	9.82243	0.76403
-	-	-	-	-	-	-	-	-	-
Q14697	2	2	0	54	54	46	4.64849	11.68015	0.00000
Q07000	4	4	3	11	12	12	1.10600	9.91619	0.02459
Q9UKM9	2	0	2	6	6	6	1.57247	8.85309	0.04271
P04233	4	5	0	0	0	0	-5.50295	7.56705	0.00201
P17066	4	5	3	4	6	9	0.11148	9.34904	1.00000
P84103	7	8	8	9	6	6	-0.67333	9.85675	0.18035
B9A064	11	10	15	19	22	18	0.16218	10.96450	0.68746
O15144	0	3	1	1	2	6	0.59570	8.09500	0.77530
P46781	6	9	6	4	9	4	-0.84341	9.64507	0.11263
P17174	0	4	2	3	0	3	-0.52795	7.98065	0.77530
P29353	17	18	20	51	47	29	0.65571	11.89821	0.00632
P05387	8	9	7	12	7	9	-0.32420	10.09698	0.49577
P20700	8	15	3	6	7	4	-1.14888	9.82439	0.01506
Q01105	13	15	15	4	3	21	-1.16015	10.54926	0.00166
P60953	4	0	7	6	5	9	0.30772	9.34903	0.58836
Q16555	6	9	9	0	0	0	-6.89797	8.98529	0.00000
P15880	8	11	8	13	13	12	-0.05620	10.41793	0.90268
P16403	45	54	29	57	67	51	-0.09830	12.63992	0.63365
P51149	0	2	1	28	25	23	4.02448	10.68955	0.00000

Uniprot Accession	MM.1S Vesicle Spectral Count			U266 Vesicle Spectral Count			Statistics		
	Replicate 1	Replicate 2	Replicate 3	Replicate 1	Replicate 2	Replicate 3	logFC	logCPM	PValue
P37802	7	7	10	19	18	18	1.61597	10.74449	0.00006
P00441	10	11	13	4	12	4	-0.33123	10.15562	0.53528
P07108	10	10	10	3	7	4	-0.66035	9.85865	0.20402
P63000	11	10	11	0	3	3	-1.94646	9.63856	0.00266
P16152	0	0	0	6	6	0	5.84196	8.00264	0.00035
Q8N0Y7	11	9	13	8	7	8	-0.08888	10.21420	1.00000
P29966	24	18	27	33	31	27	0.82781	11.75533	0.00730
P22626	13	7	18	37	13	8	1.03564	11.01199	0.00532
Q04917	11	12	14	9	8	9	-0.07724	10.38525	0.91132
P01116	0	0	3	0	3	4	1.56493	7.73580	0.23858
P46782	4	3	2	0	0	0	-5.01570	7.56975	0.00888
P61160	18	15	25	0	4	0	-3.35913	10.32501	0.00000
P16949	12	9	16	2	3	0	-2.40736	9.77623	0.00006
P14618	56	67	67	116	138	107	1.35583	13.58490	0.00000
P62701	11	10	5	6	3	3	-0.67479	9.64836	0.22450
P61026	7	6	2	6	11	1	0.68380	9.45448	0.33162
-	-	-	-	-	-	-	-	-	-
P05388	14	12	14	5	14	4	-0.36424	10.37528	0.36729
P49755	0	0	0	4	1	0	4.61371	6.73432	0.06547
Q92597	6	2	2	0	4	6	0.42071	8.73260	0.52284
P09972	5	8	8	9	8	5	0.49257	9.84021	0.40482
P30508	53	43	42	30	32	32	-0.12252	12.26186	0.71475
P68371	80	77	64	49	50	32	-0.32286	12.85035	0.19255
P52597	3	3	3	6	0	0	-0.14880	8.31330	1.00000
-	-	-	-	-	-	-	-	-	-
-	-	-	-	-	-	-	-	-	-
Q14974	7	5	5	5	6	0	-0.19338	9.20993	0.71804
Q6S8J3	86	115	129	97	89	79	0.11458	13.63465	0.65872
P49773	10	9	11	0	0	0	-6.72110	9.29190	0.00000
-	-	-	-	-	-	-	-	-	-
P46926	5	1	5	0	0	0	-5.29707	7.85646	0.00240
P43007	51	53	53	21	32	32	-0.45310	12.31283	0.11697
P38405	5	7	7	7	7	10	0.75930	9.84647	0.13013
P09104	28	20	23	16	10	11	-0.50668	11.14969	0.20164
Q99729	0	3	0	6	1	0	1.56493	7.73510	0.23858
P16104	38	38	39	27	23	19	-0.30496	11.92133	0.32260
-	-	-	-	-	-	-	-	-	-
-	-	-	-	-	-	-	-	-	-
P30499	31	21	22	16	15	17	-0.19254	11.33324	0.61047
P31150	12	24	22	11	12	3	-0.72174	10.78626	0.05768
P61020	11	6	3	3	6	4	-0.18746	9.44823	0.86963
P31943	0	0	0	6	1	0	5.08221	7.22179	0.00888
Q9Y696	15	12	24	21	23	33	1.02140	11.44171	0.00185
Q14697	3	3	6	0	0	0	-5.41954	7.98283	0.00125
Q07000	44	36	36	27	28	26	-0.08676	12.02676	0.79590
-	-	-	-	-	-	-	-	-	-
-	-	-	-	-	-	-	-	-	-
P17066	6	4	10	5	5	7	0.19408	9.62007	0.76238
P84103	4	1	0	4	3	0	0.87927	7.99338	0.40106
B9A064	103	57	88	5	3	1	-4.32105	12.31343	0.00000
O15144	7	5	7	0	0	0	-6.07003	8.63996	0.00003
P46781	7	7	7	7	2	0	-0.77709	9.30666	0.21302
P17174	6	3	2	2	0	0	-1.91950	8.10006	0.04401
P29353	9	16	13	11	15	11	0.39010	10.64584	0.37639
P05387	13	11	5	10	5	2	-0.33562	9.92499	0.58907
P20700	5	3	0	0	0	0	-4.85133	7.40024	0.01721
Q01105	16	8	12	0	1	0	-4.47175	9.58898	0.00000
P60953	20	13	17	2	10	5	-1.11554	10.45314	0.01392
Q16555	6	8	13	0	0	0	-6.57062	9.14288	0.00000
P15880	6	5	5	9	4	3	0.42457	9.41092	0.62218
P16403	0	0	5	4	5	1	1.38101	8.31937	0.13139
P51149	10	8	11	14	21	9	1.02536	10.61264	0.01148

Uniprot Accession	MM.1S Global Spectral Count			U266 Global Spectral Count			Statistics		
	Replicate 1	Replicate 2	Replicate 3	Replicate 1	Replicate 2	Replicate 3	logFC	logCPM	PValue
P62241	5	6	5	3	8	7	-0.37432	9.48330	0.61158
P07910	13	14	9	36	36	32	0.97685	11.51801	0.00043
P50914	4	3	3	3	4	4	-0.40271	8.78812	0.66581
P40429	3	2	3	2	3	5	-0.22166	8.56538	0.81562
P31146	15	12	15	2	1	4	-3.08163	10.01777	0.00000
-	-	-	-	-	-	-	-	-	-
Q13151	2	3	3	9	6	9	1.01689	9.39364	0.10204
Q92820	0	0	0	4	5	3	5.37143	7.97859	0.00201
Q04837	3	6	4	0	11	0	-0.77459	8.98121	0.31127
Q13885	39	39	42	55	67	59	0.04321	12.62834	0.83129
-	-	-	-	-	-	-	-	-	-
P62917	5	3	6	1	3	5	-1.16102	8.92041	0.09560
P08865	8	9	7	8	10	13	-0.17883	10.17702	0.68870
Q58FF8	9	7	13	10	12	15	-0.19673	10.44042	0.62744
P30042	4	3	2	5	6	8	0.51854	9.20172	0.44611
P42224	0	0	0	5	6	6	5.86364	8.48030	0.00007
-	-	-	-	-	-	-	-	-	-
Q32P51	13	26	11	32	41	38	0.59890	11.72070	0.02134
P30486	0	0	0	9	11	9	6.62387	9.24917	0.00000
P30492	3	3	3	9	11	9	1.12091	9.64101	0.06841
P0CG04	6	4	7	19	22	18	1.23563	10.63869	0.00166
Q58FF7	26	28	28	30	29	38	-0.30647	11.88200	0.20020
Q8N257	40	43	43	140	156	137	1.22994	13.49593	0.00000
P43361	0	0	0	0	1	8	4.96796	7.56357	0.00796
P63261	121	125	149	131	128	135	-0.55299	14.03782	0.00002
-	-	-	-	-	-	-	-	-	-
Q92945	3	5	4	1	1	2	-2.05548	8.39719	0.01321
-	-	-	-	-	-	-	-	-	-
Q9Y536	9	3	8	9	6	9	-0.28346	9.85574	0.65623

Uniprot Accession	MM.1S Vesicle Spectral Count			U266 Vesicle Spectral Count			Statistics		
	Replicate 1	Replicate 2	Replicate 3	Replicate 1	Replicate 2	Replicate 3	logFC	logCPM	PValue
P62241	8	7	8	5	5	3	-0.38643	9.57265	0.53210
P07910	3	0	0	3	2	0	1.09644	7.40832	0.46077
P50914	3	3	4	3	3	0	-0.29634	8.40461	0.81070
P40429	3	4	2	0	0	0	-5.01570	7.57057	0.00888
P31146	17	30	26	28	26	36	0.73093	11.78887	0.01998
P31350	9	7	9	0	0	0	-6.46080	9.03178	0.00000
-	-	-	-	-	-	-	-	-	-
-	-	-	-	-	-	-	-	-	-
-	-	-	-	-	-	-	-	-	-
Q13885	61	57	58	37	37	30	-0.32724	12.52339	0.23057
P10909	10	6	4	0	0	0	-6.14296	8.71258	0.00001
-	-	-	-	-	-	-	-	-	-
P08865	14	18	10	5	7	5	-0.86557	10.27883	0.05856
Q58FF8	21	16	19	18	17	11	0.14665	11.08101	0.74390
-	-	-	-	-	-	-	-	-	-
-	-	-	-	-	-	-	-	-	-
P02786	39	9	14	10	14	10	-0.43324	10.97487	0.29996
Q32P51	15	9	17	10	8	2	-0.59926	10.32478	0.20025
P30486	45	36	42	44	49	37	0.51000	12.40917	0.06299
P30492	54	45	44	32	41	31	-0.02822	12.35340	0.93043
P0CG04	76	36	57	5	3	0	-3.93428	11.79252	0.00000
Q58FF7	32	32	26	23	20	8	-0.38686	11.53293	0.23098
Q8N257	43	39	36	42	24	10	-0.20303	11.99560	0.46002
P43361	0	0	0	1	3	1	4.61371	6.73431	0.03350
P63261	234	288	323	200	200	206	-0.04846	14.91467	0.83581
P08754	17	20	17	13	16	20	0.28958	11.10558	0.41968
-	-	-	-	-	-	-	-	-	-
P30046	7	9	8	3	5	3	-0.68387	9.53051	0.26497
-	-	-	-	-	-	-	-	-	-